UNIVERSITY OF NAPLES FEDERICO II

Department of Agricultural Sciences
WATER MANAGEMENT and BIOSYSTEMS ENGINEERING DIVISION

32nd CYCLE of DOCTORATE in
AGRICULTURAL and AGRI-FOOD SCIENCES

Flow resistance in open channels colonized by *Phragmites australis*: field experiments and modeling

Supervisor
Prof. Giovanni Battista Chirico

PhD Candidate
Giuseppe Francesco Cesare Lama

PhD Program Coordinator
Prof. Guido D'Urso

Years 2017/2020

Dedicada a mi familia y
a una mujer muy especial en mi vida

Thesis submitted for the degree of PhD in Agricultural and Agri-Food Sciences
Portici (Napoli), Italy - March 2020

PhD Candidate: Giuseppe Francesco Cesare Lama

Supervisor: Prof. Giovanni Battista Chirico

PhD Program Coordinator (XXXII Cycle): Prof. Guido D'Urso

Reading Committee:

Prof. Federico Preti, Università degli Studi di Firenze

Prof. Nicola Fontana, Università degli Studi del Sannio

Acknowledgments

I sincerely thank my tutor, Prof. Giovanni Battista Chirico, for the priceless opportunity he had given to me to deepen my knowledge on my research topic and to improve and grow both professionally and personally during the three years of my PhD experience. I want to thank him for having believed in me.

I sincerely thank Dr. Juha Järvelä and Dr. Kaisa Västilä for having hosted me as visiting PhD student at the Environmental Hydraulics Lab of Department of Built Environment - Aalto University (Finland) and for having wisely guided me in my research activities. I am extremely grateful to them for having transmitted to me their sincere enthusiasm during all the seven months spent collaborating with them.

I want to thank Prof. Federico Preti and Prof. Luca Solari for their significant support during the first stage of my PhD Program, and for always making me feel at ease during the experimental activities conducted together.

I am profoundly thankful to the reading committee of the present Doctoral thesis and for the useful and encouraging comments and suggestions they provided.

I wish to thank Dr. Vittoro Pasquino, Dr. Alessandro Errico, Dr. Luigi Saulino and Dr. Paolo Nasta for having inspired me during all my PhD Program, and to Dr. Simona Francalanci for our interesting discussions dealing with the experimental activities in which we had the opportunity to collaborate. Special thanks go to Prof. Paola Gualtieri, Prof. Nunzio Romano, Prof. Fabrizio Sarghini, Prof. Gerardo Severino, Prof. Guido D'Urso, Prof. Mario Palladino, Prof. Stefania Pindozzi and Prof. Salvatore Faugno for having enriched these years with extremely stimulating academic activities.

I thank my colleagues at the Department of Agricultural Sciences in Portici (Napoli). Inevitable thanks go to Antonio, Carolina, Caterina, Elena, Ester, Maddalena, Marco, Mariano, Mario, Maura, Oscar, Pierre, Rossella, Sajjad, Vincenzo and Vladimir. I am profoundly thankful to Dr. Gerardo Caroppi and Dr. Ivo Martone for the unforgettable life experiences spent together in Finland and Panama, and to have shared with me part of these three years.

I am most grateful to my precious friends, for having encouraged me as a family. I hope from the bottom of my heart to be able to make their dreams come reality.

Thanks to my beloved parents Sylvia and Francesco, and to my precious zietta Anna Maria. I hope you could always be proud of me.

Thank you/Grazie di cuore ANGELiNA

Portici (Napoli) - Italy, March 2020

Giuseppe Francesco Cesare Lama

Scientific publications related to this Doctoral thesis and author's contribution

The journal papers and proceedings related to this Doctoral thesis are listed below:

I. (*Journal*) Errico, A., **Lama**, **G**.**F**.**C**., Francalanci, S., Chirico, G.B., Solari, L., Preti, F. 2019. Flow dynamics and turbulence patterns in a drainage channel colonized by common reed (*Phragmites australis*) under different scenarios of vegetation management. Ecological Engineering, 133, pp. 39-52. https://doi:10.1016/j.ecoleng.2019.04.016.

II. (*Conference*) Errico, A., **Lama**, **G**.**F**.**C**., Francalanci, S., Chirico, G.B., Solari, L., Preti, F. 2019. Validation of global flow resistance models in two experimental drainage channels covered by *Phragmites australis* (common reed), in Proceedings of the 38th IAHR World Congress - Water Connecting the World, Panama City, Panama, pp. 1313-1321. https://doi:10.3850/38WC092019-1215.

III. (*Conference*) **Lama**, **G**.**F**.**C**., Errico, A., Francalanci, S., Solari, L., Preti, F., Chirico, G.B. 2019. Hydraulic modeling of field experiments in a drainage channel under different riparian vegetation scenarios, in Book of Abstract of the AIIA International Mid-Term Conference, Matera 12-13 September, Italy, p. 54.

IV. (*Conference*) **Lama**, **G**.**F**.**C**., Errico, A., Francalanci, S., Solari, L., Preti, F., Chirico, G.B. 2019. Comparative analysis of modeled and measured vegetative Chézy's flow resistance coefficients in a drainage channel vegetated by dormant riparian reed. Proceedings of the International IEEE Workshop on Metrology for Agriculture and Forestry, Portici, Italy. pp. 180-184. ISBN: 978-1-7281-3611-0.

V. (*Journal*) **Lama**, **G**.**F**.**C**., Errico, A., Francalanci, S., Solari, L., Preti, F., Chirico, G.B. 2020. Evaluation of flow resistance models based on field experiments in a partly vegetated reclamation channel. Geosciences, 10(2), 47. https://doi.org/10.3390/geosciences10020047.

VI. (*Journal*) **Lama**, **G**.**F**.**C**. et al. 2020. Sensitivity of Ecohydraulic modeling to the uncertainty of Common reed Leaf Area Index derived by Digital Hemispherical Photography. *In preparation.*

Index

Abstract

The analysis and the prediction of the effects of the hydrodynamic interaction between water flow and riparian vegetation in natural and manmade vegetated water bodies are the main objectives of Ecohydraulics. Riparian vegetation has a paramount impact on both flow resistance and water quality in vegetated open channels. Defining the most appropriate management practice of riparian vegetation inside both natural and manmade water bodies is crucial for assuring a balance between a satisfactory level of hydraulic conveyance and a high environmental value of water. The presence of riparian vegetation significantly affects both mean and turbulent water flow fields, with important implications on oxygen production and transport of nutrients within vegetated open channels.

Experimental analysis and modeling were performed in this thesis, to provide additional understanding of the hydrodynamic interaction between riparian vegetation and water flow at field scale in an abandoned reclamation channel colonized by rigid and emergent plants of *Phragmites australis (Cav.)* Trin. ex Steud., also known as Common reed. Different riparian vegetation management scenarios were evaluated: undisturbed conditions, partial riparian vegetation cover and total riparian vegetation removal. Field hydraulic tests were carried out for investigating the experimental cross sectional distributions of streamwise velocity and main turbulence features (Reynolds stresses and Turbulent Kinetic Energy).

The outcomes of the experimental activities were employed for modeling the flow resistance of the examined vegetated reclamation channel by employing both 1D numerical simulations and literature models, which accuracies were assessed by comparing experimental and modeled vegetative global water flow resistance coefficients. In the case of partial riparian vegetation cover, a methodology based on the detailed analysis of the experimental cross sectional streamwise velocity distribution was proposed. This methodology provides estimates of global water flow resistance with prediction errors smaller than the direct application of the examined models.

In the last part of the doctoral research program, the feasibility of Digital Hemispherical Photography (DHP) technology was evaluated for assessing Leaf Area Index (LAI) of mature Common reed plants to be exploited for flow resistance modeling of vegetated streams. The uncertainty of DHP-derived LAI was evaluated from a functional perspective, by estimating its impact on the uniform water flow velocity predicted with Västilä & Järvelä model. DHP proved to be a reliable technology for ecohydraulic modeling at field scale.

Keywords: Ecohydraulics; Flow resistance; Vegetated open channels; Riparian vegetation; Field hydraulic experiments; Digital Hemispherical Photography; Leaf Area Index.

Abstract (Italiano)

L'analisi e la previsione degli effetti dell'interazione idrodinamica tra corrente idrica e vegetazione ripariale all'interno dei corpi idrici naturali e artificiali sono gli obiettivi principali dell'eco-idraulica. La vegetazione ripariale ha un significativo impatto sia sulla resistenza al moto che sulla qualità della risorsa idrica nei canali vegetati. La presenza della vegetazione ripariale ha un impatto notevole sui campi di moto medi e turbolenti, con importanti implicazioni sulla produzione di ossigeno e sul trasporto di nutrienti all'interno dei canali vegetati. E' necessario pertanto individuare buone pratiche di gestione della vegetazione ripariale all'interno di canali vegetati sia per garantire un'adeguata officiosità idraulica sia per tutelare l'ecosistema ripariale.

La presente Tesi di Dottorato si concentra su analisi idrauliche sperimentali e modellistiche volte a comprendere gli effetti dell'interazione idrodinamica tra vegetazione ripariale e corrente idrica alla scala di campo, attraverso lo studio di diversi scenari di gestione della vegetazione ripariale: condizione indisturbata, copertura parziale e totale rimozione della vegetazione ripariale. Sono stati condotti sei esperimenti idraulici a scala reale per la misura delle velocità e delle principali caratteristiche turbolente (Sforzi di Reynolds ed Energia Cinetica Turbolenta) all'interno di un canale di bonifica abbandonato, colonizzato da piante emergenti e rigide di *Phragmites australis (Cav.)* Trin. ex Steud., comunemente nota col nome di Cannuccia di palude.

I risultati delle attività sperimentali sono stati impiegati per la verifica dell'accuratezza della resistenza al moto nel canale di bonifica stimata con modelli presenti in letteratura. In particolare, nel caso di parziale copertura di vegetazione ripariale, è stata proposta una metodologia basata sull'analisi dettagliata delle distribuzioni di velocità misurate in campo. Questa metodologia ha permesso di stimare la resistenza al moto con un errore di predizione inferiore rispetto all'applicazione diretta dei modelli esaminati.

Nell'ultima parte del programma di ricerca di dottorato, è stata valutata la fattibilità di utilizzare la fotografia digitale emisferica (DHP) per la stima l'indice di area fogliare (LAI) della Cannuccia di palude da utilizzare in alcuni modelli per la stima della resitenza al moto dei canali vegetati. L'incertezza del LAI stimato con la tecnica DHP è stata valutata dal punto di vista funzionale, valutando il suo impatto sulla velocità media di corrente in condizioni di moto uniforme calcolata con il modello di Västilä & Järvelä. La tecnologia DHP si è rivelata una valida alternativa per la modellazione eco-idraulica di canali vegetati a scala reale.

Parole chiave: Eco-idraulica; Resistenza al moto; Canali vegetati; Vegetazione ripariale; Esperimenti idraulici a scala di campo; Fotografia digitale emisferica; Indice di area fogliare.

Objectives

The interaction between riparian vegetation and water flow hydrodynamic in open channels is still poorly understood, lacking both experimental evidences and robust modeling approaches. Among riparian species, Common reed is one of the most widespread weeds in natural and manmade vegetated water bodies all over the world, but the effects of its interaction with water flow dynamics have been not adequately investigated. In this context, the most remarkable unanswered research questions refer to the experimental analysis and modeling of the hydraulic resistance of natural and manmade open channels colonized by this riparian species, both at green and mature phenological stage, in most of the cases corresponding respectively to submerged and emergent conditions. At its peak phenological stage, this riparian species is characterized by a rigid bio-mechanical behaviour, showing an emergent vegetative condition. This aspect is extremely interesting for designing and scheduling appropriate riparian vegetation management activities, which aim at balancing the need of ensuring adequate hydraulic efficiency with the need of safeguarding the environmental quality of vegetated water bodies. Given these premises, the objectives of this thesis can be summarized as follows:

1. Experimental field-scale analysis and discussion of flow resistance and main turbulence features within a reclamation channel, considering different management scenarios of rigid emergent Common reed stands;

2. Validation and improvement of literature predictive models and hydraulic 1D numerical simulations of open channels, covered by rigid emergent Common reed stands;

3. Evaluation of DHP technology, as a cheap indirect tool for assessing riparian vegetation structure parameters relevant for modeling the global water flow resistance of vegetated open channels, covered by rigid emergent Common reed stands.

1. Introduction

1.1. Ecohydraulics

Riparian vegetation constitutes a fundamental natural element, dynamically interacting with water flow within vegetated water bodies (*Lama et al., 2019*). As shown in the following Figure 1, its positive environmental impacts sensibly vary depending on the water flow regimes inside the vegetated streams, moving from low flow to overflow.

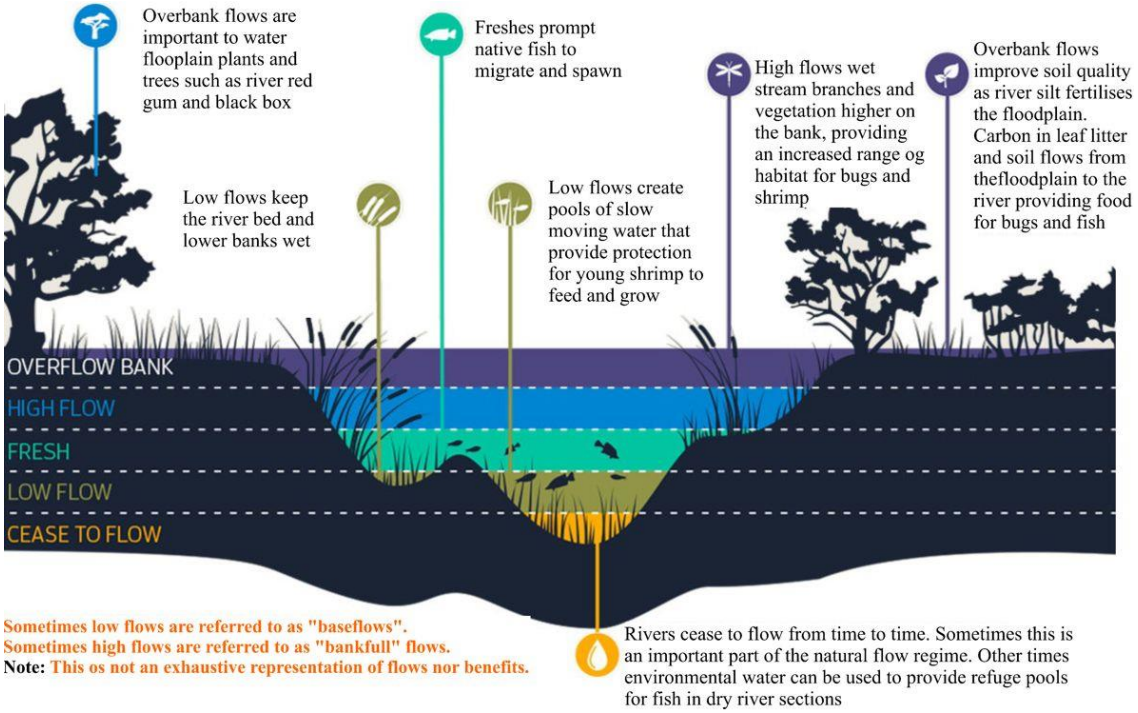

Fig. 1. Environmental benefits related to the presence of riparian vegetation in vegetated streams for different water levels (From *http://www.vewh.vic.gov.au/water-for-the-environment/environmental-benefits*).

Riparian plants dynamically interact with water flow, significantly affecting the hydrodynamics and the quality of fresh- or backwater flowing inside vegetated streams (i.e., rivers, reclamation channels, floodplains, lakes or wetlands), with a consequent increase in their water flow resistance, depending on both hydraulic and vegetative conditions (*Errico et al., 2019*; *Lama et al., 2020*).
The following Figure 2 shows a vegetated reclamation channel, colonized by *Phragmites australis (Cav.)* Trin. ex Steud. (Common reed) plants' stands.

Fig. 2. Vegetated reclamation channel, colonized by *Phragmites australis (Cav.)* Trin. ex Steud. plants (Common reed) in undisturbed conditions. The continuous white line indicates the limit of the vegetated reclamation channel bank.

More in detail, the presence of riparian vegetation in water bodies significantly alters the water flow velocity (*Wu & He, 2009*; *Errico et al., 2018*) and turbulence fields (*Pope, 2000*; *Errico et al., 2019*), as well as the mass and momentum exchanges between vegetated and non-vegetated zones (*Poggi et al., 2004*; *Nepf, 2012*; *Caroppi et al., 2019*). These effects can be examined at different scales, ranging from single branches and blades on an isolated plant to the whole riparian plant's stand (*Nepf, 2012*). As described in Figure 3a and Figure 3b, riparian plants react differently to water flow according to their peculiar bio-mechanical behaviour (flexible *vs*. rigid), submergence (emergent *vs*. submerged, depending on h/h_v, defined as the ratio between the water level, h, and the stem height measured from the channel bottom, h_v), and foliage conditions (foliated *vs*. defoliated). All these vegetative conditions depend essentially on both riparian vegetation species and its phenological stages (green *vs*. mature).

1.1.1. Riparian vegetation and streamwise velocity

Vegetated water flow refers to open channel flow with the cross section completely or partially covered by riparian vegetation (Fig. 3a-c) so that its effects on water flow dynamics cannot be neglected (*Nezu & Okamoto, 2012*; *Guo & Zhang, 2016*; *Errico et al., 2018*).

As reported in some previous studies (*Sukhodolova, 2008*; *Hopkinson & Wynn, 2009*; *Liu et al., 2017*), the presence of riparian vegetation strongly modifies the cross water flow (streamwise) streamwise velocity fields and vertical profiles. In natural open channels, riparian vegetation is organized in patches, commonly not uniformly distributed along the wetted perimeter, that dynamically interact with water flow in a non-linear manner (*Zhao & Huai, 2016*), by retarding the water flow itself, causing turbulence energy losses (*Panigrahi & Khatua, 2015*) and exerting additional hydraulic roughness to the channel

bed and banks. In the case of reclamation channels, streamwise velocity is generally low due to the small longitudinal bed slopes involved. Errico et al. (2018) outlined how Common reed canopies behave differently according to their phenological stage and their cross sectional density: leafed, young and sparse reeds show a flexible behaviour even in reclamation channels; differently, mature, emergent stems show a rigid attitude in response to the water flow. Under these latter conditions, stems bending can be neglected. Indeed, to describe the water flow - riparian vegetation hydrodynamic interaction for emergent vegetation, the stems are often assimilated to rigid cylinders arranged in regular or random patterns (*Whittaker et al., 2013*; *Caroppi et al., 2018*; *Gualtieri et al., 2018*).

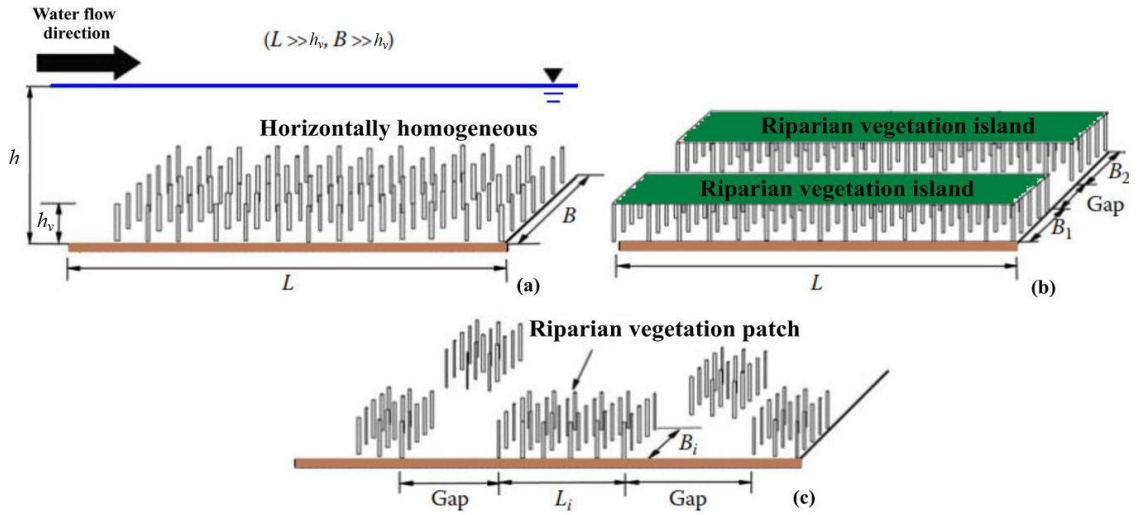

Fig. 3. Scheme of (a) uniformly, (b) partly and (c) patchy vegetated open channels (From *Nezu & Okamoto, 2012*).

For channel management and river restoration projects aiming at controlling the streambank retreat, the impact of riparian vegetation on shear stress acting on the banks needs to be necessarily understood. As shown in many studies (*Wilcox, 2010*; *Farhadi et al., 2018*), Reynolds stresses (τ'_{xz}) and Turbulent Kinetic Energy (*TKE*) distributions in the *x*-*z* vertical plan can be evaluated for the assessment of the effect of riparian vegetation on the water flow velocity dynamics at field scale. Most studies about this topic have been conducted in laboratory flumes employing both artificial and real plants, (*Luhar & Nepf, 2011*; *Panigrahi & Khatua, 2015*; *Etminan et al., 2017*; *Caroppi et al, 2019*). This approach allows one to study the water flow velocity vertical and cross sectional distributions and to measure the turbulent fluctuations with great precision. However, to characterize the riparian vegetation - water flow interaction at field scale, the measurement of the turbulent fluctuations within a real vegetated channel can offer a view which is more coherent with the actual processes of hydrodynamic interaction, especially for evaluating the hydraulic roughness (*Sime et al., 2007*; *Sukhodolova & Sukhodolov, 2012*; *Västilä et al., 2013*; *Errico et al., 2018*).

Typical examples of streamwise water flow velocity vertical profiles *u(z)* referred to non-vegetated open channels (dominated by bed turbulence), and with submerged (dominated by canopy top, defined as "Shear Layer") and emergent (dominated by steam wakes)

riparian vegetation (*Beudin et al, 2016*) are shown in the following Figures 4a-c:

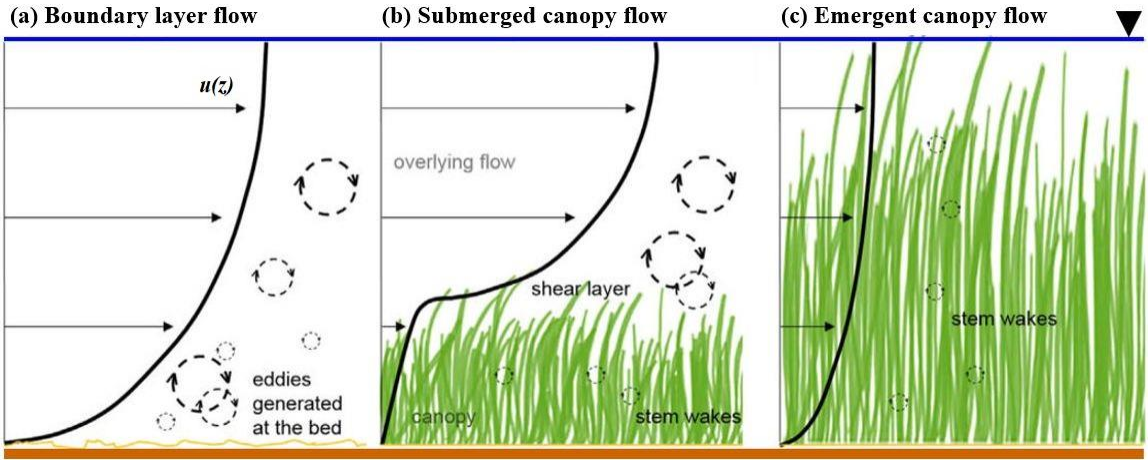

Fig. 4. Scheme of streamwise velocity vertical profiles *u(z)* for (a) non-vegetated open channels and with (b) submerged and (c) patchy and emergent riparian vegetation (From *Beudin et al, 2016*).

1.1.2. Impacts of riparian vegetation on water flow turbulence

Riparian vegetation affects turbulence across various spatial scales ranging from a single plant to canopy length up to the reach scale (*Nikora, 2010*). At the canopy scale and in the case of full submergence, vegetation modifies velocity with the formation of a vertical mixing-layer located in the proximity of the canopy top at the inflection point of the "S"-shaped velocity profile (*Ghisalberti & Nepf, 2002*). This "Mixing Layer" is characterized by large-scale coherent vortex convecting high-momentum fluid towards the low-momentum fluid region within the vegetation canopy.

This mechanism can be further modified due to the production of turbulence by organized waving canopy motion (i.e., monami). Horizontal mixing layers can be also observed in finite-width emergent canopies. In this case, shear layers grow at the edges of the canopy along the main water flow direction. When the canopy has two flow parallel edges, coherent flow structures are shed out of phase on either side (*Rominger & Nepf, 2011*). In the case of emergent canopies of finite length, the stem density must be considered as a key factor for the interaction and instability of the so-called von Kármán wakes, typically produced behind each plant stem (*Takemura & Tanaka, 2007*). When the relative stem spacing is sufficiently small - ratio spacing to stem diameter about 0.5 - a unique wake in the form of a large-scale vortex street is formed behind the whole canopy. Most importantly, the production of turbulence by stems can be greater than the bed shear production (*Nepf, 1999*; *Caroppi et al., 2019*). Therefore, in vegetated channels, sediment transport can be driven not only by bed shear stress but also by turbulence introduced by riparian vegetation wakes. Recent developments on this research topic illustrate that the onset of sediment motion can be predicted as a function of near-bed *TKE* considering both bed- and riparian vegetation-generated turbulence (*Hopkinson & Wynn, 2009*; *Yang et al., 2016*). Moreover, Tinoco & Coco (2018) found an increase in sediment re-suspension within canopies even when the water flow average velocity was considerably reduced, in the case of oscillatory water flows. This suggests that the sediment re-

suspension can be driven mainly by *TKE* induced by riparian vegetation rather than by mean water flow. Augmentation of turbulence exerted by riparian vegetation has also various implications on transport and retention of dissolved and particle matter (*Smith et al., 2014*; *Morris et al., 2015*; *Trinci et al., 2017*; *Verschoren et al., 2017*).

1.1.3. Impacts of riparian vegetation on hydraulic resistance

The estimation of the actual hydraulic roughness due to different riparian vegetation covers in vegetated streams have represented one of the most stimulating research issues in Ecohydraulics for many decades. However, most studies (i.e., *Murphy et al., 2007*; *Kothyari et al., 2009*; *Cheng & Nguyen, 2011*) have been conducted in laboratory flumes, with the relevant limitation of not studying a natural plant stand, but an artificial or grown one. Other studies investigated this problem directly in the field, but still not covering the entire variety of plant species and growth patterns that can be found in the water bodies of the world. Among these, interesting field experiments were conducted in grass-lined channels, focusing on the effect of flexible grasses-in conditions of full submergence (e.g., *Kouwen, 1988*; *Mohsen et al., 2006*). Other studies focused on the hydrodynamics of aquatic macrophytes such as *Ranunculus spp., Myriophyllum spp,* etc., which show an herbaceous habitus, not presenting rigid stems or straight emergent leaves (*Green, 2005*; *Nikora et al., 2008*; *Bal & Meire, 2009*; *Old et al., 2014*; *Verschoren et al., 2017*). Besides hydraulic resistance, these studies focused on the effects of plant growth on turbulence, on nutrients retention, as well as on the impacts of different riparian vegetation management strategies on them (*Baatrupp-Pedersen, 2018*).

1.1.4. Effects of riparian vegetation density, seasonality and management practices

In most cases, riparian vegetation cover is far to be homogeneous within a natural water body. Aquatic macrophytes, for example, are often arranged in patches, or strips, and this peculiar arrangement can be influenced, among other factors, by riparian vegetation management practices (*Old et al., 2014*). A consistent number of studies demonstrated how alterations of vegetation-induced water flow are significantly influenced by the cross sectional plants' arrangement, or even within an entire vegetated reach. Focusing on this aspect, Luhar & Nepf (2013) proposed a distinction in the water flow resistance analysis, according to three different scales (blade, patch and reach scale), as different assumption needs to be made for each of these three cases. The author observed that, for a determined value of the blockage factor (i.e., the fraction of channel cross section physically blocked by vegetation and biomass), water flow resistance induced by vegetated patches varies significantly with the number and position of patches. Patch size and blockage can be influenced by plant growth patterns, which often imply a seasonal variability in plant shapes and sizes. Interesting long-term studies demonstrated how water flow resistance varies significantly with seasonality (*Dawson, 1978*; *Gurnell & Midgley, 1994*; *Baatrupp-Pedersen, 2018*). These studies outlined how riparian vegetation growth and management practices can influence the seasonal water flow resistance, adducing interesting questions about the actual efficacy of such practices and their influence on species distribution in vegetated reclamation networks.

According to water bodies managers, choosing the most appropriate maintenance practice represents a fundamental issue to deal with (*Forzieri et al., 2012*). To our knowledge, few studies have examined the hydrodynamic impact of different riparian vegetation management scenarios at field scale. Old et al. (2014) and Verschoren et al. (2017) investigated the effects of three different riparian vegetation treatments within a lowland stream, observing a decrease in hydraulic roughness coefficients after the partial and total removal of riparian vegetation, with trends comparable with those reported in the present study. They also observed that the partial removal of riparian vegetation leads to the highest heterogeneity of streamwise velocity distribution. Just a few studies investigated the case of vegetated channels covered by Common reed, a plant species widespread almost all over the world, growing in wetlands and lowland areas (*Clevering & Lissner, 1999*; *Guo et al., 2013*). In a recent study, Errico et al. (2018) outlined that the removal of reed from a portion of the vegetated channel is an effective measure to contain the hydraulic roughness increase. This study constituted a step forward in analyzing the effects of Common reed in reclamation channels at the end of autumn when plants are at their maximum development stage.

References

Baattrup-Pedersen, A., Ovesen, N.B., Larsen, S.E., Andrsen, D.K., Riis, T., Kronvang, B., Rasmussen, J.J. 2018. Evaluating effects of weed cutting on water level and ecological status in Danish lowland streams. Freshw. Biol. https://doi.org/10.1111/fwb. 13101.

Bal, K.D., Meire, P. 2009. The influence of macrophyte cutting on the hydraulic resistance of lowland rivers. J. Aquat. Plant Manage., 47, pp. 65-68. https://hdl.handle.net/10067/765450151162165141.

Beudin, A., Kalra, T.S., Ganju, N.K., Warner, J.C. 2016. Development of a coupled wave-flow-vegetation interaction model. Computers & Geosciences, 100, pp. 76-86. https://dx.doi.org/10.1016/j.cageo.2016.12.010.

Caroppi, G., Gualtieri, P., Fontana, N., Giugni, M. 2018. Turbulence anisotropy at flow rigid vegetation interface. Geosciences 8(7), 259. https://doi.org/10.3390/geosciences8070259.

Caroppi, G., Västilä, K., Järvelä, J., Rowinski, P.M., Giugni, M. 2019. Turbulence at water-vegetation interface in open channel flow: experiments with natural-like plants. Adv. Water Resour. https://doi.org/10.1016/j.advwatres.2019.03.013.

Cheng, N.S., Nguyen, H.T. 2011. Hydraulic radius for evaluating resistance induced in simulated emergent vegetation in open-channel flows. J. Hydraul. Eng., 137 (9), pp. 995-1004. https://doi.org/10.1061/(ASCE)HY.1943-7900.0000377.

Clevering, O.A., Lissner, J. 1999. Taxonomy, chromosome numbers, clonal diversity and population dynamics of Phragmites australis. Aquat. Bot., 64 (3-4), pp. 185-208. https://doi.org/10.1016/S0304-3770(99)00059-5.

Dowson, F.H. 1978. The seasonal effects of aquatic plant growth on the flow of water in a stream. In: Proceedings of 5th European Weed Research Council Symposium on Aquatic Weeds. Vol. 71-78.

Errico, A., Pasquino, V., Maxwald, M., Chirico, G.B., Solari, L., Preti, F. 2018. The effect of flexible vegetation on flow in reclamation channels: Estimation of roughness coefficients at the real scale. Ecol. Eng., 120, pp. 411-421. https://doi.org/10.1016/j.ecoleng. 2018.06.018.

Errico, A., Lama, G.F.C., Francalanci, S., Chirico, G.B., Solari L., Preti F. 2019. Flow dynamics and turbulence patterns in a reclamation channel colonized by *Phragmites australis* (common reed) under different scenarios of vegetation management. Ecol. Eng., 133, pp. 39-52. https://doi:10.1016/j.ecoleng.2019.04.016.

Etminan, V., Lowe, R.J., Ghisalberti, M. 2017. A new model for predicting the drag exerted by vegetation canopies. Water Resour. Res., 53 (4), pp. 3179-3196. https://doi.org/10.1002/2016WR020090.

Farhadi, A., Sindelar, C., Tritthart, M., Glas, M., Blanckaert, K., Habersack, H. 2018. An investigation on the outer bank cell of secondary flow in channel bends. J. Hydro Environ. Res., 18, 1-11. https://doi.org/10.1016/j.jher.2017.10.004.

Forzieri, G., Castelli, F., Preti, F. 2012. Advances in remote sensing of hydraulic roughness. Int. J. Remote Sens., 33 (2), pp. 630-654. https://doi.org/10.1080/01431161.2010.531788.

Ghisalberti, M., Nepf, H.M. 2002. Mixing layers and coherent structures in vegetated aquatic flows. J. Geophys. Res. 107 (C2). https://doi.org/10.1029/2001JC000871.

Green, J.C. 2005. Comparison of blockage factors in modelling the resistance of channels containing submerged macrophytes. River Res. Appl., 21, pp. 671-686. https://doi.org/10.1002/rra.854.

Gualtieri, P., De Felice, S., Pasquino, V., Pulci Doria, G. 2018. Use of conventional flow resistance equations and a model for the Nikuradse roughness in vegetated flows at high submergence. J. Hydrol. Hydromech., 66 (1), pp. 107-120. https://doi.org/10.1515/johh-2017-0028.

Guo, J., Zhang, J. 2016. Velocity distributions in laminar and turbulent vegetated flows. J. Hydraul. Res. 54 (2), 117-130. https://doi.org/10.1080/00221686.2015.1136899.

Guo, W.-Y., Lambertini, C., Li, X.-Z., Meyerson, L.A., Brix, H. 2013. Invasion of old world Phragmites australis in the new world: precipitation and temperature patterns combined with human influences redesign the invasive niche. Change Biol., 19 (11), pp. 3406-3422. https://doi.org/10.1111/gcb.12295.

Gurnell, A.M., Midgley, P. 1994. Aquatic weed growth and flow resistance - influence on the relationship between discharge and stage over a 25 year river gauging station record. Hydrol. Process., 8, pp. 63-73. https://doi.org/10.1002/(ISSN)1099-1085.

Hopkinson, L., Wynn, T. 2009. Vegetation impacts on near bank flow. 418 (October), pp. 404-418. https://doi.org/10.1002/eco.87.

Kothyari, U.C., Hashimoto, H., Hayashi, K. 2009. Effect of tall vegetation on sediment transport by channel flows. J. Hydraul. Res., 47 (6), pp. 700-710. https://doi.org/10.3826/jhr.2009.3317.

Kouwen, N. 1988. Field estimation of the biomechanical properties of grass. J. Hydraul. Res., 26 (5), pp. 559-568. https://doi.org/10.1080/00221688809499193.

Lama, G.F.C., Errico, A., Francalanci, S., Solari, L., Preti, F., Chirico, G.B. 2019. Comparative analysis of modeled and measured vegetative Chézy's flow resistance coefficients in a drainage channel vegetated by dormant riparian reed. Proceedings of the International IEEE Workshop on Metrology for Agriculture and Forestry, Portici, Italy. pp. 180-184. ISBN: 978-1-7281-3611-0.

Lama, G.F.C., Errico, A., Francalanci, S., Solari, L., Preti, F., Chirico, G.B. 2020. Evaluation of flow resistance models based on field experiments in a partly vegetated reclamation channel. Geosciences, 10(2), 47. https://doi.org/10.3390/geosciences10020047.

Liu, D., Valyrakis, M., Williams, R. 2017. Flow Hydrodynamics across Open Channel Flows with Riparian Zones: Implications for riverbank stability. Water, 9 (720), pp. 1-19. https://doi.org/10.3390/w9090720.

Luhar, M., Nepf, H.M. 2011. Flow-induced reconfiguration of buoyant and flexible aquatic vegetation. Limnol. Oceanogr., 56 (6), pp. 2003-2017. https://doi.org/10.4319/lo.2011.56.6.2003.

Luhar, M., Nepf, H.M. 2013. From the blade scale to the reach scale: A characterization of aquatic vegetative drag. Adv. Water Resour. https://doi.org/10.1016/j.advwatres.2012.02.002.

Mohsen, M., Badronnisa, Y., Mohammed, T.A., Ghazali, A.H. 2006. Manning roughness coefficient for grass-lined channel, (January) - Suranaree. J. Sci. Technol., 13 (4), pp. 317-330.

Morris, M., Mohammadi, M.H., Day, S., Hondzo, M., Sotiropulus, F. 2015. Prediction of Glossosoma biomass spatial distribution in Valley Creek by field measurements and a three-dimensional turbulent open-channel flow model. Water Resour. Res., 51, pp. 1457-1471. https://doi.org/10.1002/2014WR015887.

Nepf, H.M. 1999. Drag, turbulence, and diffusion in flow through emergent vegetation. Water Resour. Res., 35 (2), 479-489. https://doi.org/10.1029/1998WR900069.

Nepf, H.M. 2012. Hydrodynamics of vegetated channels. Journal of Hydraulic Research 50(3): pp. 262-279. https://doi.org/10.1080/00221686. 2012.696559.

Nezu, I., Okamoto, T. 2012. Hydraulics of Vegetated Canopies, in: Handbook of Environmental Fluid Dynamics, Volume One, pp. 285-309. https://doi:10.1201/b14241-27\r10.1201/b14241-27

Nikora, V.I., Larned, S., Nikora, N., Debnath, K., Cooper, G., Reid, M. 2008. Hydraulic Resistance due to Aquatic Vegetation in Small Streams: Field Study. J. Hydraul. Eng. https://doi.org/10.1061/(ASCE)0733-9429(2008) 134:9(1326).

Nikora, V.I. 2010. Hydrodynamics of Aquatic Ecosystems: An Interface Between Environment, Biomechanics and Environmental Fluid Mechanics. River. Res. Appl., 26, pp. 367-384. https://doi.org/10.1002/rra.1291.

Old, G.H., Naden, P.S., Rameshwaran, P., Acreman, M.C., Baker, S., Edwards, F.K., Sorensen, J.P.R., Mountford, O., Gooddy, D.C., Stratford, C.J., Scarlett, P.M., Newman, J.R., Neal, M. 2014. Instream and riparian implications of weed cutting in a chalk river. Ecol. Eng. https://doi.org/10.1016/j.ecoleng.2014.07.006.

Panigrahi, K., Khatua, K.K. 2015. Prediction of velocity distribution in straight channel with rigid vegetation. Aquatic Procedia, 4 (Icwrcoe), pp. 819-825 Available at: http://linkinghub.elsevier.com/retrieve/pii/S2214241X15001030.

Poggi, D., Porporato, A., Ridolfi, R., Albertson, J.D., Katul, G.G. 2004. The effect of vegetation density on canopy sub-layer turbulence. Bound. Layer Meteorol., 111 (3), 565-587. https://doi.org/10.1023/B:BOUN.0000016576.05621.73.

Pope, S.B. 2000. Turbulent Flows. Cambridge University Press. https://doi.org/10.1017/CBO9780511840531.

Rominger, J.T., Nepf, H.M. 2011. Flow adjustment and interior flow associated with a rectangular porous obstruction. J. Fluid Mech., 680, pp. 636-659. https://doi.org/10.1017/jfm.2011.199.

Sime, L.C., Ferguson, R.I., Church, M. 2007. Estimating shear stress from moving boat acoustic Doppler velocity measurements in a large gravel bed river. Water Resour. Res., 43 (3), pp. 1-12. https://doi.org/10.1029/2006WR005069.

Smith, D.L., Goodwin, R.A., Nestler, J.M. 2014. Relating turbulence and fish habitat: a new approach for management and research. Rev. Fish Sci. Aquacult., 22, pp. 123-130. https://doi.org/10.1080/10641262.2013.803516.

Sukhodolova, T.A. 2008. Studies of Turbulent Flow in Vegetated River Reaches with Implications for Transport and Mixing Processes. PhD Thesis. April. http://dx.doi.org/10.18452/15843.

Sukhodolova, T.A., Sukhodolov, A.N. 2012. Vegetated mixing layer around a finite-size patch of submerged plants: 1. Theory and field experiments. Water Resour. Res., 48 (10), pp. 1-16. https://doi.org/10.1029/2011WR011804.

Takemura, T., Tanaka, N. 2007. Flow structures and drag characteristics of a colony-type emergent roughness model mounted on a flat plate in uniform flow. Fluid Dyn. Res., 39, pp. 694-710. https://doi.org/10.1016/j.fluiddyn.2007.06.001.

Tinoco, R.O., Coco, G. 2018. Turbulence as the Main Driver of Resuspension in Oscillatory Flow Through Vegetation. J. Geophys. Res. Earth Surf., 123 (5), pp. 891-904. https://doi.org/10.1002/2017JF004504.

Trinci, G., Harvey, G.L., Henshaw, A.J., Bertoldi, W., Hölker, F. 2017. Life in turbulent flows: interactions between hydrodynamics and aquatic organisms in rivers. Wiley Interdisciplinary Reviews: Water, 4(3), p. e.1213. Available at: http://doi.wiley.com/10.1002/wat2.1213.

Västilä, K., Järvelä, J., Aberle, J. 2013. Characteristic reference areas for estimating flow resistance of natural foliated vegetation. J. Hydrol., 492, pp. 49-60. https://doi.org/10.1016/j.jhydrol.2013.04.015.

Verschoren, V., Schoelynck, J., Cox, T., Schoutens, K., Temmerman, S., Meire, P. 2017. Opposing effects of aquatic vegetation on hydraulic functioning and transport of dissolved and organic particulate matter in a lowland river: A field experiment. Ecol. Eng., 105, pp. 221-230. https://doi.org/10.1016/j.ecoleng.2017.04.064.

Whittaker, P., Wilson, C., Aberle, J., Rauch, H.P., Xavier, P. 2013. A drag force model to incorporate the reconfiguration of full-scale riparian trees under hydrodynamic loading. J. Hydraul. Res., 51 (5), pp. 569-580. https://doi.org/10.1080/00221686.2013.822936.

Wilcox, B.P. 2010. Ecohydrology Bearing - Invited Commentary Transformation eco-system change and ecohydrology: ushering in a new era for watershed management. Ecohydrology, 130, pp. 126-130 Available at: http://www3.interscience.wiley.com/journal/122653919/abstract.

Wu, W., He, Z. 2009. Effects of vegetation on flow conveyance and sediment transport capacity. Int. J. Sediment Res., 24(3): pp. 247-259. https://doi.org/10.1016/S1001-6279(10)60001-7.

Zhao, F., Huai, W. 2016. Hydrodynamics of discontinuous rigid submerged vegetation patches in open-channel flow. J. Hydro-environ. Res., 12, pp. 148-160. https://doi.org/10.1016/j.jher.2016.05.004.

2. Flow resistance modeling with rigid Common reed plant's stands

2.1. Rigid-cylinder analogy

In the case of rigid bio-mechanical behaviour, riparian plants are usually described through the so-called "rigid-cylinder analogy", being the stem bending null, or, at most, negligible (*Caroppi et al., 2018*; *Pasquino et al., 2018; Errico et al., 2018*). Under both emergent (Fig. 5a) and submerged (Fig. 5b), riparian vegetation geometrical configuration with respect to water flow direction can vary between aligned (Fig. 5c) and staggered (Fig. 5d), to represent the effect of different spatial frames to be examined during laboratory flume experimental studies (*Schoneboom et al., 2011*; *Jalonen et al., 2013*).

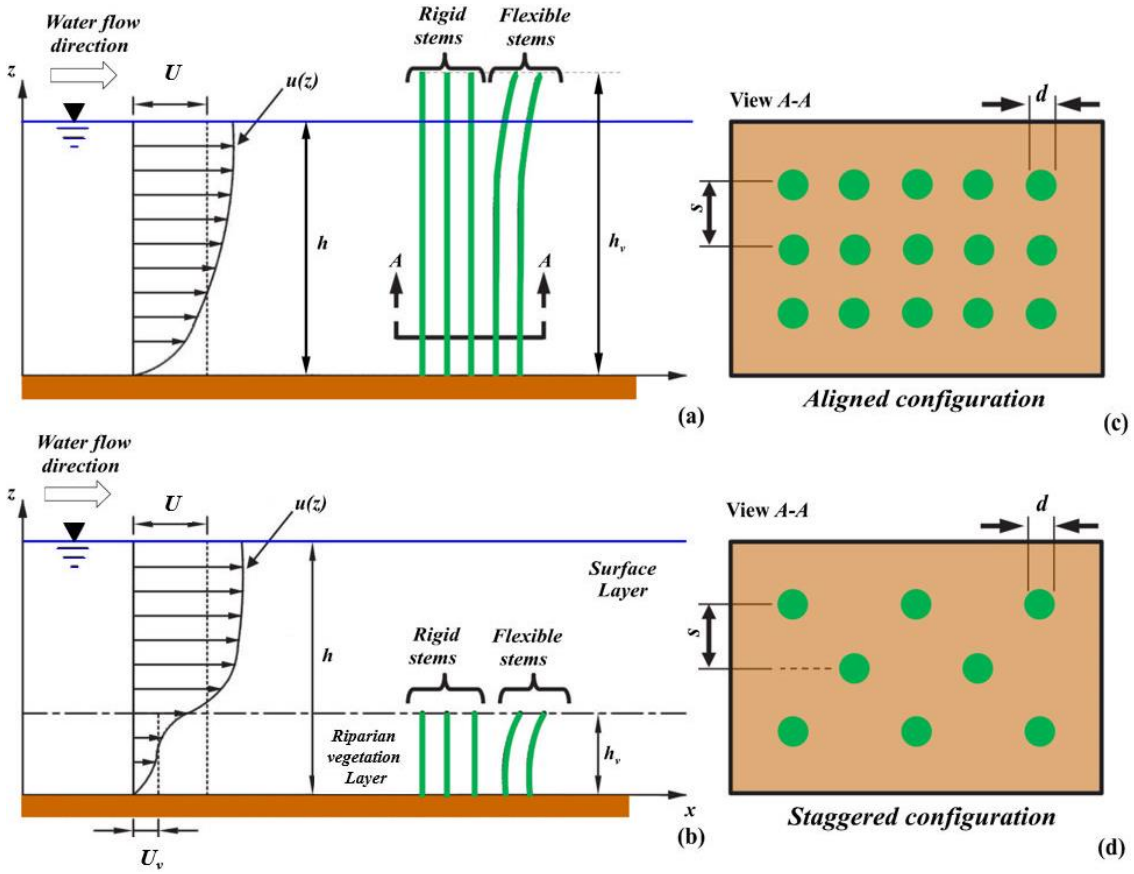

Fig. 5. Riparian vegetation conditions in open channels: view of (a) emergent and (b) submerged riparian plants, taking into account both rigid and flexible bio-mechanical behaviour. Plan view of (c) staggered and (d) aligned geometrical configurations: d (m) is the stem's average diameter, h (m) is the water level, h_v (m) is the stems' average height from the channel bottom (representing the thickness of the so-defined "riparian vegetation layer" in submerged conditions), s (m) is the distance between adjacent stems, U ($m \cdot s^{-1}$) is the uniform water flow velocity, U_v ($m \cdot s^{-1}$) is the water flow velocity averaged only over the vegetation layer, $u(z)$ is the vertical profile of the water flow velocity (From *Vargas-Luna et al., 2015*).

In Ecohydraulic modeling, riparian plants are synthetically parametrized through their characteristic diameter d (m) - typically expressed by the stem's average diameter - height form the channel bottom h_v (m), density m (m^{-2}) - defined as the number of riparian plants per unit bed surface area (*Nepf, 2019a*; *Nepf, 2012b*; *Caroppi et al, 2019*) - and by the so-called riparian vegetation "surface density" λ, as well as by the projected plant area per volume a (m^{-1}). The two latter parameters can be expressed as follows:

$$\lambda = \frac{\pi \cdot m \cdot d^2}{4} \tag{2.1}$$

$$a = m \cdot d. \tag{2.2}$$

For both flexible (Fig. 6a) and rigid (Fig. 6b) bio-mechanical behaviour, both emergent and submerged riparian vegetation is commonly represented as an agglomeration of uniformly distributed stems.

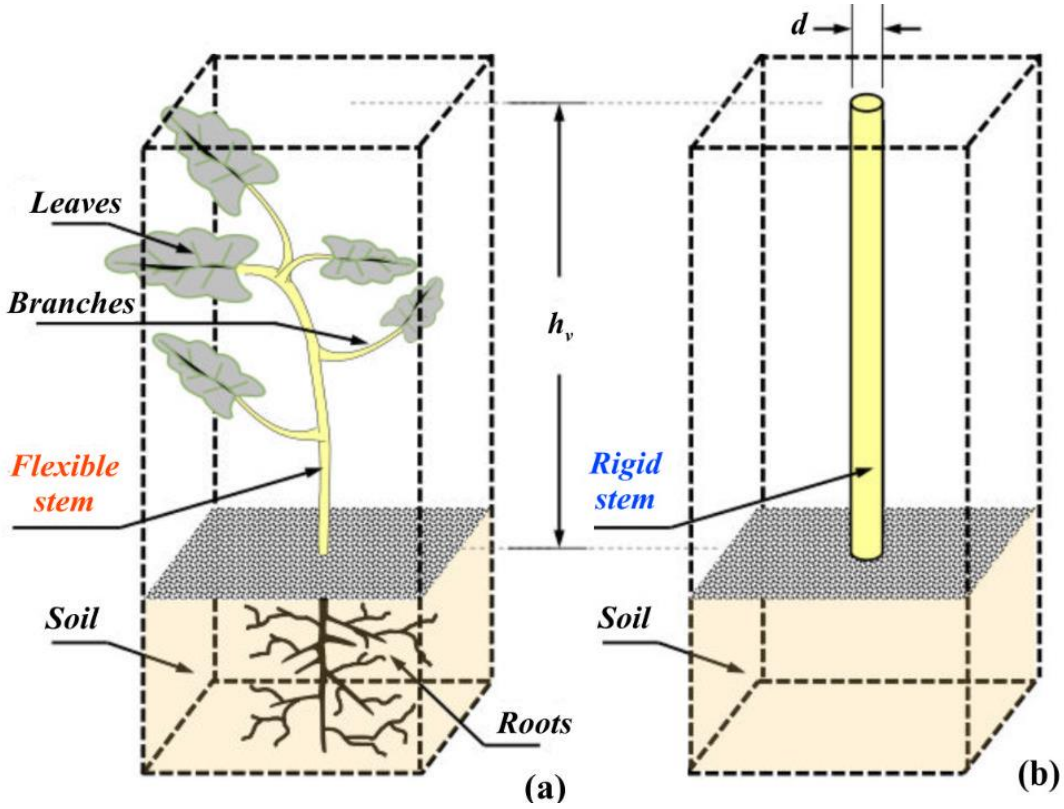

Fig. 6. Main morphometrical properties for (a) real riparian vegetation, and dimensional characteristics for (b) rigid-cylinder analogy (From *Vargas-Luna et al., 2015*).

From the fluid dynamic point of view, a still Common reed plant immersed in a water flow is subject to two main forces: the Weight W (N), proportional to the gravity acceleration g ($m^2 \cdot s^{-1}$), and the so-called resultant force F_R (N), proportional to the water flow average velocity U ($m \cdot s^{-1}$). F_R can be decomposed into two components: Lift force F_L (N), that is the component of F_R perpendicular to the water flow direction, and Drag force F_D (N), that is the component of F_R parallel to the water flow direction (Fig. 7).

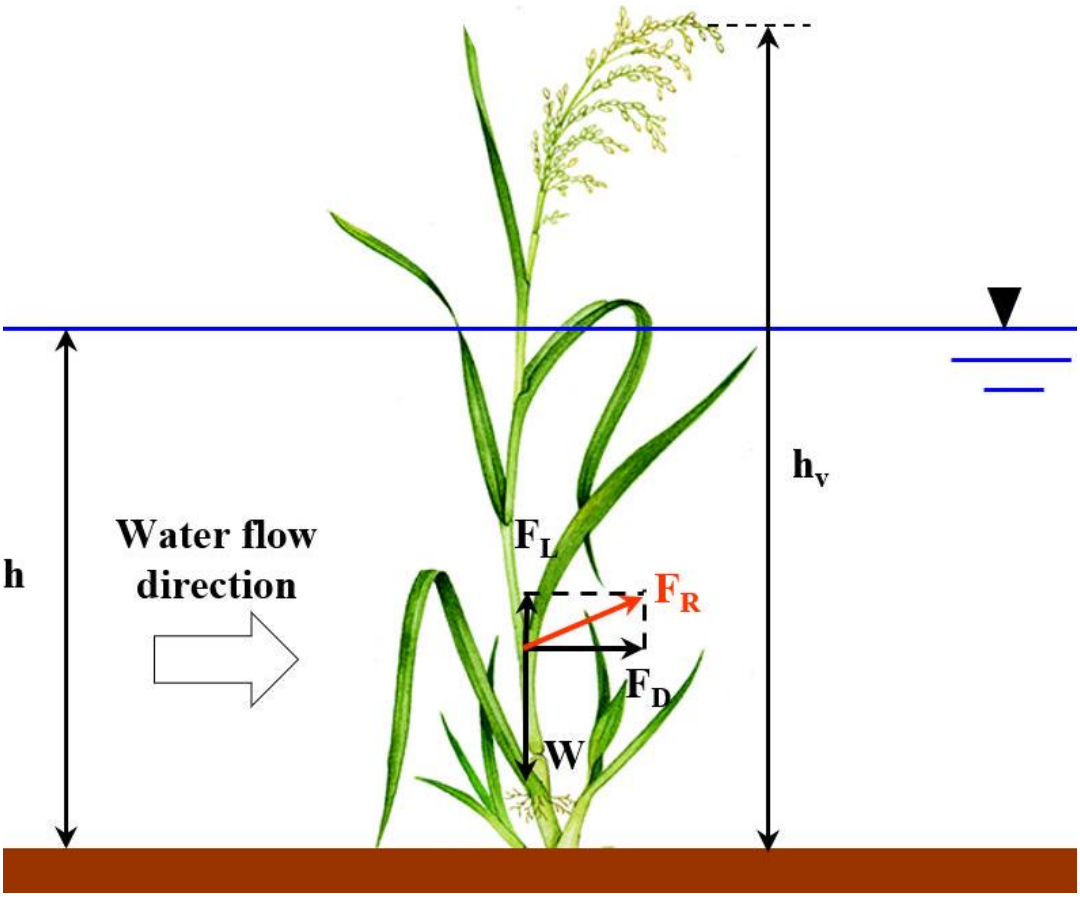

Fig. 7. Hydrodynamic forces acting on an isolated emergent Common reed plant (h/h_v < 1) immersed in water flow: F_D (N) is the Drag force, F_L (N) is the Lift force, F_R (N) is the Resultant force, h (m) is the water level and W (N) is the Weight.

F_D is proportional to the so-called "approach velocity" u_c (m·s^{-1}), that in the case of emergent riparian vegetation is generally assumed to be equal to the water flow average velocity U (m·s^{-1}). Under these assumptions, F_D can be expressed as follows (*Rouse, 1946*; *Järvelä, 2002*; *Västilä & Järvelä, 2014*):

$$F_D = \frac{1}{2} \cdot \rho \cdot C_D \cdot A_C \cdot U^2, \tag{2.3}$$

where ρ (kg·m^{-3}) is the water dynamic viscosity, equal to approximately 1000 kg·m^{-3}, C_D is the drag coefficient, and A_C (m^2) is the so-defined "reference area". In the case of rigid riparian plants, C_D can be expressed as a function of the Reynolds number $Re = u_c \cdot l_c / \nu$, where l_c (m) is the so-called "characteristic length" and ν (m^2·s^{-1}) is the kinematic viscosity of water, equal to approximately 10^{-6} m^2·s^{-1}.

Rigid bio-mechanical behaviour is typical of mature plants, which are characterized by high flexural rigidity $E \cdot I$, where E (N·m^{-2}) and I (m^4) are respectively the elastic modulus of the plant's material and the cross sectional second moment of area. Following Schlichting (1936), the global water flow resistance exerted by vegetated open channels in uniform flow conditions can be estimated by assuming that the total shear stress τ

($N \cdot m^{-2}$) can be split into two components, according to the linear superposition principle (e.g., *Yen, 2002*): bed-shear stress τ' ($N \cdot m^{-2}$) and vegetative shear stress τ'' ($N \cdot m^{-2}$):

$$\tau = \rho \cdot g \cdot h \cdot i = \tau' + \tau'', \quad (2.4)$$

where i indicates the longitudinal slope of the vegetated channel bottom.
By considering a condition of steady and uniform water flow for a spatially averaged reference framework (*Nikora et al., 2007a*; *Nikora et al., 2007b*; *Aberle & Järvelä, 2013*), Equation (2.4) can be rewritten as follows:

$$\rho \cdot g \cdot h \cdot \left(1 - \frac{m \cdot \langle V_p \rangle}{h}\right) = \frac{\tau_0}{\rho} \cdot (1 - m \cdot \langle A_B \rangle) + \frac{1}{2} \cdot m \cdot \langle C_D \rangle \cdot \langle A_C \rangle \cdot \langle u_c{}^2 \rangle, \quad (2.5)$$

where $\langle V_p \rangle$ (m^3) is the so-called "spatial average submerged plant volume". In the case of floodplain riparian vegetation, it can be verified that $m \cdot \langle V_p \rangle << h$ and $m \cdot \langle A_b \rangle << 1$. Thus, dividing Equation (2.5) by U^2, it is possible to write:

$$f = f' + f'', \quad (2.6)$$

where f ($= 8 \cdot g \cdot i \cdot h / U^2$) is the Darcy-Weisbach's friction factor, f' ($= 8 \cdot \tau_0 / \rho \cdot U^2$) is the friction factor due to bed surface and f'' ($= 4 \cdot m \cdot \langle C_D \rangle \cdot \langle A_C \rangle \cdot \langle u_c{}^2 \rangle / U^2$) is the friction factor due to the form drag. According to Aberle & Järvelä (2013), rigid stems of emergent riparian trees or reed-type vegetation (e.g., *Phragmites australis (Cav.)* Trin. ex Steud.) have often been simulated by employing simply shaped bluff elements such as cylinders (rigid-cylinder analogy) arranged in regular or random geometrical configurations (e.g., *Lindner, 1982*; *Nepf, 1999*; *Kothyari et al., 2009*). For emergent riparian vegetation, $\langle A_C \rangle$ can be easily expressed by the product $\langle h_v \cdot d \rangle$. Moreover, as reported by many Authors, $\langle C_D \rangle$ is a function of stem hydrodynamic roughness (e.g., *Tanaka et al., 2011*), stem shape (e.g. *James et al., 2008*), stem Reynolds number $Re_s = \langle u_C \rangle \cdot d/v$, density (e.g., *Li & Shen 1973*; *Lindner 1982*; *Nepf 1999*; *Ishikawa et al. 2000*; *Kothyari et al. 2009*) and the spatial arrangement of cylinders (aligned, staggered or randomly placed) (see. Fig. 3a and Fig.3b). For a cylindric stem, $\langle C_D \rangle$ can be computed according to two different approaches. First, $\langle F_D \rangle$ can be retrieved by considering heterogeneous water flow conditions. Under these conditions, it is possible to write:

$$\langle F_D \rangle = \frac{1}{2} \cdot \rho \cdot \langle C_D \rangle \cdot \langle A_C \rangle \cdot \langle u_c{}^2 \rangle, \quad (2.7)$$

where $\langle C_D \rangle$ represents the drag coefficient of an isolated cylinder, calculated as a function of Re_s. The second methodology, instead, is based on the following expression:

$$\langle F_D \rangle = \frac{1}{2} \cdot \rho \cdot \overline{C_D} \cdot \langle A_C \rangle \cdot U^2, \quad (2.8)$$

where $\overline{C_D}$ is the so-defined "bulk drag coefficient", referred to U^2. Thus, following Aberle & Järvelä (2013), it is possible to write:

$$\overline{C_D} = \langle C_D \rangle \cdot \frac{\langle u_c{}^2 \rangle}{U^2}. \tag{2.9}$$

Then, the new expression of *f''* for cylindric stems becomes the following:

$$f'' = 4 \cdot m \cdot \overline{C_D} \cdot \langle A_C \rangle. \tag{2.10}$$

Among others, Luhar et al. (2008) indicated that for randomly distributed rigid riparian vegetation, the so-called stem reference area index $m \cdot \langle A_C \rangle$ can be expressed as A_C/A_B, where A_B (m^2) is the bottom surface area. Then, Equation (2.10) can be expressed as follows:

$$f'' = 4 \cdot \overline{C_D} \cdot \frac{A_C}{A_B}. \tag{2.11}$$

As appears from Eq. (2.11), defining properly A_C is fundamental. As indicated by Armanini et al. (2005), the frontal projected area in still air A_{p_0} is typically employed in the case of leafless woody vegetation. In the case of non-submerged mature Common reed stands colonizing vegetated channels (see Fig. 2), it is possible to consider $\frac{A_{p_0}}{A_B} \equiv$ *LAI*, where *LAI* indicates the Leaf Area Index. Thus, Equation (2.11) can be rewritten as follows:

$$f'' = 4 \cdot \overline{C_D} \cdot LAI. \tag{2.12}$$

Due to the existence of wake water flow features (e.g., *Pope & Whitelaw, 1976*) in a cylinder array, $\overline{C_D}$ may sensibly vary from C_D of a single and isolated emergent cylinder for a wide range of Re_s values (*Aberle & Järvelä, 2013*). In fact, many previous works have recognized a decreasing trend of $\overline{C_D}$ with increasing Re_s (e.g., *Lindner, 1982*; *Nepf, 1999*; *Ishikawa et al., 2000*; *Tanino and Nepf, 2008*; *Kothyari et al., 2009*) and that, for the same *U* and density values, $\overline{C_D}$ was larger for a staggered than for an aligned cylinder configuration (e.g., *Li & Shen, 1973*; *Lindner, 1982*; *Schoneboom et al., 2011*; *Nepf, 2012b*). However, Ishikawa et al. (2000), Tanino & Nepf (2008), Kothyari et al. (2009) & Stoesser et al. (2010) have observed that $\overline{C_D}$ increases with increasing stem density, whilst, according to Nepf (1999) an opposite trend was detected, even for similar Re_s and densities values. As reported by Lindner (1982), the wake water flow due to an upstream cylinder could be considered as negligible for a longitudinal relative cylinder spacing of $a_x/d > 40$, where a_x is the longitudinal cylinders' spacing, and that u_c remained approximately constant after a distance of $20 \cdot a_x$ to the leading edge of the entire array.

2.2. Models for predicting water flow resistance of vegetated water bodies colonized by rigid Common reed plants' stands

According to Galema (2009), the global water flow resistance of vegetated water bodies can be predicted by employing several empirical or semi-empirical equations and physically-based models. The models' input parameters have been mostly retrieved from laboratory flume experiments under controlled hydrodynamic conditions and riparian vegetation species. To assess the predictive efficiency of several resistance models, Vargas-Luna et al. (2015) carried out a comparative analysis between estimated ($C_{r,\,est.}$) and measured ($C_{r,\,meas.}$) vegetative Chézy's water flow resistance coefficients, based on the outcomes of 234 experiments referred to real riparian vegetation. The examined datasets are summarized in the following Table 1.

Tab. 1. Experimental datasets analyzed by Vargas-Luna et al. (2015) referred to real riparian vegetation, under different hydraulic and vegetative conditions: *NL* indicates No leaves, *LL* indicates Low leaves concentration, and *HL* indicates High leaves concentration; *F* indicates Field experiments and *L* indicates Laboratory experiments; *E* indicates Emergent riparian vegetation and *S* indicates Submerged riparian vegetation (From *Vargas-Luna et al., 2015*)

Dataset	Tests	Type	Foliage	Exp.	Condition
Ree & Crow (1977)	24	Grass,	NL;	F	E
	31	Shrub	LL		
Turner & Chanmeesri (1984)	17	Wheat	NL	L	E
Hall & Freeman (1994)	12	Bulrush	NL	L	
Meijer & van Velzen (1999)	2	Reeds	NL	L	E
Freeman et al. (2000)	37	Shrubs	NL;	L	E
	50		HL		E
Järvelä (2003)	12	Wheat and Sedges	NL	L	S
James et al. (2004)	8	Reeds	NL	L	E
Nikora et al. (2008)	1	Aquatic	-	F	E
	24				S
Righetti (2008)	2	Willows	LL	L	E
	4				S
Velasco et al. (2008)	9	Barley	NL	L	S
King et al. (2012)	2	Aquatic	-	L	E
	4				S

The resistance models based on the rigid-cylinder analogy consider either submerged or emergent riparian vegetation conditions, or both. Petryk & Bosmajian (1975), Ishikawa et al. (2003), Hoffmann (2004) and James et al. (2004) take into account the only cases of emergent riparian vegetation while Klopstra et al. (1997), van Velzen et al. (2003), Huthoff (2007) and Yang & Choi (2010), among others, consider the only submerged

conditions. Stone & Shen (2002), Baptist et al. (2007) and Cheng (2011) consider emergent and submerged conditions. In their review, Vargas-Luna et al. (2015) have analyzed the performance of Stone & Shen (2002) and Baptist et al. (2007) models for the prediction of the Chèzy water flow resistance coefficient (C_r). These two models can be expressed according to different equations, depending on the plants' submergence:

Stone & Shen *(2002)* resistance model for submerged riparian vegetation ($h/h_v \geq 1$):

$$C_r = 1.385 \cdot \left(\frac{h}{h_v} - d \cdot \sqrt{m}\right) \cdot \sqrt{\frac{g}{a \cdot h}}, \quad (2.13)$$

where g (m·s^2) is the gravity acceleration and $a = m \cdot d$.
Stone &Shen (2002) resistance model for emergent riparian vegetation ($h/h_v < 1$):

$$C_r = 1.385 \cdot \left(1 - d \cdot \sqrt{m}\right) \cdot \sqrt{\frac{g}{a \cdot h}}. \quad (2.14)$$

Baptist et al. (2007) resistance model for submerged riparian vegetation ($h/h_v \geq 1$):

$$C_r = \sqrt{\frac{1}{\frac{1}{{C_b'}^2} + \frac{C_D \cdot a \cdot h_v}{2 \cdot g}}} + \sqrt{\frac{g}{k}} \cdot ln\left(\frac{h}{h_v}\right), \quad (2.15)$$

where k is the von Kármán's constant, equal to 0.40, C_D (= 1) is the drag coefficient for rigid stems, and C_b' (m$^{1/2}$·s^{-1}) is the water flow resistance coefficient associated with bed roughness in submerged conditions, expressed as:

$$C_b' = C_b + \sqrt{\frac{g}{k}} \cdot ln\left(\frac{h}{h_v}\right) \sqrt{1 + \frac{C_D \cdot a \cdot h_v \cdot {C_b}^2}{2 \cdot g}}, \quad (2.16)$$

where C_b (m$^{1/2}$·s^{-1}) is the water flow resistance associated with bed roughness in emergent conditions (*van Velzen et al., 2003*), expressed as:

$$C_b = 18 \cdot log\left(\frac{12 \cdot h}{k_s}\right), \quad (2.17)$$

with k_s (m$^{1/2}$·s^{-1}) is the characteristic bed roughness, imposed equal to 50 m$^{1/2}$·s^{-1}.
Baptist et al. (2007) resistance model for emergent riparian vegetation ($h/h_v < 1$):

$$C_r = \sqrt{\frac{1}{\frac{1}{{C_b}^2} + \frac{C_D \cdot a \cdot h}{2 \cdot g}}}. \quad (2.18)$$

The results of the comparative analysis between $C_{r,\,est.}$ and $C_{r,\,meas.}$ carried out by Vargas-Luna et al. (2015) have shown that Baptist et al. (2007) resistance model could lead to reasonably acceptable predictions of $C_{r,\,meas.}$, and performed similarly for submerged and emergent riparian vegetation conditions (Fig. 8a), whilst Stone & Shen (2002) resistance model tended to overestimate it (Fig. 8b).

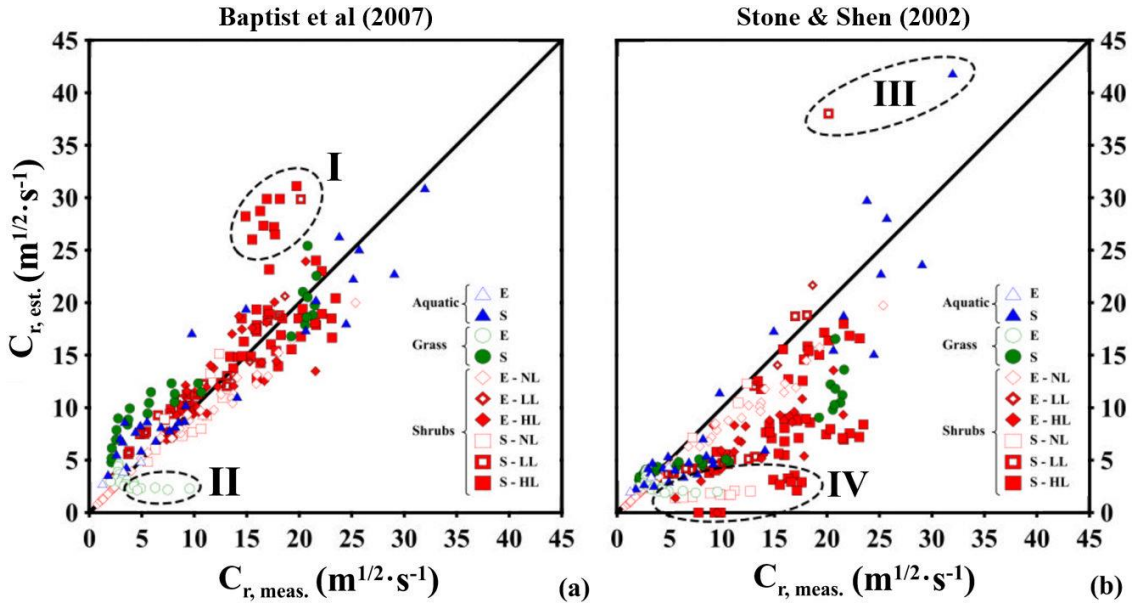

Fig. 8. Measured and estimated C_r ($m^{1/2}\cdot s^{-1}$), referred to (a) Baptist et al. (2007) and (b) Stone & Shen (2002) resistance models for: *E* stands for Emergent riparian vegetation and *S* stands for Submerged riparian vegetation, and for *NL* stands for No leaves, *LL* and *HL* stand for Low and High leaves concentration, respectively. The black dashed ellipses define classes of data showing different riparian vegetation properties (From *Vargas-Luna et al., 2015*).

In Figures 8a-b, the black dashed ellipses circumscribe some specific classes of experimental data. In detail, "Class I" referred to the experimental outcomes for which Baptist et al. (2007) resistance model underestimated the global water flow resistance. This group of data consisted of submerged shrubs characterized by high leaves density (a ranging between 1.45 and 3.25 m^{-1}). "Class I" also included one experiment characterized by low leaves density and a relatively high degree of submergence, expressed by a = 0.04 m^{-1} and h/h_v = 2.1, respectively. "Class II" included experimental measurements performed by Freeman et al. (2000), for which $C_{r,\,meas}$ was overestimated by Baptist et al. (2007) resistance model. "Class III" was referred to two experimental setups, both corresponding to high degrees of submergence, one with low and one with high leaves density (a = 1.20 m^{-1} and h/h_v = 7.9), for which $C_{r,\,meas}$ was underestimated by Stone & Shen (2002) resistance model. In the end, "Class IV" was referred to experimental measurements characterized by high $a\cdot d$ values, to which Stone & Shen (2002) resistance model resulted to be extremely sensitive. Based on these observed trends, it could be stated that riparian vegetation density and degree of submergence played a leading role in the ranges of applicability of the two resistance models tested by Vargas-Luna et al. (2015) in their review. In particular, $C_{r,est}$ have been analyzed referred to both Stone & Shen (2002) and Baptist et al. (2007) resistance models, by taking into account a vegetated reclamation channel with bed roughness C_b, equal to 50 $m^{1/2}\cdot s^{-1}$, riparian vegetation patch with drag coefficient C_D equal to 1, and stems' average diameter d equal to 0.004 m. The Authors have investigated two riparian vegetation heights h_v of 0.05 and 0.25 m, and the water levels have been varied for obtaining degrees of submergence

ranging between 0.04 and 17.0. In their analyses, the Authors selected two different values of riparian vegetation densities (number of stems per unit bed surface) equal to 250 and 750 m^{-2}, respectively corresponding to a plant area per unit of volume *a* of 1.0 and 3.0 m^{-1}. The results of this comparative analysis are shown in the following Figure 9.

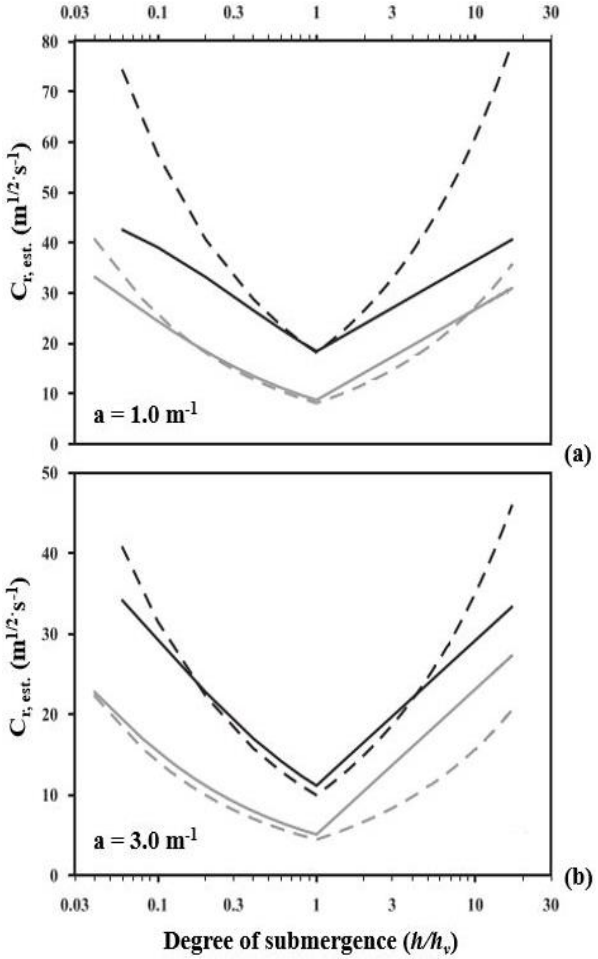

Fig. 9. $C_{r,est.}$ ($m^{1/2}\cdot s^{-1}$) as a function of the degree of submergence, according to Stone & Shen (2002) and Baptist et al. (2007) models for (a) a = 1.0 m^{-1} and (b) a = 3.0 m^{-1}. Two vegetated layer heights have been considered: 0.05 m (dashed and continuous black line for Stone & Shen (2002) and Baptist et al. (2007), respectively) and 0.25 m (dashed and continuous grey line for Stone & Shen (2002) and Baptist et al. (2007) respectively) (From *Vargas-Luna et al., 2015*).

By considering the lowest canopy density value (Fig. 9a), no significant spreads have been noticed between the performances of the two resistance models for tall riparian vegetation, whereas substantial deviations have been observed by the Authors for the shorter plants. These discrepancies led to extremely high $C_{r,est}$ values referred to Stone & Shen (2002) resistance model. For denser canopies, lower spreads between the outcomes of the two resistance models have been observed in the case of emergent riparian vegetation. Stone & Shen (2002) resistance model exhibited a high sensitivity to water level variations in the case of submerged riparian vegetation (Fig. 9b). In fact, it was more sensitive to the variations in water level than Baptist et al. (2007) resistance model, which led to some discrepancies in $C_{r,est}$.

References

Aberle, J., Järvelä, J. 2013. Flow resistance of emergent rigid and flexible floodplain vegetation. J. Hydraul. Res. 51 (1), pp. 33-45. https://doi.org/10.1080/00221686.2012.754795.

Armanini, A., Righetti, M., Grisenti, P. 2005. Direct measurement of vegetation resistance in prototype scale. J. Hydraulic Res. 43(5), pp. 481-487. https://doi.org/10.1080/00221680509500146.

Baptist, M.J., Babovic, V., Rodríguez, J., Keijzer, M., Uittenbogaard, R., Mynett, A., Verwey, A. 2007. On inducing equations for vegetation resistance. J. Hydraul. Res., 45(4), pp. 435-450. https://doi.org/10.1080/00221686.2007.9521778.

Caroppi, G., Gualtieri, P., Fontana, N., Giugni, M. 2018. Vegetated channel flows: turbulence anisotropy at flow-rigid canopy interface. Geosciences, 8, 259. https://doi.org/10.3390/geosciences8070259.

Caroppi, G., Västilä, K., Järvelä, J., Rowinski, P.M., Giugni, M. 2019. Turbulence at water-vegetation interface in open channel flow: experiments with natural-like plants. Adv. Water Resour. https://doi.org/10.1016/j.advwatres.2019.03.013.

Cheng, N.S. 2011. Representative roughness height of submerged vegetation. Water Resources Research 47(8): W08517. https://doi.org/10.1029/ 2011WR010590.

Errico, A., Pasquino, V., Maxwald, M., Chirico, G.B., Solari, L., Preti, F. 2018. The effect of flexible vegetation on flow in reclamation channels: Estimation of roughness coefficients at the real scale. Ecol. Eng. 120, pp. 411-421. https://doi.org/10.1016/j.ecoleng. 2018.06.018.

Freeman, G.E., Rahmeyer, W.H., Copeland, R.R. 2000. Determination of resistance due to shrubs and woody vegetation. Technical Report, ERDC/CHL TR-00-25, US Army Engineer Research and Development Center, Vicksburg, MS.

Galema, A. 2009. Vegetation resistance; evaluation of vegetation resistance models for flood management. Master Thesis, University of Twente, Enschede, The Netherlands.

Hall, B., Freeman, G. 1994. Study of hydraulic roughness in wetland vegetation takes new look at Manning's n. Technical Report. The Wetlands Research Program Bulletin 4(1), pp. 1-4.

Hoffmann, M.R. 2004. Application of a simple space-time averaged porous media model to flow in densely vegetated channels. Journal of Porous Media 7(3): pp. 183-192. https://doi:10.1615/JPorMedia.v7.i3.30.

Huthoff, F. 2007. Modelling hydraulic resistance of floodplain vegetation. PhD Thesis, Department of Water Engineering, University of Twente, The Netherlands.

Ishikawa, Y., Mizuhara, K., Ashida, S. 2000. Effect of density of trees on drag exerted on trees in river channels. J. For. Res. 5(4), pp. 271-279. https://doi.org/10.1007/BF02767121.

Ishikawa, Y., Sakamoto, T., Mizuhara, K. 2003. Effect of density of riparian vegetation on effective tractive force. Journal of Forest Research 8(4): pp. 235-246. https://doi:10.1061/10.1007/s10310-003-0032-4.

Jalonen, J., Järvelä, J., Aberle J. 2013. Leaf area index as a vegetation density measure for hydraulic analyses, J. Hydraul. Eng., 139(5), pp. 461-469, https://doi:10.1061/(ASCE)HY.1943-7900.0000700.

James, C.S., Birkhead, A.L., Jordanova, A.A., O'Sullivan, J.J. 2004. Flow resistance of emergent vegetation. Journal of Hydraulic Research 42(4): pp. 390-398. https://10.1080/00221686.2004.9728404.

Järvelä, J. 2002. Flow resistance of flexible and stiff vegetation: A flume study with natural plants. J. Hydrology 269, pp. 44-54. https://doi.org/10.1016/S0022-1694(02)00193-2.

Järvelä, J. 2003. Influence of vegetation on flow structure in floodplains and wetlands. In River, Coastal and Estuarine Morphodynamics 2003 (Vol. II, pp. 845-856), Sánchez-Arcilla A, Bateman A (eds). IAHR: Barcelona, Spain.

King, A.T., Tinoco, R.O., Cowen, E.A. 2012. A k-ε turbulence model based on the scales of vertical shear and stem wakes valid for emergent and submerged vegetated flows. Journal of Fluid Mechanics 701: pp. 1-39. https://doi.org/10.1017/jfm.2012.113.

Klopstra, D., Barneveld, H.J., van Noortwijk, J., van Velzen, E. 1997. Analytical model for hydraulic roughness of submerged vegetation. Conference Proceedings of the 27th IAHR Conference, San Francisco. HKV publication, pp. 775-780.

Kothyari, U.C., Hayashi, K., Hashimoto, H. 2009. Drag coefficient of unsubmerged rigid vegetation stems in open channel flows. J. Hydraulic Res. 47(6), pp. 691-699. https://doi.org/10.3826/jhr.2009.3283.

Li, R.M., Shen, W. 1973. Effect of tall vegetations on flow and sediment. J. Hydraulic Div. 99(5), pp. 793-814.

Lindner, K. 1982. Der Strömungswiderstand von Pflanzenbeständen. Mitt. Leichtweiß-Institut für Wasserbau No. 75, Braunschweig, Technische Universität Braunschweig, Germany, in German.

Luhar, M., J. Rominger, Nepf, H.M. 2008. Interaction between flow, transport and vegetation spatial structure, Environ. Fluid Mech., 8, pp. 423-439, https://doi.org/10.1007/s10652-008-9080-9.

Nepf, H.M. 1999. Drag, turbulence, and diffusion in flow through emergent vegetation. Water Resour. Res. 35(2), pp. 479-489. https://doi.org/10.1029/1998WR900069.

Meijer, D.G., van Velzen, E.H. 1999. Prototype-scale flume experiments on hydraulic roughness of submerged vegetation. XXVIII IAHR Conference, Technical University of Graz, Graz, Austria.

Nepf, H.M. 2012a. Hydrodynamics of vegetated channels. Journal of Hydraulic Research 50(3): pp. 262-279. https://doi.org/10.1080/00221686. 2012.696559.

Nepf, H.M. 2012b. Flow and transport in regions with aquatic vegetation. Annual Review of Fluid Mechanics 44(1): pp. 123-142. https://doi.org/10.1146/annurev-fluid-120710-101048.

Nikora, V., McLean, S., Coleman, S., Pokrajac, D., McEwan, I., Campbell, L., Aberle, J., Clunie. D., Koll, K. 2007. Double-averaging concept for rough-bed open-channel and overland flows: Applications. J. Hydraulic Eng. 133(8), pp. 884-895. https://doi.org/10.1061/(ASCE)0733-9429(2007)133:8(884).

Nikora, V., McEwan, I., McLean, S., Coleman, S., Pokrajac, D., Walters, R. 2007. Double-averaging concept for rough-bed open-channel and overland flows: Theoretical background. J. Hydraulic Eng. 133(8), pp. 873-883. https://doi.org/10.1061/(ASCE)0733-9429(2007)133:8(873).

Nikora, V., Larned, S., Nikora, N., Debnath, K., Cooper, G., Reid, M. 2008. Hydraulic resistance due to aquatic vegetation in small streams: field study. Journal of Hydraulic Engineering 134(9): pp. 1326-1332. https://10.1061/(ASCE)0733-9429(2008)134:9(1326).

Pasquino, V., Saulino, L., Pelosi, A., Allevato, E., Rita, A., Todaro, L., Saracino, A., Chirico, G.B. 2018. Hydrodynamic behaviour of European black poplar (Populus nigra L.) under coppice management along Mediterranean river ecosystem. River Res. Appl., 34, 586-594. https://doi.org/10.1002/rra.3276.

Petryk S., Bosmajian, G. 1975. Analysis of flow through vegetation. Journal of the Hydraulics Division, 101(7): pp. 871-884.

Pope, S.B. 2000. Turbulent Flows. Cambridge University Press. https://doi.org/10.1017/CBO9780511840531.

Pope, S.B., Whitelaw, J.H. 1976. The calculation of near-wake flows. J. Fluid Mech. 73, part 1, pp. 9-32. https://doi.org/10.1017/S0022112076001213.

Ree, W.O., Crow., F. 1977. Friction factors for vegetated waterways of small slope. Technical Report Publication S-151, US Department of Agriculture, Agricultural Research Service.

Righetti, M. 2008. Flow analysis in a channel with flexible vegetation using double-averaging method. Acta Geophysica 5(3): pp. 801-823. https://doi.org/10.2478/s11600-008-0032-z.

Rouse, H. 1946. Elementary Mechanics of Fluids. John Wiley & Sons.

Schlichting, H. 1936. Experimental investigations of the problem of surface roughness. NASA Technical Memorandum 823, Washington, DC.

Schoneboom, T., Aberle, J., Dittrich, A. 2011. Spatial variability, mean drag forces, and drag coefficients in an array of rigid cylinders. In: Experimental methods in hydraulic research, geoplanet: earth and planetary sciences. Vol. 1, pp. 255-265, P. Rowinski, ed. Springer, Berlin.

Stone, B.M., Shen, H.T. 2002. Hydraulic resistance of flow in channels with cylindrical roughness. J. Hydraulic Eng., 128(5), pp. 500-506. https://doi.org/10.1061/(ASCE)0733-9429(2002)128:5(500).

Tanaka, N., Takenaka, H., Yagisawa, J., Morinaga, T. 2011. Estimation of drag coefficient of a real tree considering the vertical stand structure of trunk, branches, and leaves. Int. J. River Basin Manag. 9(3-4), pp. 221-230. https://doi.org/10.1080/15715124.2011.606427.

Turner, A.K., Chanmeesri, N. 1984. Shallow flow of water through non-submerged vegetation. Agricultural Water Management 8(4): pp. 375-385. https://doi.org/10.1016/0378-3774(84)90065-9.

Vargas-Luna, A., Crosato, A., Uijttewaal, W.S.J. 2015. Effects of vegetation on flow and sediment transport: Comparative analyses and validation of predicting models. Earth Surf. Proc. Land. 40 (2), pp. 157-176. https://doi.org/10.1002/esp.3633.

Västilä, K., Järvelä, J. 2014. Modeling the flow resistance of woody vegetation using physically based properties of the foliage and stem. Water Resour. Res., 50, pp. 229-245. https://doi.org/10.1002/2013WR013819.

Velasco, D., Bateman, A., Medina, V. 2008. A new integrated, hydro-mechanical model applied to flexible vegetation in riverbeds. Journal of Hydraulic Research 46(5): pp. 579-597. https://doi.org/10.3826/jhr.2008.2986.

van Velzen, E., Jesse, P., Cornelissen, P., Coops, H. 2003. Stroming-sweerstand vegetatie in uiterwaarden; Handboek. Part 1 and 2. Technical Report, RIZA Reports, 2003.028 and 2003.029, Arnhem, The Netherlands.

Watson, D.J. 1947. Comparative physiological studies in the growth of field crops. I. Variation in net assimilation rate and leaf area between species and varieties, and within and between years. Annals of Botany, 11: pp. 41-76.

Yang, W., Choi, S.U. 2010. A two-layer approach for depth-limited open channel flows with submerged vegetation. Journal of Hydraulic Research 48(4): pp. 466-475. https://doi.org/10.1080/00221686.2010.491649.

3. Measurement of riparian vegetation canopy structure parameters

3.1 Leaf Area Index (LAI)

The Leaf Area Index (*LAI*) is one of the most basic and utilized parameters for characterizing the riparian vegetation canopy structure (Fig. 10a). Defined for the first time by Watson (1947) as the total one-sided area of leaf tissue (Fig. 10b) per unit ground surface (Fig. 10c), *LAI* has been broadly employed in many agricultural, forestry and environmental studies dealing with evapotranspiration (*Pelosi et al., 2016*; *Chirico et al., 2018*), biomass productivity (*Archontoulis et. al, 2012*; *Bai et al., 2016*), irrigation efficiency (*Djaman et al., 2013*; *Vitale et al., 2016*), as well as in Ecohydraulic modeling (*Järvelä, 2004*; *Aberle & Järvelä, 2013*; *Västilä & Järvelä, 2014*).

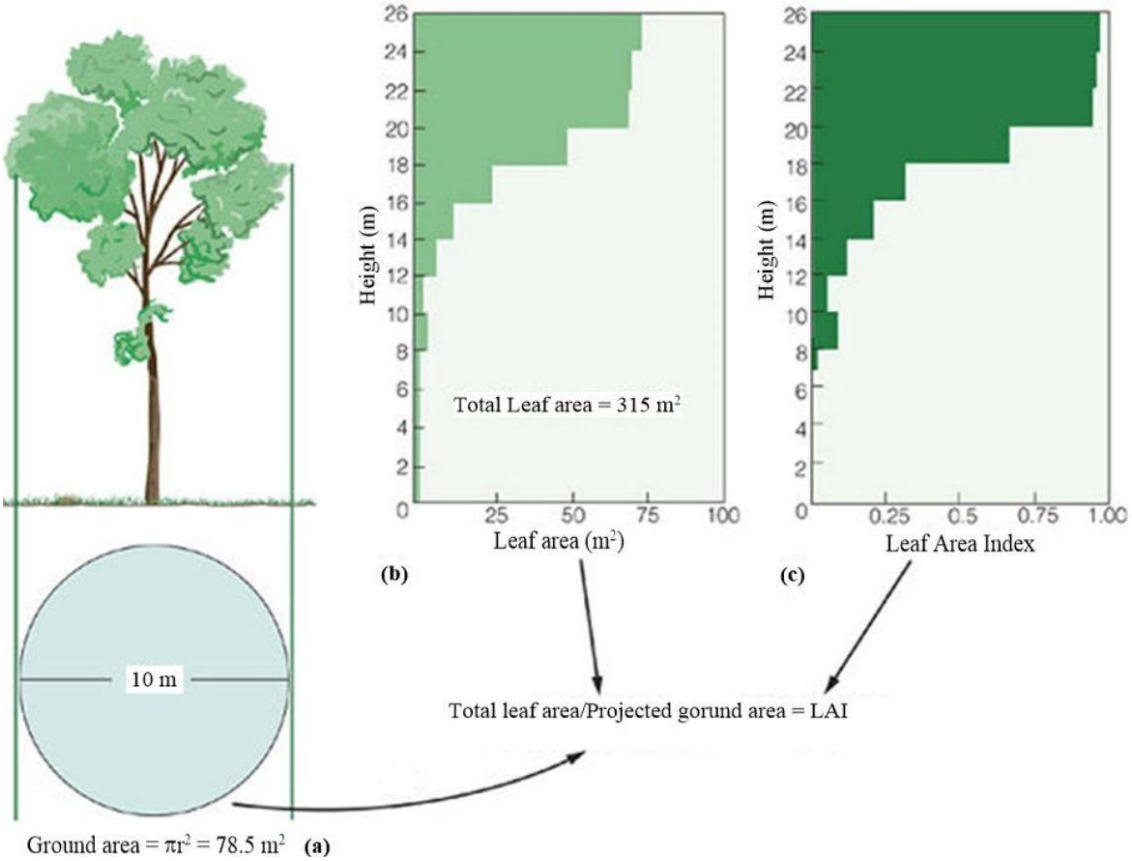

Fig. 10. Schemes of (a) Canopy Structure, (b) Total leaf area and (c) Project ground area for *LAI* calculation (i.e., *Breda, 2003*).

The methods employed for determining *LAI* at field can be essentially divided into two classes: direct and indirect methods (*Breda, 2003*; *Al Mamun Hossain et al., 2017*; *Saulino et al., 2019*). Direct methods are based on destructive - harvesting - riparian plants' sampling and image processing (Fig. 11a-b), while indirect methods involve the analysis of physical parameters acquired by using proximity sensors of ground-calibrated devices (*Jonkeree, 2004*; *Chianucci et al., 2015*; *Fang et al., 2019*).

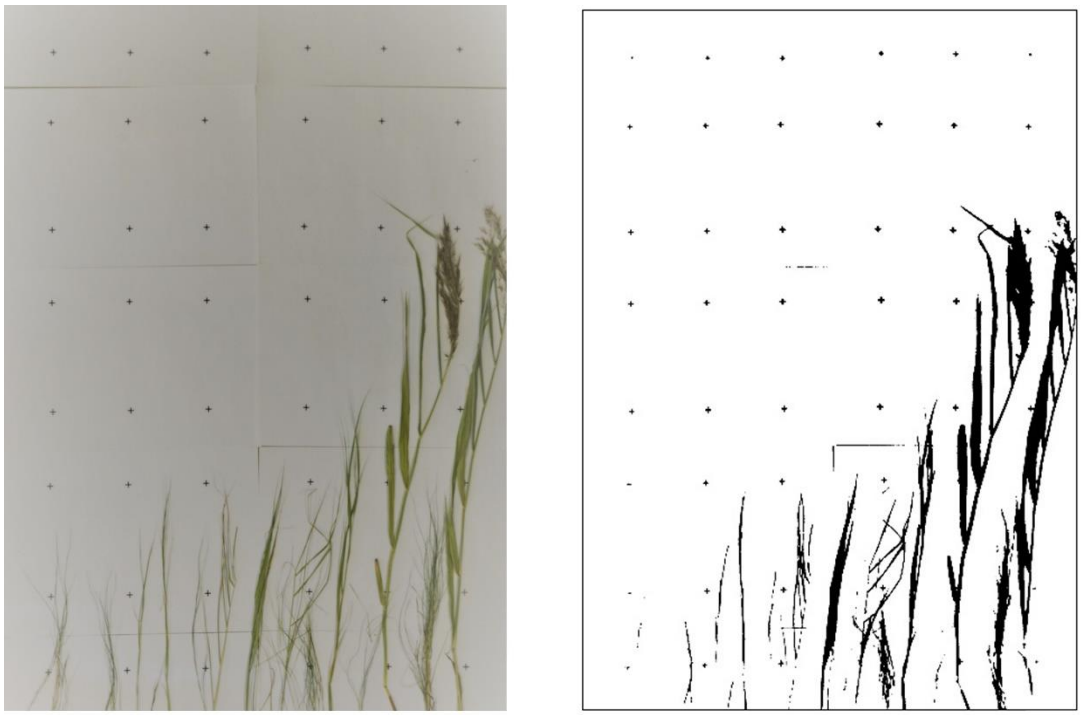

Fig. 11. Examples of (a) original and (b) binarized images referred to the same riparian vegetation harvested sample.

One of the most diffuse indirect methods for obtaining ground-based *LAI* measurements refers to the LI-COR® LAI-2000 Plant Canopy Analyzer (hereinafter referred to as *LI-COR*), a portable device equipped with an optical sensor measuring the amount of incident solar light reflected by riparian vegetation canopy. It has been widely exploited in both forestry and agricultural activities since it provides *LAI* values having accuracy comparable to those retrieved utilizing direct methods. Moreover, it allows repeatability of measurements which much fewer time costs with respect to direct methods, especially in short plants (*Sonnentag et al., 2007*; *Lopez-Lozano & Casterad, 2013*; *Hedley et al., 2017*).

3.2 LI-COR® LAI-2000 Plant Canopy Analyzer (LI-COR)

The *LI-COR* portable device provides ground-based *LAI* estimations, operating the inversion of canopy transmittance according to Beer-Lambert's law, recorded under uniform sky conditions. The device measures the attenuation of the diffusive sky radiation at five zenith angles simultaneously (Fig. 12a), considering the above ($LI\text{-}COR_A$) and below ($LI\text{-}COR_B$) canopy pair readings for the same plant (Fig. 12b), for calculating the transmittance $T_j(\theta_i)$ at arbitrary point *j*.

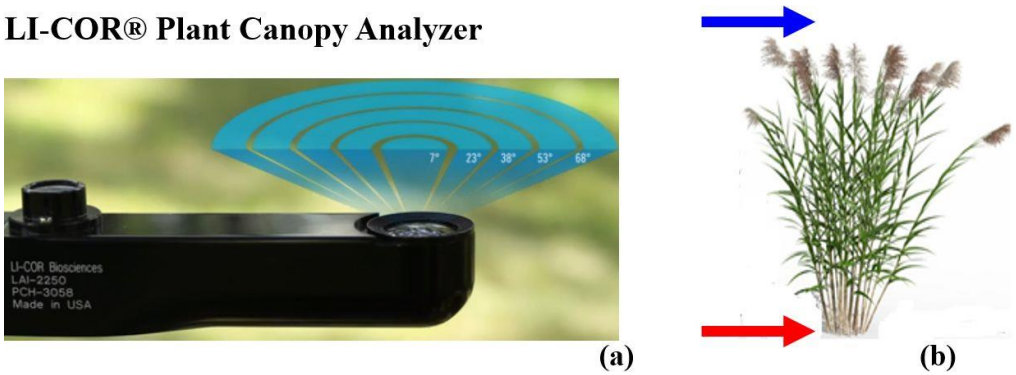

Fig. 11. (a) LI-COR's sensor. (b) Above (blue arrow) and below (red arrow) pair readings.

The optical sensor projects the image of its nearly hemispheric view onto 5 sensors arranged in concentric rings, and five transmittances are then calculated by diving the *A* and *B* corresponding pairs (i.e., *Rautiainen et al., 2004*; *Majasalmi, 2013*;). Thus, *LI-COR* measures the transmittance in different directions through plant canopies in the blue wavelength region (320 - 490 nm). Thus, transmittance corresponds to angular canopy gap fractions. The sensor's FOV extends over almost 150° and is divided into five concentric rings (*i*) centred at view zenith angles θ_i, that are given weights (W_i) according to the part of the hemisphere that they cover. Thus, *LAI* is computed as follows:

$$LAI = 2\sum_{i=1}^{5} K_i\, Q_i, \tag{3.1}$$

where $K_i = ln\left|T_j(\theta_i)\right|$ and $Q_i = sin\theta_i d\theta_i$ represent the leaves contact frequencies and the weights, respectively, for each view zenith angle θ_i.

3.3 Digital Hemispherical Photography (DHP) processing

In the last twenty years, Digital Hemispherical Photography (*DHP*) was exploited in many studies with different aims, being a cheaper and less time-consuming alternative to *LI-COR* (*Majasalmi et al., 2013*; *Chianucci et al., 2015*; *Loffredo et al; 2016*), based on Fisheye - or wide-angle - lenses (Fig. 13a), with an Angle-Of-View (*AOV*) ≥ 180°, also known as hemispherical view (Fig. 13b).

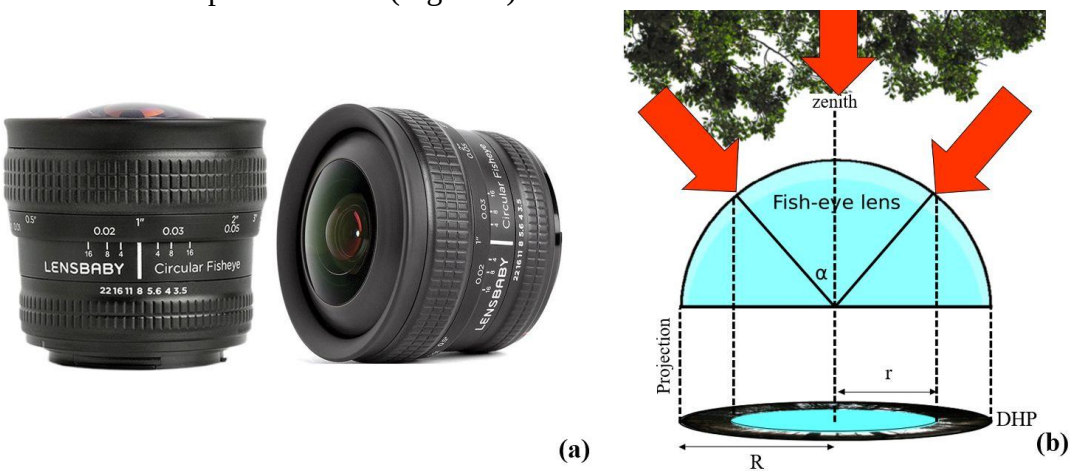

Fig. 11. (a) View of Fish-eye lens. (b) Scheme of *DHP* after image projection from a Fish-eye lens (From *Loffredo et al., 2016*).

LAI can be retrieved from *DHP* processing by using commercial or freeware dedicated softwares, which have been calibrated and validated for many plant species (e.g. *Liu et al., 2015*; *Liu et al., 2019*). Among others, INRA (Insitut National de la Recherche Agronomique) freeware CAN_EYE software (available at *https://www6.paca.inra.fr/can_eye*) is broadly utilized in both forestry and agricultural studies since it allows the user to improve the binarization process manually and, at the same time, to reduce the misclassification errors which are generally produced by automated threshold methods. The software implements a statistical analysis of gap fraction for different zenith angles under the assumption of Poisson's distribution for the leaf normal orientation (*Garrigues et al., 2008*; *Weiss & Baret, 2016*; *Guangjian et al., 2019*). Thus, this procedure is not applicable for analyzing the gap fraction of a single *DHP*, rather an ensemble, based on a minimum number of 8 *DHP*s for each Elementary Sampling Units (*ESU*) is required (*Weiss et al., 2004*; *Morisette et al., 2006*; *Weiss & Baret, 2016*). This condition was exposed in detail by Weiss et al. (2004): in fact, they suggest considering between 5 and 15 *DHP*s per *ESU*, after having analyzed the distribution of *RMSE* referred to *DHP*-derived *LAI* of Wheat and Pine canopies. CAN_EYE software analyses more than one picture a time. In fact, the CAN_EYE *LAI* calculations are performed considering between 8 and 12 (at most 25) *DHPs* a time. This proceeding was highlighted by Weiss et al. (2004); they suggested considering between 5 and 15 pictures per *ESU* as optimum, after analyzing the *RMSE* distribution of Fisheye based *LAI* assessments referred to Wheat and Pine canopies, varying the number of *DHP*s analyzed in each *ESU*. The input parameters required by CAN_EYE software for the camera+lens optical centre calibration are the coordinates of the centre (indicated as x_C and y_C) and the radius of the hemispherical lens, both expressed in pixels. After imposing them as input parameters, the lens projection (or mapping) function was automatically generated by the software itself. It can be defined as the function that gives the position of any pixel from the *DHP* centre as a function of the focal length and angular distance from the optical axis. As indicated in the Instruction Manual, the software supports only polar (or equidistant) projection functions, for which the angular distances (in degrees) in the object region are proportional to radial distances in pixels on the image plane. It is important to underline that CAN_EYE software considers a *FOV* corresponding to a zenith angle of 60° (defined as *COI*) to avoid distortions, and the angular resolutions for zenith and azimuth directions were set to 10° (*Fang et al., 2018*). According to the CAN_EYE software User Manual (Version 6.4.91), *COI* is defined as the limit of the *DHP* in degrees used during the imagery. By default, it is set to 0° - 60° because zenith angles higher than 60° are not considered, due to the large occurrence of mixed pixels in these areas. After the calibration, the software allows the user to create appropriate masks (Fig. 14a) for eliminating external elements (i.e. other plants and/or built-up structures) from the images. Then, it executes an *RGB* colour classification to discriminate the vegetation elements from the sky (Fig. 14b):

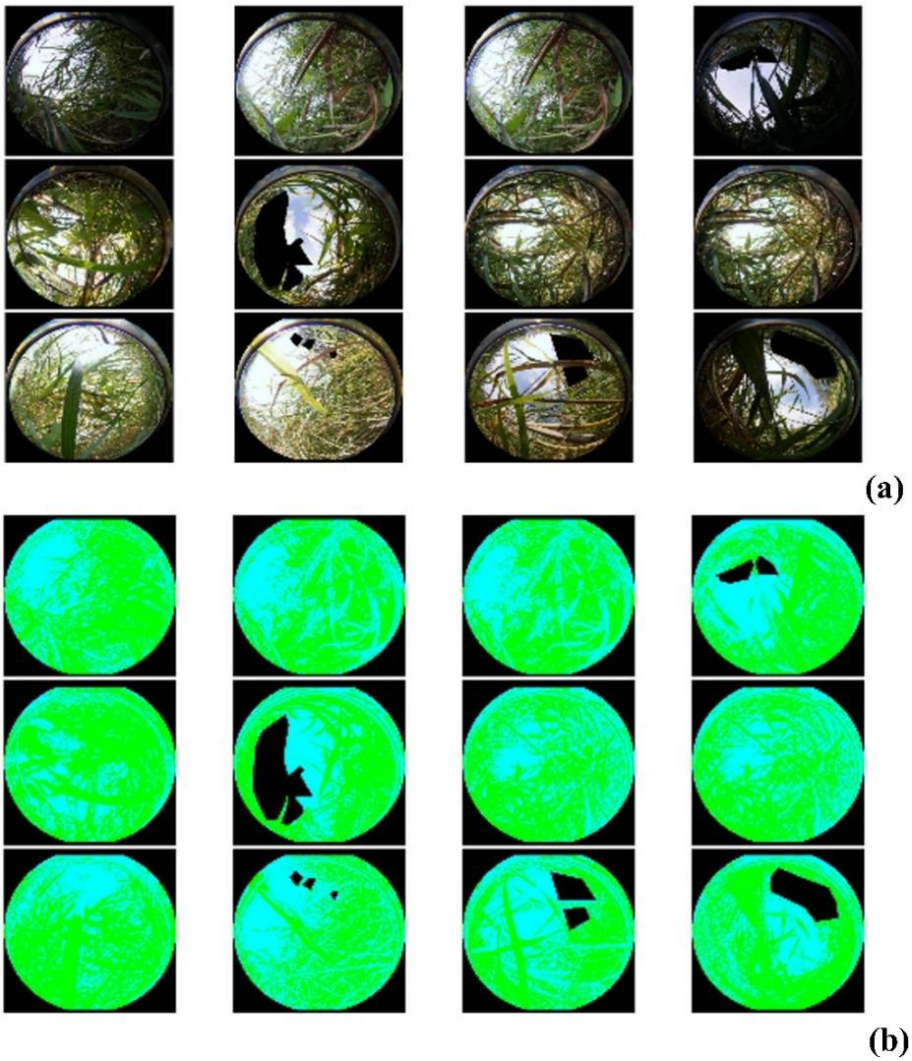

Fig. 13. Example of *DHPs* (a) masking and (b) binarization processes operated by CAN_EYE software *ESU* by *ESU*. The masks are indicated by the black shapes, while riparian vegetation and sky are indicated in soft green and soft blue, respectively.

The CAN_EYE software calculates *LAI* from the inversion of the gap fraction $P_0(\theta_v, \varphi_v)$, expressed by the following equation (*Weiss et al., 2004*):

$$P_0(\theta_i, \varphi_i) = e^{-G(\theta_i,\varphi_i)LAI/cos\theta_i}, \quad (3.2)$$

where $P_0(\theta_i, \varphi_i)$ is the gap fraction - or probability for having no contact between sunrays and leaves - θ_i and φ_i are respectively the zenith and azimuth angles of the incident light beam penetrating inside the canopy, $G(\theta_i, \varphi_i)$ is the mean projection of the leaf area per unit surface in a plane perpendicular to the sunrays (*Jockheere et al., 2004*).

The software inverts Equation 3.2 according to two different assumptions on leaf average orientation (*Weiss & Baret, 2016*), corresponding to two different *LAI* values, indicated as C_1 and C_2. For C_1, the Average Leaf Inclination angle (*ALA*), defined as the averaged angle between the zenith and the normal to the leaf surface, is assumed to be contained in the range 60° ± 30°. Instead, C_2 is based on a view angle of 57°, with no limitations for *ALA* values (*Ross, 1981; Chen et al., 1997*). This latter calculation is possible only when $COI \geq 60°$.

References

Aberle, J., Järvelä, J. 2013. Flow resistance of emergent rigid and flexible floodplain vegetation. J. Hydraul. Res. 51(1), pp. 33-45. https://doi.org/10.1080/00221686.2012.754795.

Al Mamun Hossain, S.A., Wang, L., Chen, T., Li, Z. 2017. Leaf area index assessment for tomato and cucumber growing period under different water treatments, 6(10), pp. 461-467. https://doi.org/10.17221/568/2017-PSE.

Archontoulis, S.V., Yin, X., Vos, J., Danalatos, N.G., Struik, P.C. 2012. Leaf photosynthesis and respiration of three bioenergy crops in relation to temperature and leaf nitrogen: How conserved are biochemical model parameters among crop species? Journal of Experimental Botany, 63(2), pp. 895-911. https://doi.org/10.1093/jxb/err321.

Bai, Z., Mao, S., Han, Y., Feng, L., Wang, G., Yang, B., Zhi, X., Fan, Z., Lei, Y., Du, W., Li, Y. 2016. Study on Light Interception and Biomass Production of Different Cotton Cultivars. PLoS ONE 11(5): e0156335. doi:10.1371/journal.pone.0156335.

Breda, N.J.J. 2003. Ground-based measurements of leaf area index: a review of methods, instruments and current controversies. Journal of Experimental Botany, 54(39), pp. 2403-2417. https://doi.org/10.1093/jxb/erg263.

Chen, J.M., Rich, P.M., Gower, J.M., Norman, S.T., Plummer, S.P. 1997. Leaf area index of boreal forests: Theory, techniques, and measurement. Atmospheres, 102(D24), pp. 29429-29443. https://doi.org/10.1029/97JD01107.

Chianucci, F., Ferrara, C., Pollastrini, M., Corona, P. 2015. Development of digital photographic approaches to assess leaf traits in broadleaf tree species. Ecological Indicators, 106, 105547. https://doi.org/10.1016/j.ecolind.2019.105547.

Chirico, G.B., Pelosi, A., De Michele, C., Falanga Bolognesi, S., D'Urso, G. 2018. Forecasting potential evapotranspiration by combining numerical weather predictions and visible and near-infrared satellite images: an application in southern Italy. The Journal of Agricultural Science, pp. 1-9. https://doi.org/10.1017/S0021859618000084.

Djaman, K., Irmak, S., Rathje, W.R., Martin D.L, Eisenhauer, D.E. 2013. Maize evapotranspiration, yield production functions, biomass, grain yield, harvest index, and yield response factors under full and limited irrigation. Transactions of the ASABE, 56(2), pp. 273-293.

Fang, H., Ye, Y.C., Liu, W.W., Wei, S.S., Ma, L. 2018. Continuous estimation of canopy leaf area index (LAI) and clumping index over broadleaf crop fields: an investigation of the PASTIS-57 instrument and smartphone applications. Agricultural and Forest Meteorology, 253, pp. 48-61. https://doi.org/10.1016/j.agrformet.2018.02.003.

Fang, H., Baret, Plummer, S., Schaepman-Strub, G. 2019. An Overview of Global Leaf Area Index (LAI): Methods, Products, Validation, and Applications. 57(3), pp. 739-799. Reviews of Geophysics. https://doi.org/10.1029/2018RG000608.

Garrigues, S., Lacaze, R., Baret, F., Morisette, J.T., Weiss, M., Nickeson, J.E., Fernandes, R., Plummer, S., Shabanov, N.V., Myneni, R.B., Knyazikhin, Y., Yang, W. 2008.

Validation and intercomparison of global Leaf Area Index products derived from remote sensing data. Journal of Geophysical Research, 113, G02028. https://doi.org/10.1029/2007JG00063.

Guangjian, Y., Ronghaia, H., Jinghui, L., Weiss, M., Hailan, J., Xihan, M., Donghui, X., Wuming, Z. 2019. Review of indirect optical measurements of leaf area index: Recent advances, challenges, and perspectives. Agricultural and Forest Meteorology, 265, pp. 390-411. https://doi.org/10.1016/j.agrformet.2018.11.033.

Hedley, J.D., Russell, B.J., Randolph, K., Pérez-Castro, M.Á., Vásquez-Elizondo, R.M., Enríquez, S., Dierssen, H.M. 2017. Remote Sensing of Seagrass Leaf Area Index and Species: The Capability of a Model Inversion Method Assessed by Sensitivity Analysis and Hyperspectral Data of Florida Bay. Frontiers in Marine Science, 4, 326. https://doi.org/10.3389/fmars.2017.00362.

Jonckheere, I., Fleck, S., Nackaerts, K., Muys, B., Coppin, P., Weiss, M., Baret, F. 2004. Review of methods for in situ leaf area index determination Part I. Theories, sensors and hemispherical photography. https://doi.org/10.1016/j.agrformet.2003.08.027.

Liu, J., Wang, T., Skidmore, A.K., Jones, S., Heurich, M., Beudert, B., Premier, J. 2019. Comparison of terrestrial LiDAR and digital hemispherical photography for estimating leaf angle distribution in European broadleaf beech forest. ISPRS Journal of Photogrammetry and Remote Sensing, 158, pp. 76-89. https://doi.org/10.1016/j.isprsjprs.2019.09.015.

Liu, Z., Jin, G., Zhou, M. 2015. Evaluation and correction of optically derived leaf area index in different temperate forests. iForest - Biogeosciences and Forestry, 9, pp. 55-62. https://doi.org/10.3832/ifor1350-008.

Loffredo, N., Sun, X., Onda, Y. DHPT 1.0: New software for automatic analysis of canopy closure from under-exposed and over-exposed digital hemispherical photographs. Computers and Electronics in Agriculture, 125, pp. 39-47. http://dx.doi.org/10.1016/j.compag.2016.04.028.

Lopez-Lozano, R., Casterad, M.A. 2013. Comparison of different protocols for indirect measurement of leaf area index with ceptometers in vertically trained vineyards. Australian Journal of Grape and Wine Research, 19, pp. 116-122. https://doi.org/10.1111/ajgw.12005.

Majasalmi, T., Rautiainen, M., Stenberg, P., Lukeš, P. 2013. An assessment of ground reference methods for estimating LAI of boreal forests. Forest Ecology and Management, 292, pp. 10-18. http://dx.doi.org/10.1016/j.foreco.2012.12.017.

Morisette, J.T., Baret, F., Privette, J.L., Myneni, R.B., Nickeson, J.E., Garrigues, S., Shabanov, N.V., Weiss, M., Fernandes, R.A., Leblanc, S.G., Kalacska, M., Sánchez-Azofeifa, G.A.,Chubey, M., Rivard, B., Stenberg, P., Rautiainen, M., Voipio, P., Manninen, T., Pilant, A.N., Lewis, T.E., Iiames, J.S., Colombo, R., Meroni, M., Busetto, L., Cohen, W.B., Turner, D.P., Warner, E.D., Petersen, G.W., Seufert, G., Cook, R. 2006. Validation of Global Moderate-Resolution LAI Products: A Framework Proposed Within the CEOS Land Product Validation Subgroup. IEEE Transactions on Geoscience and Remote Sensing, 44(7).

Pelosi, A., Medina, H., Villani, P., D'Urso, G., Chirico, G.B. 2016. Probabilistic forecasting of reference evapotranspiration with a limited area ensemble prediction system. Agricultural Water Management, 178, pp. 106-118. https://doi.org/10.1016/j.agwat.2016.09.015.

Rautiainen, M., Stenberg, P., Nilson, T., Kuusk, A. 2004. The effect of crown shape on the reflectance of coniferous stands. Remote Sensing of Environment, 89, pp. 41-52. https://doi.org/10.1016/j.rse.2003.10.001.

Saulino, L., Allevato, E., Todaro, L., Rossi, S., Bonanomi, G., Saracino, A. 2019. Comparative study of hybrid and wild black poplar genotypes in the first three-year cycle of multi-stem short-rotation coppice. Biomass and Bioenergy, 122, pp. 17-27. https://doi.org/10.1016/j.biombioe.2019.01.001.

Sonnentag, O., Talbot, J., Chen, J.M., Roulet, N.T. 2007. Using direct and indirect measurements of leaf area index to characterize the shrub canopy in an ombrotrophic peatland. Agricultural and Forest Meteorology, 144, pp. 200-212.

Västilä, K., Järvelä, J. 2014. Modeling the flow resistance of woody vegetation using physically based properties of the foliage and stem. Water Resour. Res. 4, 50, pp. 229-245. https://doi.org/10.1002/2013WR13819.

Vitale, L., Di Tommasi, P., D'Urso, G., Magliulo, V. 2016. The response of ecosystem carbon fluxes to LAI and environmental drivers in a maize crop grown in two contrasting seasons. International journal of biometeorology, 60(3), pp. 411-420.

Watson, D.J., 1947. Comparative physiological studies in the growth of field crops. I: Variation in net assimilation rate and leaf area between species and varieties, and within and between years. Ann. Bot., 11, pp. 41-76. www.jstor.org/stable/42907023.

Weiss, M., Baret, F. 2016. Can_eye V6.4.6 User Manual. EMMAH (Mediterranean Environment and Agro-Hydro System Modelisation) Laboratory. French National Institute of Agricultural Research (INRA).

Weiss, M., Baret, F., Smith, G.J., Jonckheere, I., Coppin, P. 2004. Review of methods for in situ leaf area index determination Part II: Estimation of LAI, errors and sampling. Agricultural and Forest Meteorology, 121, pp. 37-53. https://doi:10.1016/j.agrformet.2003.08.001.

4. Measurement of flow dynamic characteristics in vegetated open channels

4.1. Acoustic Doppler velocimeter (ADV)

The experimental measurements of mean and turbulent flow features in vegetated and non-vegetated open channels (*Sukhodolova & Sukhodolov, 2012; Caroppi et al., 2019*; *Errico et al., 2019; Lama et al., 2020*) are usually carried out by employing the acoustic Doppler velocimetry (*ADV*) device (Fig. 15 and 16).

Fig. 15. *ADV* device. In Figure is reported the Vectrino II Profiler (*Nortek®, U.S.A.*).

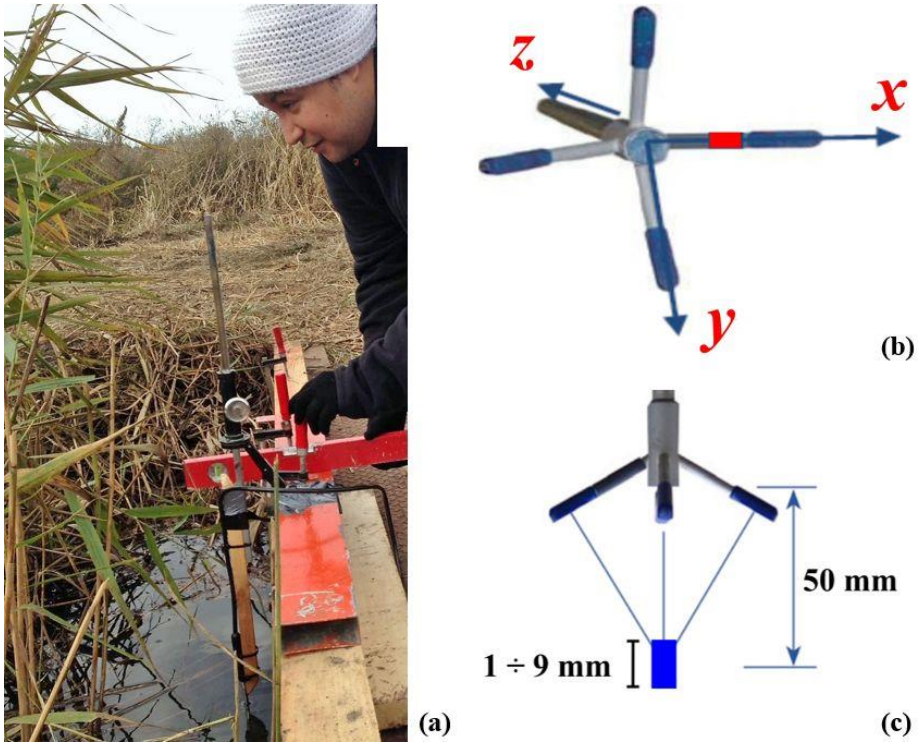

Fig. 16. (a) Experimental set-up for field-scale *ADV* measurements within a real vegetated reclamation channel. (b) *ADV* 4-beam downlooking probe with indicated the *x*, *y* and *z* axes, where *x* is the water flow (streamwise, *u*) direction, *y* is the direction transversal (spanwise, *v*) to the water flow direction and *z* is the vertical (*w*) direction. (c) 1 - 9 mm high sampling water volume, which center is located at 50 mm from the *ADV* probe (From

Vectrino II Profiler manual - Nortek®, U.S.A.)
ADV device is employed under different hydraulic and vegetative conditions (Fig. 16a). It is composed of one transmitter and four acoustic receivers (Fig. 16b), in order to intersect with the transmit beam pattern at a certain sampling volume (Fig. 16c). *ADV* measures velocity ta each receiver, combining them by considering the relative orientation of *x*,*y* and *z* axes, to calculate the 3D water velocity components (*u*, *v* and *w*). One of the most important elements to be taken into account in *ADV* measurements is represented by the probe orientation respect to the water flow main direction. In fact, as reported by Peltier et al., (2013), the misorientation of the probe can produce erroneous mean velocity and Reynolds stresses assessments.

4.2. ADV Data acquisitions

The first aspect strongly affecting the quality of *ADV* data is the so-called "velocity range setting", defining the highest value of velocity that can be measured. More in detail, the *ADV* device generates noise in velocity data (*McLelland & Nicholas, 2000*; *García et al., 2005*). This noise is directly proportional to the velocity range setting. Another source of noise is the so-called Doppler noise, characterized by a random distribution.
Moreover, *ADV* data are characterized by accuracy of ±0.5% as declared by the manufacturer. They are usually characterized using two parameters indicating the quality of the acquisitions (*Caroppi et al., 2018*; *Caroppi et al., 2019*): the signal averaged Correlation (*CORR*) and the Signal-to-Noise Ratio (*SNR*). The *CORR* represents the average correlation (in percentage) between the acoustic signals recorded by each pair of the *ADV* receivers. It theoretically ranges from 0% (records dominated by noise) to 100% (negligible noise in the records). As reported in the SonTek® Handled *ADV*® Technical manual (*SonTek, 2007*), the *SNR* measures the intensity of the received acoustic signal ($\text{amplitude}_{\text{Signal}}$) concerning the intensity of the ambient noise level ($\text{amplitude}_{\text{Noise}}$). It is usually measured in dB, and could be expressed as follows:

$$SNR = 20 \cdot log_{10}(\text{amplitude}_{\text{Signal}}/\text{amplitude}_{\text{Noise}}). \quad (4.1)$$

The *ADV* raw measurements must be pre-filtered by employing different techniques. In the study reported in Chapter 5, the WinADV freeware software was employed. It applies a phase-space threshold despiking method (*Goring & Nikora, 2002*) based on fixed threshold values of both *CORR* and *SNR* for each acquired *ADV* signal: *CORR* > 65% and *SNR* > 15 dB, to obtain a high-quality signal to be processed.

References

Caroppi, G., Gualtieri, P., Fontana, N., Giugni, M. 2018. Turbulence anisotropy at flow rigid vegetation interface. Geosciences 8(7), 259. https://doi.org/10.3390/geosciences8070259.

Caroppi, G., Västilä, K., Järvelä, J., Rowinski, P.M., Giugni, M. 2019. Turbulence at water-vegetation interface in open channel flow: experiments with natural-like plants. Adv. Water Resour. https://doi.org/10.1016/j.advwatres.2019.03.013.

Errico, A., Lama, G.F.C., Francalanci, S., Chirico, G.B., Solari L., Preti F. 2019. Flow dynamics and turbulence patterns in a reclamation channel colonized by *Phragmites australis* (common reed) under different scenarios of vegetation management. Ecol. Eng., 133, pp. 39-52. https://doi:10.1016/j.ecoleng.2019.04.016.

García, M.C., Cantero, I.M., Niño, Y., García, H.M., 2005. Turbulence Measurements with Acoustic Doppler Velocimeters. J. Hydraul. Eng., pp. 1062-1073. https://doi:10.1061/(ASCE)0733-9429(2005)131:12(1062).

Goring, D.G., Nikora, V.I. 2002. Despiking Acoustic Doppler Velocimeter Data. J. Hydraul. Eng. 128 (1), 117-126. https://doi.org/10.1061/(ASCE)0733-9429(2002)128:1(117).

Lama, G.F.C., Errico, A., Francalanci, S., Solari, L., Preti, F., Chirico, G.B. 2020. Evaluation of flow resistance models based on field experiments in a partly vegetated reclamation channel. Geosciences, 10(2), 47. https://doi.org/10.3390/geosciences10020047.

McLelland, S.J., Nicholas, A.P. 2000. A new method for evaluating errors in high-frequency ADV measurements. Hydrol. Process., 14, pp. 351-366. https://doi:10.1002/(SICI)1099-1085(20000215)14:2<351::AID-HYP963>3.0.CO;2-K.

Peltier, Y., Rivière, N., Proust, S., Mignot, E., Paquier, A., Shiono, K. 2013. Estimation of the error on the mean velocity and on the Reynolds stress due to a misoriented ADV probe in the horizontal plane: Case of experiments in a compound open-channel. Flow Meas. Instrum., 34, pp. 34-41. https://doi:10.1016/j.flowmeasinst.2013.08.002

Sukhodolova, T.A., Sukhodolov, A.N. 2012. Vegetated mixing layer around a finite-size patch of submerged plants: 1. Theory and field experiments. Water Resour. Res. 48 (10), pp. 1-16. https://doi.org/10.1029/2011WR011804.

5. Field experimental analysis of water flow dynamics and main turbulence features in an abandoned reclamation channel colonized by rigid emergent Common reed plants' stands.

The present Chapter is based on the following articles:

- Errico, A., **Lama**, **G**.**F**.**C**., Francalanci, S., Chirico, G.B., Solari, L., Preti, F. 2019. Flow dynamics and turbulence patterns in a drainage channel colonized by common reed (*Phragmites australis*) under different scenarios of vegetation management. Ecological Engineering, 133, pp. 39-52. https://doi:10.1016/j.ecoleng.2019.04.016.

- Errico, A., **Lama**, **G**.**F**.**C**., Francalanci, S., Chirico, G.B., Solari, L., Preti, F. 2019. Validation of global flow resistance models in two experimental drainage channels covered by *Phragmites australis* (common reed), in Proceedings of the 38th IAHR World Congress - Water Connecting the World, Panama City, Panama, pp. 1313-1321. https://doi:10.3850/38WC092019-1215.

5.1. Introduction

Reclamation channel networks are a widespread manmade component of lowland landscapes all over the world. In agricultural areas, their main role is to collect runoff and control the water table elevation, lowering it to improve crop root growth in soils with poor internal reclamation. In those areas affected by the phenomenon of urban sprawl, these elements play also the role of flood control, collecting rainwater coming from urbanized surfaces. The presence of water in reclamation channels enhances the growth of riparian vegetation both in-stream and on the banks. This vegetation contributes to creating a wetland habitat for many animal and plant species (*Szabo-Meszaros et al., 2018*). It also enhances the water quality, by reducing bank erosion and retaining suspended load (*Afzalimehr et al., 2011*; *Old et al., 2014*; *Verschoren et al., 2017*), providing growth substrate for the appearance of bio-films which supply to denitrification (*Soana et al., 2018*), removing nutrients (*Novotny & Chesters, 1981*; *Needelman et al., 2007*; *Giannini et al., 2017*) and producing oxygen (*Tabacchi et al., 1998*; *Dodds et al., 2017*). However, vegetation growth, if left uncontrolled, can lower the hydraulic conveyance of the channel, by increasing the global water flow resistance, and thus raise the risk of overflow and inundation of nearby land (*Aberle & Järvelä, 2013*; *Vargas-Luna et al., 2015*; *Chen & Chen, 2016*; *Pasquino et al., 2018*). The experimental survey of water flow dynamics in vegetated open channels at field scale provides some useful insights toward the identification of a balanced practice for managing riparian vegetation growth in vegetated reclamation channels so that effective land reclamation and hydraulic risk mitigation are achieved without negatively affecting the water quality.
The field experiments presented in this Chapter were designed with the specific objective to provide insights about the impact of different management strategies of Common reed management on velocity distribution, hydraulic roughness, and main turbulence features.

5.2. Materials and methods

5.2.1. Field vegetative and hydrodynamic measurements: Piaggetta reclamation channel

The field measurements were conducted in the Versilia - Massaciuccoli lowland, northern Tuscany, Italy. The study area (Fig. 17) is a natural depression delimited to the West by a dunal system and to the East by the Apuan Alps mountain chain. At the beginning of the 20th century, a reclamation plan was implemented in the area, aiming at recovering agricultural lands. Consequently, a complex reclamation network was built: reclamation channels have been dug across the fields, while the Massaciuccoli Lake and the natural streams have been delimited by levees.

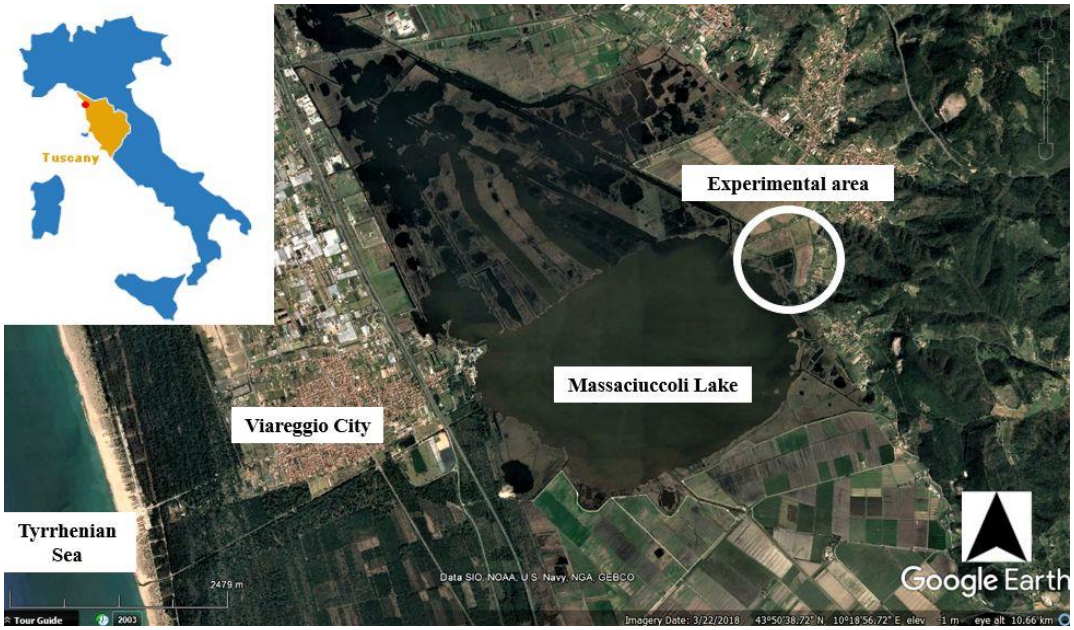

Fig. 17. Location of the experimental area.

The Versilia - Massaciuccoli lowland is now partly a protected area under the patronage of a Regional Natural Park. Fields are intensively cultivated with cereals, horticulture, and floriculture. The lake, that receives most of the water drained from the fields, is threatened by the risk of eutrophication, caused by the high load of Nitrogen and Phosphorus. For this reason, according to the classification introduced by the EU Nitrogen Directive (1991), the lake and the connected fields are designated as Nitrate Vulnerable Zones. The entire reclamation network is maintained by the Consorzio di Bonifica 1 Toscana Nord. The riparian and aquatic vegetation was removed from the banks and the bed twice per year, following the traditional management practice which points at maximizing the conveyance capacity of the network. However, in recent years part of the local stand was raising concerns about the impact of this traditional practice and was asking for the identification of maintenance practices that could preserve the key environmental function of vegetated water bodies. The field hydrodynamic and vegetative measurements were performed inside a vegetated reclamation channel named Piaggetta (Fig. 18), located nearby the Massaciuccoli Lake. It has a length of 500 m, an average width of 5 m and an average bankfull depth of 0.80 m.

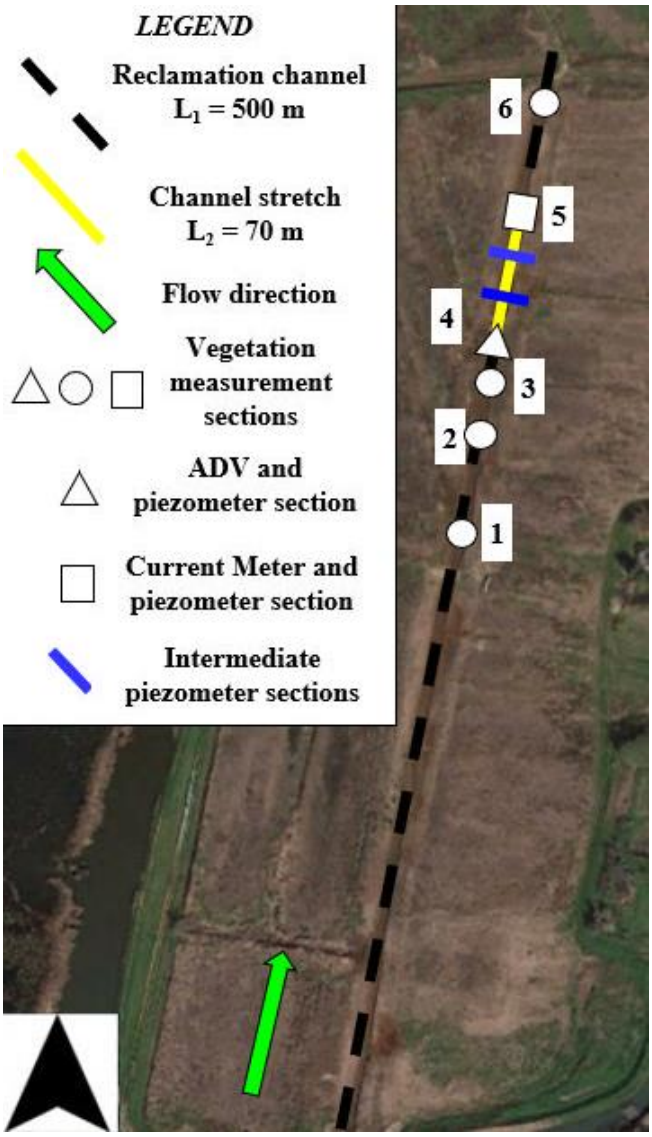

Fig. 18. Surveyed cross sections (1 - 6) along the 500 m long vegetated reclamation channel, indicated by the black dashed line. The experimental channel stretch is indicated by the continuous yellow line. The white circles indicate all the surveyed cross sections employed for the measurements of the vegetative morphometrical properties, while the white triangle and square represent the *ADV* and the Current Meter measuring cross sections, both equipped with field piezometers, respectively coinciding to the upstream (Section 4) and the downstream (Section 5) cross section of the 70 m long channel stretch. The continuous dark blue lines indicate the intermediate piezometers cross sections along the experimental stretch, located at approximately 23 m apart.

The Piaggetta vegetated reclamation channel was characterized by a slightly counter-slope bed (-0.3%). Thus, to guarantee an adequate water flow motion moving from the Massacciucoli lake, it was imposed and controlled inside the 500 m long channel by a pumping system during the field hydrodynamic experiments. The vegetated reclamation channel drains an area of 23 ha, annexed to a Regional Natural Park (Parco Regionale Migliarino - San Rossore - Massaciuccoli) and abandoned from cultivation for 5 years for rewilding purposes. The only recorded riparian species was *Phragmites australis (Cav.)*

Trin. ex Steud., covering 100% of the vegetated reclamation channel. It was characterized by a rife canopy, resulting from an undisturbed time-lapse of four vegetative seasons. The distances between pairs of adjacent cross sections were the following:

- *Cross section 1* - *Cross section 2*: 39 m;
- *Cross section 2* - *Cross section 3:* 28 m;
- *Cross section 3* - *Cross section 4*: 27 m;
- *Cross section 4* - *Cross section 5*: 70 m;
- *Cross section 5* - *Cross section 6*: 35 m.

The field hydrodynamic measurements and vegetative surveys were designed to characterize the hydraulic properties (cross sectional water flow velocity fields and hydraulic gradient), and the reed plant density and morphometrical properties (stems' average and height from the channel bottom). As indicated by Errico et al. (2019), to reduce the uncertainties during the field hydrodynamic measurements, the hydrodynamic analyses were restricted to a 70 m long experimental stretch (Fig. 18) of the 500 m long channel, since in this stretch the cross sections were almost uniform in shape. The vegetational measurements were taken along only half of the 500 m long channel because the other half was not easily accessible, due to the presence of gas pipes, hydraulic crossings and small bridges (Fig. 18 and Fig. 19).

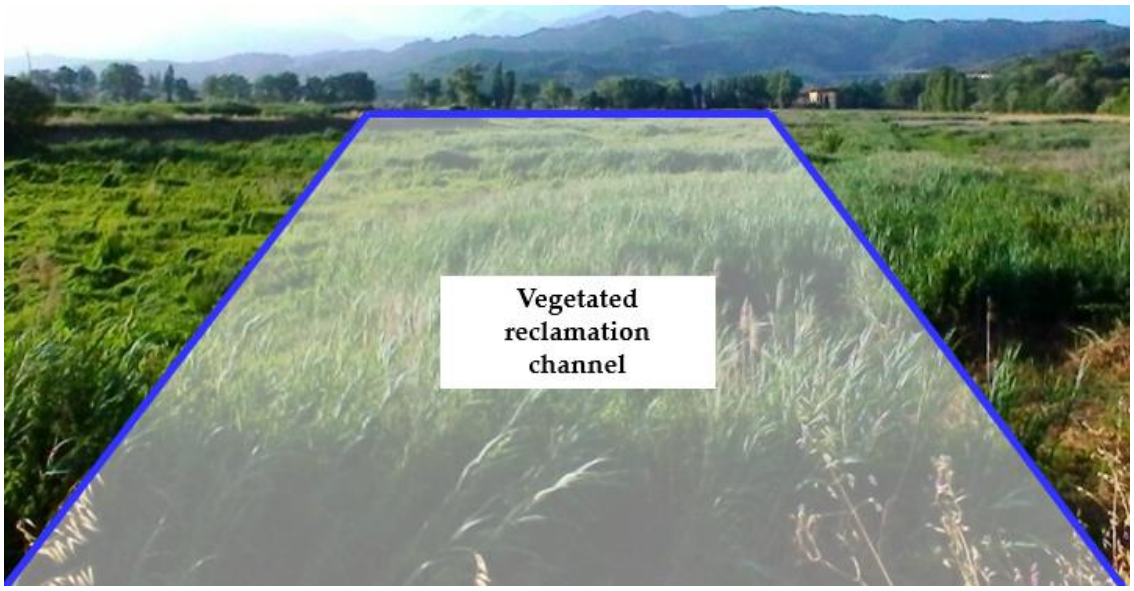

Fig. 19. View of the 500 m long vegetated reclamation channel. The continuous blue lines indicate the banks of the vegetated reclamation channel.

A detailed topographic survey of the examined cross sections was carried out by employing a topographic total station, georeferenced using fixed target points located in the surroundings of the experimental reclamation channel, characterized by a sub-centimetric precision rate (*Errico et al., 2019*; *Lama et al., 2020*).

5.2.2. Morphometrical properties of riparian vegetation and management scenarios

Field water flow measurements were carried out under three different riparian vegetation scenarios (Fig. 20a-c), to compare the impact of the different management practices on water flow characteristics:

1) Undisturbed riparian Vegetation (*UV*) along the entire examined vegetated reclamation channel (Fig. 20a);

2) Central Cut (*CC*), intended as an example of gentle management strategy, practiced by mechanically removing the riparian vegetation cover in the channel center for a width of 2.70 m, preserving two vegetated side buffers (Fig. 20b);

3) Extensive Cut (*EC*), obtained by mechanically removing the riparian vegetation along the entire reclamation channel (Fig. 20c).

(a)

(b)

(c)

Fig. 20. View of the three riparian vegetation management scenarios: (a) *UV*; (b) *CC*;

(c) *EC*.

The cutting operations were practiced utilizing an excavator equipped with cutting bucket, towed below the water surface. The machinery was not able to cut the reed stems at the channel bottom due to the excessive strain exerted by the very high hardness of stems at the base. After the cutting, residual sections of 0.15 - 0.20 m high riparian plant stems remained at the bottom of the examined vegetated reclamation channel (Fig. 21).

Fig. 21. Common reed rhizomes, with remaining 0.15 - 0.20 m high plant stems after the riparian vegetation maintenance operated by the mechanical cutting machinery.

Leaves and stems of the previous year have been not completely degraded, being the Common reed stand at undisturbed conditions for several years. Dead and fallen stems, rhizomes and leaves jams were still present within the vegetated water body, but they have been not monitored as most of this material was accumulated below the water surface and could not be detected due to high backwater turbidity. The Common reed plants were surveyed following a simple quadrant sampling methodology at six cross sections (Sections 1 - 6 in Fig. 2) along the vegetated reclamation channel. A wooden survey plots 1 m x 1 m was positioned at the bank edge and moved towards the opposite bank to survey the riparian vegetation parameters across the whole wetted perimeter, employing five sample plots. Stem number, stems' average diameter and heights were recorded within each sample plot, obtaining the distribution of the morphometrical properties along the wetted perimeters of the six measuring cross sections distributed along the reclamation channel (Fig. 22).

Fig. 22. Common reed stems surveyed using 1 m x 1 m woody plots at Section 4.

In Figure 23 is shown an example of the experimental set-up for the measurement of the morphometrical parameters of riparian vegetation at Section 4 for UV_1, obtained by employing the five survey plots 1 m x 1 m (S1 - S5).

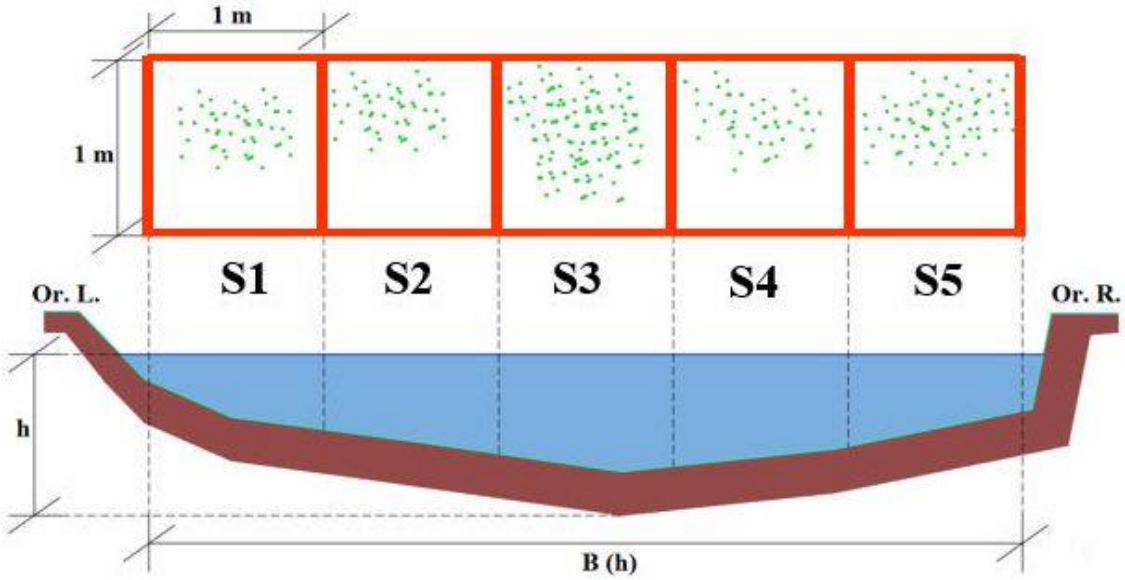

Fig. 23. Location of the five survey plots (S1 - S5) along the wetted perimeter of Section 4.

The values of the morphometrical parameters of riparian vegetation are summarized in the following Table 2, where *num*. is the total number of stems, *d* (m) is the stems' average diameter measured at 0.40 m from the reclamation channel bottom, *m* (m^{-2}) is the number

of plants per unit bed surface, also defined as riparian vegetation density, λ ($=\pi \cdot m \cdot d^2/4$) is the so-called areal vegetation density, a synthetic parameter employed for parametrizing the cross sectional distribution of stems, and h_v (m) is the average vegetation height from the examined channel bottom.

Tab. 2. Morphometrical riparian properties recorded at the six measuring cross sections: *num.* is the total number of stems in each cross section, *d* (m) is the stems' average diameter measured at 0.40 m from the channel bottom, *m* (m^{-2}) is the vegetation density, λ ($= \pi \cdot m \cdot d^2/4$) is the vegetation surface density, and h_v (m) is the average vegetation height from the channel bottom.

Section	num.	d (m)	m (m^{-2})	λ	h_v (m)
1	198	0.0062	47	0.00142	2.10
2	165	0.0065	39	0.00130	2.30
3	159	0.0065	38	0.00126	2.23
4	270	0.0054	54	0.00124	2.50
5	182	0.0069	43	0.00161	2.35
6	245	0.0055	58	0.00138	2.50

The cross sectional distributions of stems resulted to be very similar for all the six cross sections and thus it was assumed to be homogeneous along the entire reclamation channel.

5.2.3. Pumping system

The water was pumped through four mobile hydro-pumps regulated by the engines of four agricultural tractors, in order to obtain different water flow conditions within the experimental reach. The upstream end of the channel was placed in correspondence of the levee that separates the Massaciuccoli Lake from the surrounding fields, while the downstream end was placed where the channel underpasses a white road throughout an iron culvert, which was closed by a gate during the field experiments. Two tractors carrying mobile pumps were positioned on the top of the levee, taking the water from the lake and entering it into the channel. Two other pumps were placed at the downstream end, on the white road, to lift the water from the channel and discharge it into another channel located on the opposite side of the road. Discharges were controlled by regulating the rotation regime of each of the four pumps directly at the tractors' power outlets. No water losses were observed along the monitored channel stretch, guaranteeing the continuity of the discharges, which has also been double-checked by means of simultaneous discharge measurements at the upstream and downstream cross sections.
As shown in the next Table 4, the analyses of water flow dynamics were performed considering three different riparian vegetation management scenarios (*UV*, *CC*, and *EC*) for a total of six different discharges: UV_1, CC_1, CC_2, EC_1, EC_2 and EC_3. The pumping regimes at the inlet and outlet were adjusted aiming at ensuring the water flow steadiness

along the experimental channel reach. In detail, it was just possible running a single discharge (referred to experiment UV_1) for the Undisturbed Vegetation scenario because at the minimum pumping regime the bankfull level was already reached. Differently, for the Central Cut scenario it was possible investigating two values of discharge (referred to experiments CC_1 and CC_2), respectively corresponding to the minimum and maximum pumping regimes compatible with the topographical and mechanical constraints of the experimental setup and the bankfull level. Three values of discharges were examined (referred to experiments EC_1, EC_2, and EC_3) for the Extensive Cut scenario.

5.2.4. Water flow velocity measurements

The water flow velocity measurements were carried out by employing two steel footbridges placed in Section 4 and Section 5 for all three investigated riparian vegetation management scenarios. A 3-component *ADV* Vectrino II - Nortek® device equipped with a down-looking 4-beam probe was installed on a 6 m long wooden bar at the upstream steel footbridge. The down-looking 4-beam probe was oriented to identify the main water flow (streamwise) direction with the x axis of the *ADV* probe. Thus, y is the spanwise direction (positive leftwards) and z the vertical direction (positive upwards). The verticality and the appropriate alignment of *ADV* probe were addressed by employing a pair of three-dimensional bubble levels.

The water flow velocity measurements were carried out at five different vertical hydrometric lines ($ADV_{1\text{-}5}$), equally spaced from one channel bank to the other, by sliding the *ADV* probe on the 6 m long woody binary (Fig. 24a and Fig. 24b). The *ADV* was located at three different depths along each vertical, starting from 0.05 m below the water surface and moving to 0.17 and 0.27 m (in Fig. 24c, orange dots represent the *ADV* measuring positions, indicated as $A_{1\text{-}5}$, $B_{1\text{-}5}$ and $C_{1\text{-}5}$). It was not possible to have *ADV* measurements below the depth of 0.27 m from the water surface, due to the presence of dead material on the channel bottom. A propeller-type OTT® C31 Universal Current Meter (Fig. 25b and Fig. 25d) was employed for obtaining a second discharge estimation at the downstream cross section, corresponding to the stretch end, and to check for water mass losses. In this case, the water flow velocity measurements were taken along three vertical hydrometric lines equally spaced within the reclamation channel ($CM_{1\text{-}3}$) at three different depths, by keeping a vertical spacing of 10 cm (in Fig. 24d, orange dots represent the Current Meter locations, indicated as $D_{1\text{-}3}$, $E_{1\text{-}3}$ and $F_{1\text{-}3}$). The *ADV* measurement depths from the water surface were maintained fixed for all the cases, regardless of the water level recorded for the three riparian vegetation management scenarios. The water flow was considered steady when the water level in each of them was stable for a time interval of 30 minutes, with an accepted residual of ±0.01 m.

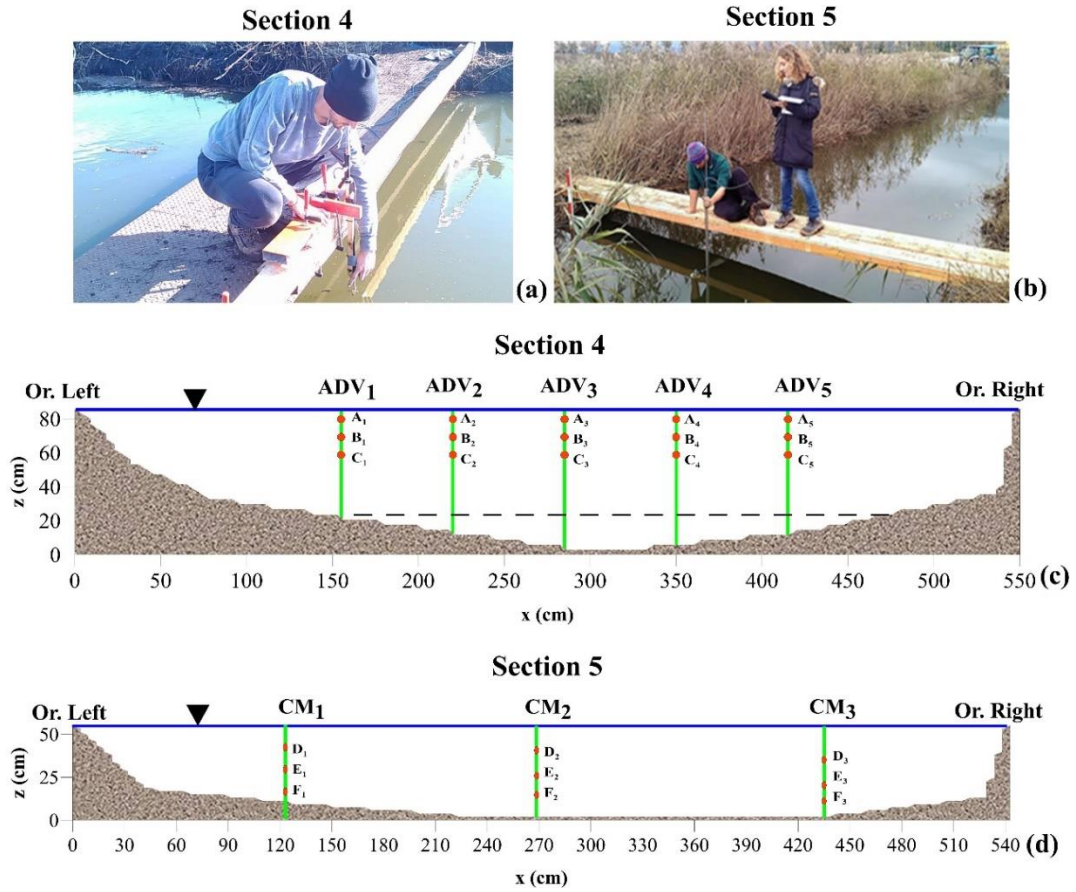

Fig. 24. Scheme of water flow velocity measurements at reclamation channel's Section 4 (a) and Section 5 (b) for *EC* riparian vegetation management scenario, respectively coinciding with the upstream and downstream cross sections of the experimental channels stretch. For both *ADV* (c) and Current Meter (d) measurements, the water level is indicated with the horizontal dark blue continuous line. The investigated vertical hydrometric lines are indicated with green continuous lines, while the measuring points with orange dots. The horizontal black dashed line indicates the top of the submerged rhizomes.

The discharge values were assessed by linear interpolation of the local water flow velocities measured at Sections 4 and Section 5 of the experimental channel stretch. The discharge values referred to the two cross sections were comparable (relative differences lower than 12.5%), thus confirming that no significant deep or lateral water losses occurred along the monitored reclamation channel stretch during the field experiments. The *ADV* measurements were carried out by choosing an acquisition frequency equal to 100 Hz, for a time interval of 3 min at each of the 15 measuring points. Consequently, the whole measurements lasted 45 min in total, under a condition of stable water profile for each examined discharge.

The *ADV* raw measurements were filtered by employing the WinADV freeware software, which applies a phase-space threshold despiking method (*Goring & Nikora, 2002*) based on fixed threshold values of *CORR* and *SNR* for each acquired *ADV* signal: *CORR* > 65% and *SNR* > 15 dB, aiming at obtaining a high-quality signal to be processed. The values

of discharges, average *CORR* and *SNR* of all the examined measuring points for each experiment are summarized in the following Table 3:

Tab. 3. Phase-space despiking method analysis based on fixed threshold values of *CORR* (%) and *SNR* (dB): *CORR* > 65% and *SNR* > 15 dB.

Experiment	Discharge ($m^3 \cdot s^{-1}$)	CORR (%)	SNR (dB)
UV_1	0.126	78.88	37.26
CC_1	0.164	82.93	38.05
CC_2	0.335	80.40	55.77
EC_1	0.086	85.69	38.27
EC_2	0.175	85.30	40.45
EC_3	0.277	86.05	53.27

5.2.5. Measured Manning's n hydraulic roughness coefficients: $n_{,meas}$

The measured (or experimental) Manning's hydraulic roughness coefficients n ($s \cdot m^{-1/3}$), hereinafter indicated as $n_{,meas}$, were estimated under the hypothesis of gradually-varied steady water flow conditions (e.g., *Kirby et al., 2005*; *Rhee et al., 2008*; *Errico et al., 2018).* The average measured Manning's *n* hydraulic roughness coefficients for the entire experimental channel stretch were calculated by applying the well-known "Energy Equation" to upstream (Section 4) and downstream (Section 5) cross sections for each experimental discharge regime:

$$n_{,meas} = \frac{J^{\frac{1}{2}} \cdot R^{\frac{2}{3}}}{U}, \tag{5.2}$$

where R (m) and U ($m \cdot s^{-1}$) are respectively the average hydraulic radius and the water flow average velocity, and J is the slope of the total energy line, calculated as the slope of the water table retrieved from the water level measurements performed at the piezometers located at Section 4 and Section 5. The values of these parameters for *UV* and *CC* riparian vegetation management scenarios are reported in the following Table 4.

5.2.6. Measured Chézy's C_r water flow resistance coefficients: $C_{r,\,meas}$

The measured vegetative Chézy's water flow resistance coefficients C_r ($m^{1/2} \cdot s^{-1}$) for the six experimental discharges, hereinafter referred to as $C_{r,meas}$, were calculated according to the following expression, under the assumptions of uniform water flow in the examined vegetated reclamation channel:

$$C_{r,meas} = \frac{U}{\sqrt{R \cdot J}}. \tag{5.3}$$

As reported in the previous paragraph, J, already defined as the slope of the total energy line, was estimated as the slope of the water table, obtained from the water level

measurements realized at the piezometers located at Section 4 and Section 5.

5.3. Results

5.3.1. Riparian vegetation management scenarios and water flow velocity

The three similar discharges UV_1, CC_1 and EC_2 were compared to better highlight the differences in the cross sectional distributions of the average streamwise velocity and main turbulence parameters, obtained by means of a linear interpolation of the local measurements carried out at Section 4. The hydraulic and geometric characteristics of the quasi-steady sub-critical water flow developed during the field hydrodynamic experiments performed inside the examined reclamation channel stretch are summarized in the following Table 4.

Tab. 4. Hydraulic and geometric features for all the three investigated riparian vegetation management scenarios in the examined reclamation channel: σ (m^2) is the water flow cross sectional area; U ($m \cdot s^{-1}$) is the water flow average velocity; R (m) is the hydraulic radius; h (m) is the water level; J is the slope of the total energy line, while $n_{,meas}$ ($s \cdot m^{-1/3}$) and $C_{r,meas}$ ($m^{1/2} \cdot s^{-1}$) are respectively the measured Manning's n hydraulic roughness coefficient and vegetative Chézy water flow resistance coefficients.

Exp.	**Dis.** ($m^3 \cdot s^{-1}$)	**σ** (m^2)	**U** ($m \cdot s^{-1}$)	**R** (m)	**h** (m)	**J**	**$n_{,meas}$** ($s \cdot m^{-1/3}$)	**$C_{r,meas}$** ($m^{1/2} \cdot s^{-1}$)
UV_1	0.126	78.88	0.035	0.57	0.68	0.0019	0.49	1.09
CC_1	0.164	82.93	0.051	0.53	0.71	0.0003	0.27	4.31
EC_2	0.175	85.30	0.049	0.58	0.72	0.0006	0.30	3.05

From the analysis of Table 4, it can be noticed that the highest values of C_r were observed for the experiment CC_1, characterized by the presence of side buffers riparian vegetation at the reclamation channel banks.

Aiming at defining the flow dynamics of vegetated channels at field scale, streamwise velocity and turbulence features were analyzed in this study. As reported in previous field-scale studies (*Sukhodolova, 2008*; *Hopkinson & Wynn, 2009*; *Rominger & Nepf, 2011*; *Liu et al., 2017*; *Errico et al., 2018*), the presence of riparian vegetation strongly modifies the average streamwise velocity fields, computed by separating the instantaneous velocity fluctuation (u', v' and w') from the mean velocity ($\bar{u}$, $\bar{v}$ and $\bar{w}$) for each velocity component along x, y and z axes. In order to obtain the contour plots, the measuring grid composed by the original 15 measuring points distributed along five vertical hydrometric lines (see Fig. 24c) was integrated with an additional list of points. For streamwise velocity measurements, they were set equal to zero at all the points corresponding to the wetted perimeter. Then, at all the points located at the water surface were assigned the same value of parameters measured at the measuring points located at

0.05 m below it. All the remaining values were obtained by triangular linear interpolation by employing a mesh composed of 30 rows x 120 columns.

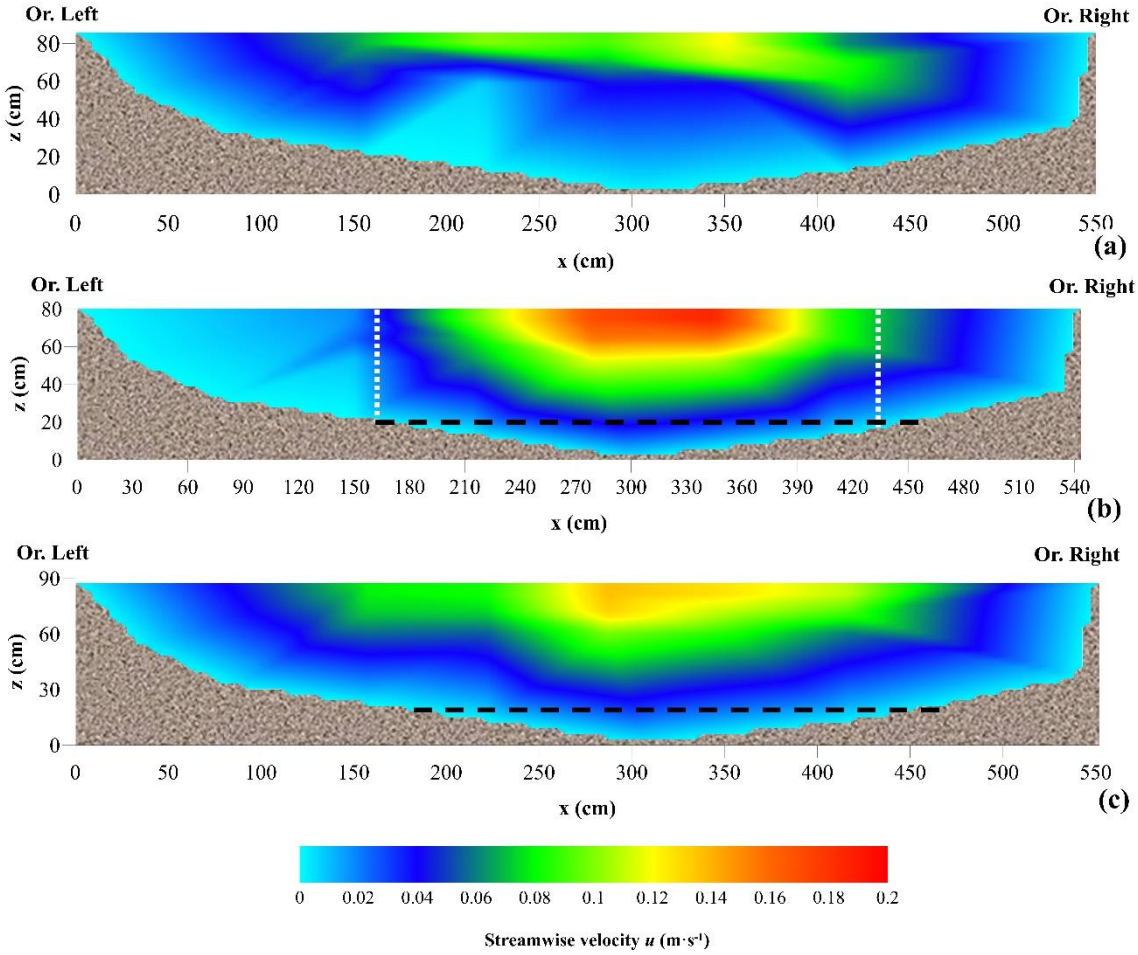

Fig. 25. Streamwise velocity u (m·s^{-1}) fields at Section 4, respectively referred to (a) UV_1 (b) CC_1, and (c) EC_2. The vertical white dashed lines indicate the limits of the side vegetation buffers for CC_1, while the horizontal black dashed line indicates the top of the submerged rhizomes.

The three riparian vegetation management scenarios were characterized by different streamwise velocity patterns. Due to the presence of vegetation, the water flow cross sectional field was highly irregular in UV_1 (Fig. 25a). The effect of the undisturbed riparian vegetation side buffers in CC_1 was such to concentrate the water flow in the reclamation channel center (Fig. 25b), where there was no influence of the emergent reed stems. The water flow velocity in the bank region was negligible, compared with the previous riparian vegetation management scenario. As expected, a regular water flow field was recognizable from the cross sectional streamwise velocity contour plot in EC_2 (Fig. 25c). The peak streamwise velocity values highly change from one scenario to the other: in UV_1 (Fig. 25a), the streamwise velocity at the surface reached a peak value equal to approximately 0.10 m·s^{-1} in correspondence of ADV_1 and ADV_5 vertical hydrometric lines. In CC_1 (Fig. 25b), this value was doubled to 0.20 m·s^{-1} at the cross section center. This was due to the blockage effect that the riparian vegetation side buffers exerted on

approximately 50% of the entire cross section. In *EC₂* (Fig. 25c) the peak was reduced by 30% compared with *CC₁*, remaining located at the cross section center, with higher values also on the sides free from riparian vegetation cover.

5.3.2. Main turbulence features

Reynolds shear stress per unit mass in the *x*-*z* plan τ'_{xz}/ρ, where ρ (kg·m^{-3}) is the water density, equal to 1000 kg·m^{-3}, representing the vertical flux of longitudinal momentum (i.e.,, *Lu & Willmarth, 1973*; *Nakagawa & Nezu, 1977*), were calculated as follows:

$$\tau'_{xz}/\rho = -\overline{u' \cdot w'}. \quad (5.4)$$

Different scales were employed in Figures 26a-c for representing the τ'_{xz}/ρ values, due to the large variability in the peak values from one riparian vegetation scenario to another.

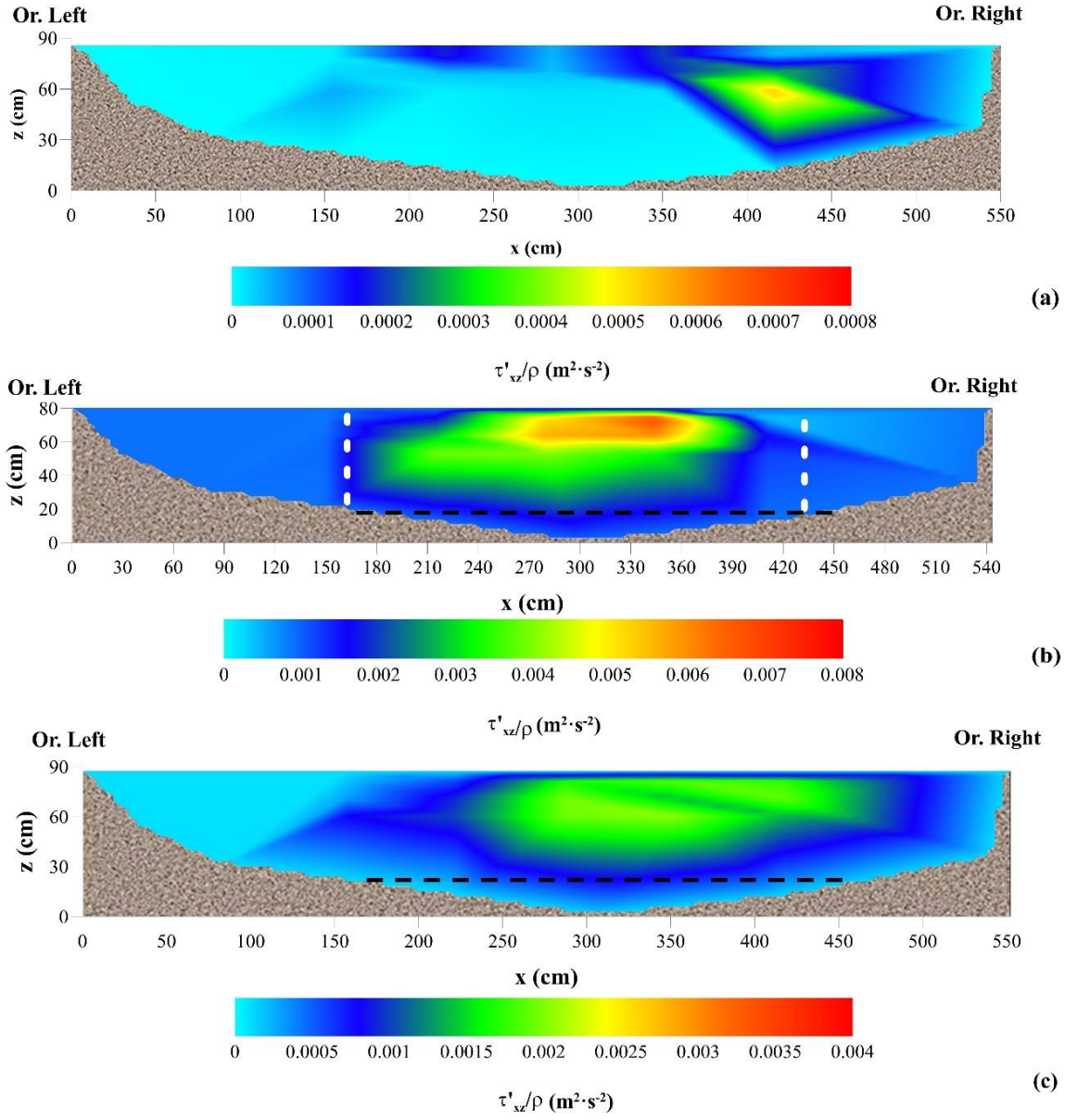

Fig. 26. Reynolds shear stress per unit mass τ'_{xz}/ρ (m^2·s^{-2}) fields at Section 4, referred

to (a) *UV₁* (b) *CC₁*, and (c) *EC₂*. The vertical white dashed lines indicate the limits of the side vegetation buffers for *CC₁*. The horizontal black dashed line indicates the top of the submerged rhizomes.

For *UV₁*, the lateral τ'_{xz}/ρ gradients on the orographic right bank were steeper than on the left one (Fig. 26a). The τ'_{xz}/ρ peak value of 0.0005 $m^2 \cdot s^{-2}$ was reached at approximately 1.40 m from the orographic right bank. In *CC₁* the water flow was concentrated essentially in the cross section center, characterized by the complete absence of riparian vegetation (Fig. 26b). The τ'_{xz}/ρ peak value was equal to 0.007 $m^2 \cdot s^{-2}$, which was about 18 times higher than the one referred to *UV₁*. For concluding, the τ'_{xz}/ρ peak for *EC₂* was equal to 0.002 $m^2 \cdot s^{-2}$; it was located at the cross section center (Fig. 26c).
The Turbulent Kinetic Energy (*Pope, 2000*; *Poggi et al., 2004*; *Nezu & Sanjou, 2008*; *Dei et al., 2011*) was calculated as follows:

$$TKE = \frac{1}{2} \cdot \left(\overline{u'^2} + \overline{v'^2} + \overline{w'^2}\right). \quad (5.5)$$

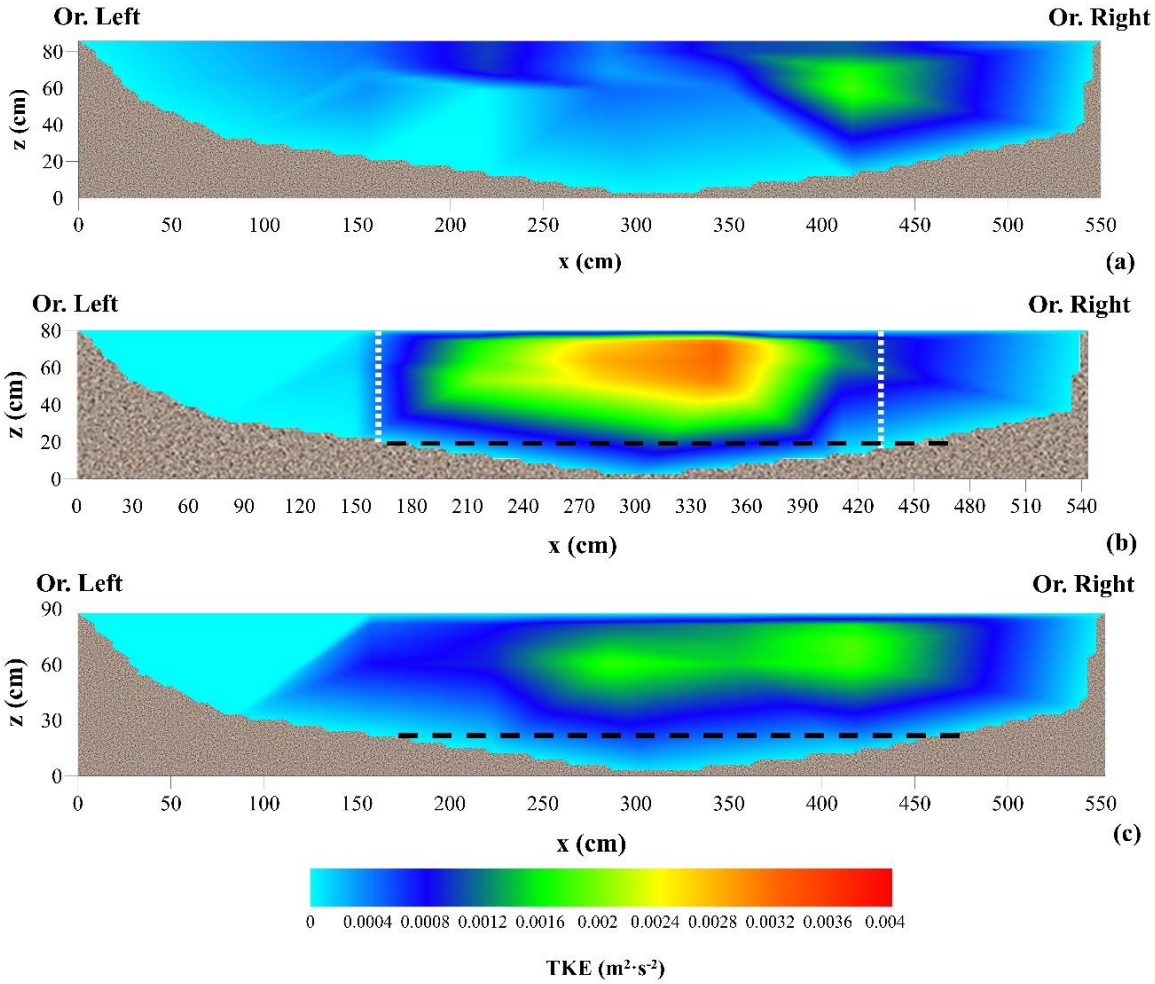

Fig. 27. Turbulent Kinetic Energy *TKE* ($m^2 \cdot s^{-2}$) fields at Section 4, respectively referred to (a) *UV₁* (b) *CC₁*, and (c) *EC₂*. The vertical white dashed lines indicate the limits of the side vegetation buffers for *CC₁*, while the horizontal black dashed line indicates the top of the submerged rhizomes.

In *UV₁*, *TKE* displays the same behaviour exhibited by τ'_{xz}/ρ, with the only difference that, in this case, the gradients on the orographic right bank were steeper than for τ'_{xz}/ρ. The *TKE* peak value was equal to 0.002 $m^2 \cdot s^{-2}$ (Fig. 27a), located at approximately 1 m from the orographic right bank, while it reached a peak value of 0.001 $m^2 \cdot s^{-2}$ at the opposite side. For *CC₁*, the *TKE* peak value doubled to 0.004 $m^2 \cdot s^{-2}$ at 2 m from the orographic right bank (Fig. 27b). In the end, in the *EC₂* (Fig. 27c), the *TKE* peak equal to 0.002 $m^2 \cdot s^{-2}$ was located at the cross section center and at the orographic right bank.

5.3.3. Measured Manning's n hydraulic roughness coefficients: $n_{,meas}$

The measured Manning's *n* hydraulic roughness coefficients were obtained for each investigated discharge (Table 3). The computed values could be considered as "equivalent" Manning's *n* hydraulic roughness coefficients as they represent the global water flow resistance value of the experimental reach obtained without considering any partitioning of the wetted perimeter due to different riparian vegetation cover. For Piaggetta reclamation channel, the values of the Manning's *n* ranged between 0.129 and 0.495 $s \cdot m^{-1/3}$, with the maximum value observed for *UV₁*, characterized by the presence of an emergent reed canopy over the entire reach; the minimum values were observed for *CC₂* and *EC₃*, corresponding to the highest discharges. The Manning's *n* hydraulic roughness coefficients slightly decreased with increasing discharges, both in the *CC* and *EC* scenarios, despite the conditions changed from emergent riparian vegetation to submerged plant stalks of 0.20 m in height. Given the values of stem density and diameter, which can be referred to as "sparse" vegetation according to the classification proposed by Yang et al. (2016), all the Manning's *n* values were significantly higher than expected. The channel substrate was observed to be very smooth, composed of peat and silt. Therefore, for all the scenarios, the water flow resistance had to be related to the presence of disturbances other than just the stems and the reclamation channel bottom. Most of the water flow resistance might be related to dead stems, rhizomes and leaves, due to the relatively low density of the living stems.

5.4. Discussion

5.4.2. Effects of riparian vegetation management on the Manning's n hydraulic roughness coefficients: $n_{,meas}$

As expected, the experimental Manning's *n* hydraulic roughness coefficients $n_{,meas}$ resulted to be strongly related to the discharge, rather than to changes in the three riparian vegetation management scenarios. In the *CC* and *EC* scenarios, their values decreased for increasing discharges (Fig. 28), suggesting that the remnant vegetative dead material acted as a submerged layer of rigid riparian vegetation.

The upper stems, bare and sparse, had a small influence in terms of global water flow resistance at reach scale, and this explains why the differences between before- and after-cut scenarios resulted to be so small. Nikora et al. (2008), within a variety of different vegetation patterns, investigated the hydraulic roughness related to the presence of

remnant plant stalks, observing that their global water flow resistance followed the same pattern of undisturbed riparian vegetation scenario, due to the partial cross section blockage. However, when these were sparse, their effect was found to be small with respect to the vegetation scenario before cutting. Indeed, Nikora et al. (2008) observed low global water flow resistances for remnant plant stalks. The difference with the present study lied in the presence of clogging material.

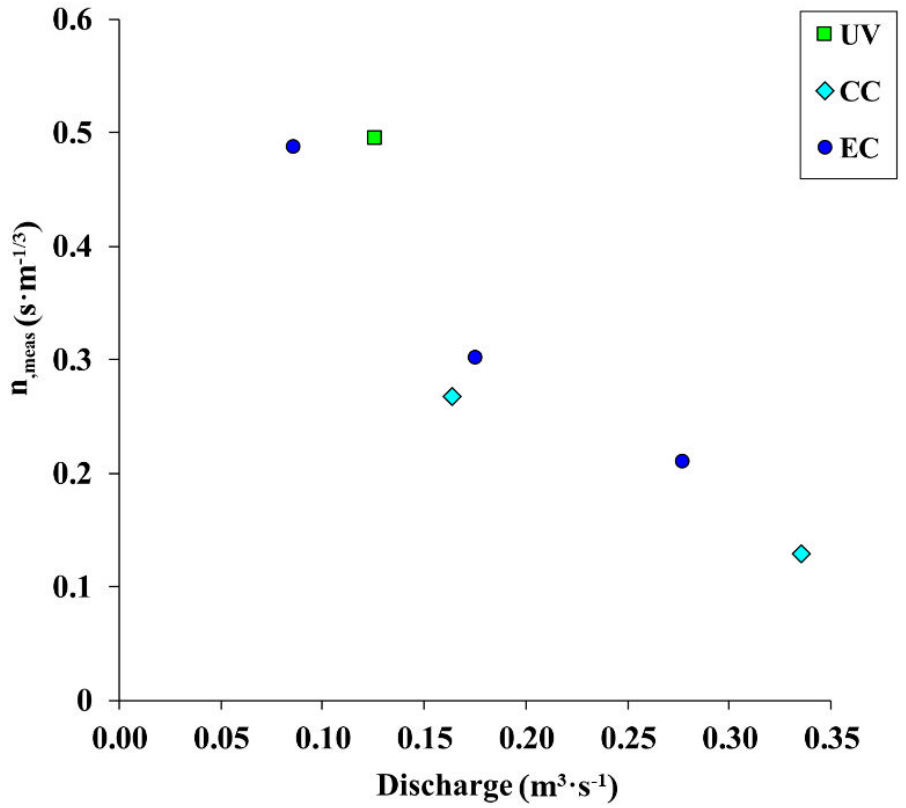

Fig. 28. Discharge *vs*, $n_{,meas}$ for *UV* (green squares), *CC* (soft blue diamonds) and *EC* (dark blue circles) riparian vegetation management scenarios.

In a previous experimental study, Errico et al. (2018) obtained significantly lower values of Manning's *n* hydraulic roughness coefficients for the same riparian species - $n_{,meas}$ varying between 0.063 and 0.074 s·m$^{-1/3}$ in a condition of full vegetation. This can be explained by the different management practice applied to the Bresciani reclamation channel studied by Errico et al. (2018) in years preceding the field experiments. This channel was managed by totally removing the stems and dredging the sediments from the channel bottom every year. This practice, besides highly affecting the aquatic environment, controlled the development of rhizomes in the central part of the reclamation channel and the accumulation of plant residuals at the foot of the re-sprouting living plants. Consequently, in the full vegetated scenario of the Bresciani reclamation channel, stems densities and sizes, as well as the amount of clogging material at the bottom, were much lower than in the Piaggetta reclamation channel. The measured values of Manning's *n* hydraulic roughness coefficient computed in the present study, referring

to a vegetated reclamation channel colonized by rigid and emergent riparian Common reed under different vegetation scenarios, are consistent with those published in previous studies and referring to channels covered by aquatic macrophytes at the maximum development stage. Dawson (1978) studied the seasonal variability of hydraulic roughness coefficients in a vegetated stream and observed values of $n_{,meas}$ in the range 0.30 - 0.40 $s \cdot m^{-1/3}$ at the maximum plant development, comparable to the experiment UV_1 of the present study. Zhao et al. (2017) investigated the hydraulic resistance of three emergent species naturally colonizing reclamation ditches and observed $n_{,meas}$ values larger than 0.43 $s \cdot m^{-1/3}$. Bal & Meire (2009) examined lowland rivers colonized by various flexible aquatic macrophytes and obtained $n_{,meas}$ values in the range 0.34 - 0.71 $s \cdot m^{-1/3}$ at the maximum phenological stage. Similar evidences were discussed by Nikora et al. (2008), who observed a value of $n_{,meas}$ equal to 0.56 $s \cdot m^{-1/3}$ in a small stream with low water flow velocity and under "dense" riparian vegetation conditions.

5.5. Conclusions

Field hydraulic experiments in vegetated channels can provide relevant data for identifying balanced riparian vegetation management practices, that can help to reconcile the need to ensure an adequate channel hydraulic efficiency with the need to reduce the environmental impacts of removing the riparian vegetation from vegetated water bodies. The present study compared the effects of three different riparian vegetation management scenarios on streamwise velocity distribution, turbulence patterns and global water flow resistance in a lowland vegetated reclamation channel, naturally colonized by rigid emergent Common reed plants' stands. The first riparian vegetation management scenario corresponded to an undisturbed canopy cover (*UV*), in which a conspicuous mattress of dead rhizomes, leaves and stems at the reclamation channel bottom was found, resulting in almost in the clogging of the deeper layer of the vegetated cross section. The second and the third riparian vegetation management scenarios were obtained by clearing, respectively, the central part (*CC*) and the entire (*EC*) channel by means of an excavator equipped with a cutting bucket. The machinery employed in the cutting operations was not able to to completely remove the riparian vegetation form the channel boundary. Common reed stalks clogged by dead vegetation residuals have been left along the boundary, thus significantly affecting the hydraulic roughness. The hydraulic conveyance obtained by removing Common reed at just the central part (*CC*) of the reclamation channel was comparable to that obtained by its total clearance (*EC*), but with much less environmental and environmental repercussion. In fact, the central cut riparian vegetation management scenario (*CC*) allowed the release of wide vegetated side buffers, fundamental for the preservation of the functionality aquatic and terrestrial habitat within the examined vegetated reclamation channel.

Moreover, the outcomes of this study showed that from an Ecohydraulic modeling mindset, classic Manning's *n* assessments based on stem density only might not be suitable for undisturbed plant stands, as they might not be able to represent the increase in frontal area caused by dead vegetative material, which naturally deposits at the reclamation channel bottom every vegetative season. Accordingly, the most suitable

models for representing natural riparian reed canopies are those that directly quantify the patch blockage factor, rather than the effect of plant elements matrices. Indeed, the results of the present study underpin the relevance of field experiments for the development of more realistic theories and models of water flow resistance within vegetated open channels.

References

Aberle, J., Järvelä, J. 2013. Flow resistance of emergent rigid and flexible floodplain vegetation. J. Hydraul. Res. 51 (1), pp. 33-45. https://doi.org/10.1080/00221686.2012.754795.

Afzalimehr, H., Moghbel, R., Gallichand, J., Sui, J. 2011. Investigation of turbulence characteristics in channel with dense vegetation. Int. J. Sediment Res. 26 (3), pp. 269-282. https://doi.org/10.1016/S1001-6279(11)60093-0.

Baattrup-Pedersen, A., Ovesen, N.B., Larsen, S.E., Andrsen, D.K., Riis, T., Kronvang, B., Rasmussen, J.J. 2018. Evaluating effects of weed cutting on water level and ecological status in Danish lowland streams. Freshw. Biol. https://doi.org/10.1111/fwb. 13101.

Bal, K.D., Meire, P. 2009. The influence of macrophyte cutting on the hydraulic resistance of lowland rivers. J. Aquat. Plant Manage. 47, pp. 65-68. https://hdl.handle.net/10067/765450151162165141.

Caroppi, G., Gualtieri, P., Fontana, N., Giugni, M. 2018. Turbulence anisotropy at flow rigid vegetation interface. Geosciences 8(7), 259. https://doi.org/10.3390/geosciences8070259.

Caroppi, G., Västilä, K., Järvelä, J., Rowinski, P.M., Giugni, M. 2019. Turbulence at water-vegetation interface in open channel flow: experiments with natural-like plants. Adv. Water Resour. https://doi.org/10.1016/j.advwatres.2019.03.013.

Chen, L., Chen, X. 2016. Comments on "An improved Cauchy number approach for predicting the drag and reconfiguration of flexible vegetation" by Peter Whittaker, Catherine A.M.E. Wilson, Jochen Aberle. Adv. Water Resour. Available at: http://linkinghub.elsevier.com/retrieve/pii/S0309170816305875.

Cheng, N.S., Nguyen, H.T. 2011. Hydraulic radius for evaluating resistance induced in simulated emergent vegetation in open-channel flows. J. Hydraul. Eng. 137 (9), pp. 995-1004. https://doi.org/10.1061/(ASCE)HY.1943-7900.0000377.

Chow, V.T. 1959. Open-channel Hydraulics. McGrow-Hill Book Co., New York, NY. https://doi.org/10.1126/science.131.3408.1215-a.

Clevering, O.A., Lissner, J. 1999. Taxonomy, chromosome numbers, clonal diversity and population dynamics of Phragmites australis. Aquat. Bot. 64 (3-4), pp. 185-208. https://doi.org/10.1016/S0304-3770(99)00059-5.

Dey, S., Sarkar, S., Solari, L. 2011. Near-bed turbulence characteristics at the entrainment threshold of sediment beds. J. Hydraul. Eng. (ASCE) 137, pp. 945-958. https://doi.org/10.1061/(ASCE)HY.1943-7900.0000396.

Dodds, W.K., Tromboni, F., Saltarelli, W.A., Fernandes Cunha, D.G. 2017. The root of the problem: Direct influence of riparian vegetation on estimation of stream ecosystem metabolic rates. Available at: Limnol. Oceanogr. Lett. 2 (1), pp. 9-17. http://doi.wiley.com/10.1002/lol2.10032.

Dowson, F.H. 1978. The seasonal effects of aquatic plant growth on the flow of water in a stream. In: Proceedings of 5th European Weed Research Council Symposium on Aquatic Weeds. Vol. 71-78.

Errico, A., Pasquino, V., Maxwald, M., Chirico, G.B., Solari, L., Preti, F. 2018. The effect of flexible vegetation on flow in reclamation channels: Estimation of roughness coefficients at the real scale. Ecol. Eng. 120, pp. 411-421. https://doi.org/10.1016/j.ecoleng. 2018.06.018.

Errico, A., Lama, G.F.C., Francalanci, S., Chirico, G.B., Solari L., Preti F. 2019. Flow dynamics and turbulence patterns in a reclamation channel colonized by *Phragmites australis* (common reed) under different scenarios of vegetation management. Ecol. Eng. 2019, 133, pp. 39-52. https://doi:10.1016/j.ecoleng.2019.04.016.

Errico, A., Lama, G.F.C., Francalanci, S., Chirico, G.B., Solari L., Preti F. 2019. Validation of global flow resistance models in two experimental reclamation channels covered by *Phragmites australis* (common reed), Proceedings of the 38t^{h} IAHR World Congress, Panama City, Panama, pp. 1313-1321. https://doi:10.3850/38WC092019-1215.

Etminan, V., Lowe, R.J., Ghisalberti, M. 2017. A new model for predicting the drag exerted by vegetation canopies. Water Resour. Res. 53 (4), pp. 3179-3196. https://doi.org/10.1002/2016WR020090.

Farhadi, A., Sindelar, C., Tritthart, M., Glas, M., Blanckaert, K., Habersack, H. 2018. An investigation on the outer bank cell of secondary flow in channel bends. J. Hydro Environ. Res. 18, 1-11. https://doi.org/10.1016/j.jher.2017.10.004.

Forzieri, G., Castelli, F., Preti, F. 2012. Advances in remote sensing of hydraulic roughness. Int. J. Remote Sens. 33 (2), pp. 630-654. https://doi.org/10.1080/01431161.2010.531788.

Ghisalberti, M., Nepf, H.M. 2002. Mixing layers and coherent structures in vegetated aquatic flows. J. Geophys. Res. 107 (C2). https://doi.org/10.1029/2001JC000871.

Giannini, V., Silvestri, N., Dragoni, F., Pistocchi, C., Sabbatini, T., Bonari, E. 2017. Growth and nutrient uptake of perennial crops in a paludicultural approach in a drained Mediterranean peatland. Ecol. Eng. 103 (Part B), pp. 478-487. https://doi.org/10.1016/j.ecoleng.2015.11.049.

Goring, D.G., Nikora, V.I. 2002. Despiking Acoustic Doppler Velocimeter Data. J. Hydraul. Eng. 128 (1), 117-126. https://doi.org/10.1061/(ASCE)0733-9429(2002)128:1(117).

Green, J.C. 2005. Comparison of blockage factors in modelling the resistance of channels containing submerged macrophytes. River Res. Appl. 21, pp. 671-686. https://doi.org/10.1002/rra.854.

Gualtieri, P., De Felice, S., Pasquino, V., Pulci Doria, G. 2018. Use of conventional flow resistance equations and a model for the Nikuradse roughness in vegetated flows at high submergence. J. Hydrol. Hydromech. 66 (1), pp. 107-120. https://doi.org/10.1515/johh-2017-0028.

Guo, J., Zhang, J. 2016. Velocity distributions in laminar and turbulent vegetated flows. J. Hydraul. Res. 54 (2), 117-130. https://doi.org/10.1080/00221686.2015.1136899.

Guo, W.-Y., Lambertini, C., Li, X.-Z., Meyerson, L.A., Brix, H. 2013. Invasion of old world Phragmites australis in the new world: precipitation and temperature patterns

combined with human influences redesign the invasive niche. Change Biol. 19 (11), pp. 3406-3422. https://doi.org/10.1111/gcb.12295.

Gurnell, A.M., Midgley, P. 1994. Aquatic weed growth and flow resistance - influence on the relationship between discharge and stage over a 25 year river gauging station record. Hydrol. Process. 8, pp. 63-73. https://doi.org/10.1002/(ISSN)1099-1085.

Hopkinson, L., Wynn, T. 2009. Vegetation impacts on near bank flow. 418 (October), pp. 404-418. https://doi.org/10.1002/eco.87.

Kirby, J.T., Durrans, S.R., Pitt, R., Johnson, D. 2005. Hydraulic resistance in grass swales designed for small flow conveyance. J. Hydraul. Eng. 131 (1), pp. 65-68. https://doi.org/10.1061/(ASCE)0733-9429(2005)131:1(65).

Kothyari, U.C., Hashimoto, H., Hayashi, K. 2009. Effect of tall vegetation on sediment transport by channel flows. J. Hydraul. Res. 47 (6), pp. 700-710. https://doi.org/10.3826/jhr.2009.3317.

Kouwen, N. 1988. Field estimation of the biomechanical properties of grass. J. Hydraul. Res. 26 (5), pp. 559-568. https://doi.org/10.1080/00221688809499193.

Liu, D., Valyrakis, M., Williams, R. 2017. Flow Hydrodynamics across Open Channel Flows with Riparian Zones: Implications for riverbank stability. Water 9 (720), pp. 1-19. https://doi.org/10.3390/w9090720.

Lu, S.S., Willmarth, W.W. 1973. Measurements of the structure of the Reynolds stress in a turbulent boundary layer 60, pp. 481-511. J. Fluid Mech. https://doi.org/10.1017/S0022112073000315.

Luhar, M., Nepf, H.M. 2011. Flow-induced reconfiguration of buoyant and flexible aquatic vegetation. Limnol. Oceanogr. 56 (6), pp. 2003-2017. https://doi.org/10.4319/lo.2011.56.6.2003.

Luhar, M., Nepf, H.M. 2013. From the blade scale to the reach scale: A characterization of aquatic vegetative drag. Adv. Water Resour. https://doi.org/10.1016/j.advwatres.2012.02.002.

Mohsen, M., Badronnisa, Y., Mohammed, T.A., Ghazali, A.H. 2006. Manning roughness coefficient for grass-lined channel, (January) - Suranaree. J. Sci. Technol. 13 (4), pp. 317-330.

Morris, M., Mohammadi, M.H., Day, S., Hondzo, M., Sotiropulus, F. 2015. Prediction of Glossosoma biomass spatial distribution in Valley Creek by field measurements and a three-dimensional turbulent open-channel flow model. Water Resour. Res. 51, pp. 1457-1471. https://doi.org/10.1002/2014WR015887.

Murphy, E., Ghisalberti, M., Nepf, H.M. 2007. Model and laboratory study of dispersion in flow with submerged vegetation. Water Resour. Res. 45 (5), W05438. https://doi.org/10.1029/2006WR005229.

Nakagawa, H., Nezu, I. 1977. Prediction of the contributions to the Reynolds stress from bursting events in open-channel flows. J. Fluid Mech. 80, 99. https://doi.org/10.1017/S0022112077001554.

Needelman, B.A., Kleinman, P.A., Allen, A.L. 2007. Improved management of agricultural reclamation ditches for water quality protection: An overview, 62(4).

Nepf, H.M. 1999. Drag, turbulence, and diffusion in flow through emergent vegetation. Water Resour. Res. 35 (2), 479-489. https://doi.org/10.1029/1998WR900069.

Nepf, H.M., Mugnier, C.G., Zavistoski, R.A. 1997. The effects of vegetation on longitudinal dispersion. Estuar. Coast. Shelf Sci. 44 (6), pp. 675-684. https://doi.org/10.1006/ecss.1996.0169.

Nezu, I., Sanjou, M. 2008. Turbulence structure and coherent motion in vegetated canopy open channel flows. J. Hydro-Environ. Res. 2, pp. 62-90. https://doi.org/10.1016/j.jher.2008.05.003.

Nikora, V.I., Larned, S., Nikora, N., Debnath, K., Cooper, G., Reid, M. 2008. Hydraulic Resistance due to Aquatic Vegetation in Small Streams: Field Study. J. Hydraul. Eng. https://doi.org/10.1061/(ASCE)0733-9429(2008) 134:9(1326).

Nikora, V.I. 2010. Hydrodynamics of Aquatic Ecosystems: An Interface Between Environment, Biomechanics and Environmental Fluid Mechanics. River. Res. Appl. 26, pp. 367-384. https://doi.org/10.1002/rra.1291.

Novotny, V., Chesters, G. 1981. Handbook of Nonpoint Pollution: Sources and Management. Van Nostrand Reinhold Company, New York.

Old, G.H., Naden, P.S., Rameshwaran, P., Acreman, M.C., Baker, S., Edwards, F.K., Sorensen, J.P.R., Mountford, O., Gooddy, D.C., Stratford, C.J., Scarlett, P.M., Newman, J.R., Neal, M. 2014. Instream and riparian implications of weed cutting in a chalk river. Ecol. Eng. https://doi.org/10.1016/j.ecoleng.2014.07.006.

Panigrahi, K., Khatua, K.K. 2015. Prediction of velocity distribution in straight channel with rigid vegetation. Aquatic Procedia 4 (Icwrcoe), pp. 819-825 Available at: http://linkinghub.elsevier.com/retrieve/pii/S2214241X15001030.

Pasquino, V., Saulino, L., Pelosi, A., Allevato, E., Rita, A., Todaro, L., Saracino, A., Chirico, G.B. 2018. Hydrodynamic behaviour of European black poplar (Populus nigra L.) under coppice management along Mediterranean river ecosystem. River Res. Appl., 34, 586-594. https://doi.org/10.1002/rra.3276.

Poggi, D., Porporato, A., Ridolfi, R., Albertson, J.D., Katul, G.G. 2004. The effect of vegetation density on canopy sub-layer turbulence. Bound. Layer Meteorol. 111 (3), 565-587. https://doi.org/10.1023/B:BOUN.0000016576.05621.73.

Pope, S.B. 2000. Turbulent Flows. Cambridge University Press. https://doi.org/10.1017/CBO9780511840531.

Rhee, D.S., Woo, H., Kwon, B., Ahn, H.K. 2008. Hydraulic resistance of some selected vegetation in open channel flows. River Res. Appl. 24 (5), pp. 673-687. https://doi.org/10.1002/rra.1143.

Rominger, J.T., Nepf, H.M. 2011. Flow adjustment and interior flow associated with a rectangular porous obstruction. J. Fluid Mech. 680, pp. 636-659. https://doi.org/10.1017/jfm.2011.199.

Sime, L.C., Ferguson, R.I., Church, M. 2007. Estimating shear stress from moving boat acoustic Doppler velocity measurements in a large gravel bed river. Water Resour. Res. 43 (3), pp. 1-12. https://doi.org/10.1029/2006WR005069.

Smith, D.L., Goodwin, R.A., Nestler, J.M. 2014. Relating turbulence and fish habitat: a new approach for management and research. Rev. Fish Sci. Aquacult. 22, pp. 123-130. https://doi.org/10.1080/10641262.2013.803516.

Soana, E., Gavioli, A., Tamburini, E., Fano, E.A., Castaldelli, G. 2018. To mow or not to mow: reed biofilms as denitrification hotspots in reclamation canals. Ecol. Eng. 113, pp. 1-10. https://doi.org/10.1016/j.ecoleng.2017.12.029.

SonTek® Handled ADV® Technical manual. 2007. SonTek® - YSI incorporated - San Diego, CA.

Sukhodolova, T.A. 2008. Studies of Turbulent Flow in Vegetated River Reaches with Implications for Transport and Mixing Processes. PhD Thesis. April. http://dx.doi.org/10.18452/15843.

Sukhodolova, T.A., Sukhodolov, A.N. 2012. Vegetated mixing layer around a finite-size patch of submerged plants: 1. Theory and field experiments. Water Resour. Res. 48 (10), pp. 1-16. https://doi.org/10.1029/2011WR011804.

Szabo-Meszaros, M., Navaratnam, C.U., Aberle, J., Silva, A.T., Forseth, T., Calles, O., Fjeldstad, H.-P., Alfredsen, K. 2018. Experimental hydraulics on fish-friendly trash-racks: an ecological approach. Ecol. Eng. 113, pp. 11-20. https://doi.org/10.1016/j.ecoleng.2017.12.032.

Tabacchi, E., Cornell, D., Hauer, R., Pinay, G., Planty-Tabacchi, A., Wissmar, R.C. 1998. Development, maintenance and role of riparian vegetation in the river landscape. Freshw. Biol. 40 (3), pp. 497-516. https://doi.org/10.1046/j.1365-2427.1998.00381.x.

Takemura, T., Tanaka, N. 2007. Flow structures and drag characteristics of a colony-type emergent roughness model mounted on a flat plate in uniform flow. Fluid Dyn. Res. 39, pp. 694-710. https://doi.org/10.1016/j.fluiddyn.2007.06.001.

Tanino, Y., Nepf, H.M. 2008. Laboratory Investigation of Mean Drag in a Random Array of Rigid, Emergent Cylinders. ReCALL 3-441. J. Hydraul. Eng. 134, 1(34). https://doi.org/10.1061/(ASCE)0733-9429(2008).

Tinoco, R.O., Coco, G. 2018. Turbulence as the Main Driver of Resuspension in Oscillatory Flow Through Vegetation. J. Geophys. Res. Earth Surf. 123 (5), pp. 891-904. https://doi.org/10.1002/2017JF004504.

Trinci, G., Harvey, G.L., Henshaw, A.J., Bertoldi, W., Hölker, F. 2017. Life in turbulent flows: interactions between hydrodynamics and aquatic organisms in rivers. Wiley Interdisciplinary Reviews: Water, 4(3), p. e.1213. Available at: http://doi.wiley.com/10.1002/wat2.1213.

Vargas-Luna, A., Crosato, A., Uijttewaal, W.S.J. 2015. Effects of vegetation on flow and sediment transport: Comparative analyses and validation of predicting models. Earth Surf. Proc. Land. 40 (2), pp. 157-176. https://doi.org/10.1002/esp.3633.

Västilä, K., Järvelä, J., Aberle, J. 2013. Characteristic reference areas for estimating flow resistance of natural foliated vegetation. J. Hydrol. 492, pp. 49-60. https://doi.org/10.1016/j.jhydrol.2013.04.015.

Västilä, K., Järvelä, J. 2014. Modeling the flow resistance of woody vegetation using physically based properties of the foliage and stem. Water Resour. Res. 4, 50, pp. 229-245. https://doi.org/10.1002/2013WR13819.

Verschoren, V., Schoelynck, J., Cox, T., Schoutens, K., Temmerman, S., Meire, P. 2017. Opposing effects of aquatic vegetation on hydraulic functioning and transport of dissolved and organic particulate matter in a lowland river: A field experiment. Ecol. Eng. 105, pp. 221-230. https://doi.org/10.1016/j.ecoleng.2017.04.064.

Whittaker, P., Wilson, C., Aberle, J., Rauch, H.P., Xavier, P. 2013. A drag force model to incorporate the reconfiguration of full-scale riparian trees under hydrodynamic loading. J. Hydraul. Res. 51 (5), pp. 569-580. https://doi.org/10.1080/00221686.2013.822936.

Wilcox, B.P. 2010. Ecohydrology Bearing - Invited Commentary Transformation eco-system change and ecohydrology: ushering in a new era for watershed management.

Ecohydrology 130, pp. 126-130 Available at: http://www3.interscience.wiley.com/journal/122653919/abstract.

Yang, J.Q., Chung, H., Nepf, H.M. 2016. The onset of sediment transport in vegetated channels predicted by Turbulent Kinetic Energy. Geophys. Res. Lett. 43, pp. 11261-11268. https://doi.org/10.1002/2016GL071092.

Yang, S., Wang, P., Lou, H., Wang, J., Zhao, C., Gong, T. 2019. Estimating River Discharges in Ungauged Catchments Using the Slope-Area Method and Unmanned Aerial Vehicle. Water. 11(11), 2361. https://doi.org/10.3390/w11112361.

Zhao, F., Huai, W. 2016. Hydrodynamics of discontinuous rigid submerged vegetation patches in open-channel flow. J. Hydro-environ. Res. 12, pp. 148-160. https://doi.org/10.1016/j.jher.2016.05.004.

Zhao, S., Cui, Y., Luo, Y., Li, Y.P. 2017. Experimental study on wetland hydraulic characteristics of vegetated reclamation ditches. Water 9 (5), 311. https://doi.org/10.3390/w9050311.

6. Water flow resistance modeling of Piaggetta vegetated reclamation channel.

The present Chapter is based on the following articles:

- **Lama**, **G**.**F**.**C**., Errico, A., Francalanci, S., Solari, L., Preti, F., Chirico, G.B. 2019. Hydraulic modeling of field experiments in a drainage channel under different riparian vegetation scenarios, in Book of Abstract of the AIIA International Mid-Term Conference, Matera 12-13 September, Italy, p. 54.

- **Lama**, **G**.**F**.**C**., Errico, A., Francalanci, S., Solari, L., Preti, F., Chirico, G.B. 2019. Comparative analysis of modeled and measured vegetative Chézy's flow resistance coefficients in a drainage channel vegetated by dormant riparian reed. Proceedings of the International IEEE Workshop on Metrology for Agriculture and Forestry, Portici, Italy. pp. 180-184. ISBN: 978-1-7281-3611-0.

- **Lama**, **G**.**F**.**C**., Errico, A., Francalanci, S., Solari, L., Preti, F., Chirico, G.B. 2020. Evaluation of flow resistance models based on field experiments in a partly vegetated reclamation channel. Geosciences, 10(2), 47. https://doi.org/10.3390/geosciences10020047.

6.1. Introduction

The presence of backwater in manmade reclamation channels enhances the growth of riparian plants, promoting the expansion of aquatic and terrestrial habitats and improving water quality (*Rowinski et al., 2018*). In this context, the analysis of the interaction between riparian plants and water flow in real vegetated channels can provide relevant hints to the administrators of land reclamation areas, about the most useful approaches to be followed when managing the riparian vegetation, which can ensure the conveyance capacity of the channel with limited impacts on the natural habitats (*Errico et al., 2019a*). One of the most challenging tasks when programming the management of riparian vegetation in reclamation channels is the definition of simple and accurate models for assessing the global water flow resistance coefficients (e.g., the vegetative Chèzy water flow resistance coefficient C_r (*Vargas-Luna et al., 2015*; *Lama et al., 2019*), the Manning's *n* hydraulic roughness coefficient (*Errico et al., 2018*), the vegetative Darcy-Weisbach's friction factor *f"* (*Västilä & Järvelä, 2014)*). However, the predictive efficiencies of these models have been rarely evaluated with field experimental data, especially in partly vegetated channels. Among others, Errico et al. (2018) and Errico et al. (2019a) have analyzed the effect of a condition of partial riparian vegetation cover on water flow dynamics related to both flexible (*Errico et al., 2018*) and rigid (*Errico et al., 2019b*) invasive riparian vegetation.

The aim of the present study is the evaluation of the accuracy of a 1D Ecohydraulic simulation performed employing HEC-RAS (Hydrologic Engineering Center - River

Analysis System) freeware software (US Army Corps of Engineers, available at *https://www.hec.usace.army.mil/software/hec-ras/download.aspx*) and of two literature models of the global flow resistance in vegetated open channels (*Stone & Shen, 2002*; *Baptist et al., 2007*) referred to field hydraulic experiments carried out in real vegetated open channels colonized by Common reed plants. The outcomes of these comparative analyses constitute a suitable tool for future researches on Ecohydraulic modeling, especially for the computation of the effect of partial riparian vegetation cover on global water flow resistance modeling for natural and manmade vegetated open channels (*Lama et al., 2019b*).

6.1.1. Estimated Manning's n hydraulic roughness coefficients: $n_{,est}$

A 1D Ecohydraulic simulation was carried out employing the HEC-RAS freeware software, considering variable hydraulic roughness along the wetter perimeter of the cross sections for reproducing the effects of the three different riparian vegetation management scenarios examined in the experimental study conducted by Errico et al (2019a), already described in Chapter 5.
The outcomes of the 1D simulation (*Lama et al., 2019a*) in terms of water flow average velocity U ($m \cdot s^{-1}$) and Manning's n hydraulic roughness coefficients ($s \cdot m^{-1/3}$) were compared with those derived from the selected experimental study.

6.1.2. Estimated vegetive Chézy's C_r water flow resistance coefficients: $C_{r,est}$

The global water flow resistance generated in vegetated channels could be estimated by employing many predictive models (e.g., *Vargas-Luna, 2015*). Each model was derived under distinct hydraulic (laboratory flumes or real vegetated channels) and vegetative (real or artificial riparian plants) conditions. Among others, the two resistance models proposed by Baptist et al. (2007) and the Stone & Shen (2002), hereinafter referred to as *Bp* and *S&S*, have been validated for real riparian vegetation, by considering both emergent and submerged vegetative conditions, depending on the ratio between the water level (h) and the plants height above the vegetated channel bottom (h_v).
This study aimed at evaluating the efficiency of *Bp* and *S&S* resistance models in terms of C_r by exploiting experimental data retrieved from field hydrodynamic and vegetative measurements, performed by Errico et al. (2019a) within an abandoned vegetated reclamation channel located in northern Tuscany (Italy), as described in Chapter 5. The main species observed along the entire reclamation channel was the Common reed a riparian species widespread in lowlands and wetlands. The examined emergent riparian reed plants were at a mature phenological stage, characterized by rigid stems. In the field hydrodynamic experiments carried out by Errico et al. (2019a), the Authors have originally examined six different discharge regimes. In this study, we examine just the two discharge regimes, both referred to the condition of partial riparian vegetation cover. Following Errico et al. (2019a), hereinafter these two discharge regimes are respectively indicated as CC_1 = 0.16 $m^3 \cdot s^{-1}$ and CC_2 = 0.33 $m^3 \cdot s^{-1}$ (See Chapter 5). The other flow rates not examined in this study are: one with undisturbed vegetation cover, equal to 0.126 $m^3 \cdot s^{-1}$; three with no vegetation cover, respectively equal to 0.086 $m^3 \cdot s^{-1}$, 0.175 $m^3 \cdot s^{-1}$

and 0277 $m^3 \cdot s^{-1}$. Due to time constraints and limited available resources for the field campaign, we have not been able to explore a larger number of flow rates and water levels. A first comparison between estimated and measured C_r was carried out without considering the variability of the cross sectional water flow velocity field induced by the partial vegetation cover. Thus, *Bp* and *S&S* resistance models were applied under the assumption that the entire cross section homogenously contributes to the global water flow resistance process. A second comparative analysis was performed by applying a methodology based on the combination of the well-known Divided Channel Method (*DCM*) with four composite cross section methods, as respectively proposed by Colebatch (1941), Horton (1933), Pavlovskii (1931) and Yen (2002). *DCM* was applied to represent the impact of the non-homogenous distribution of the riparian reed along the wetted perimeter by dividing the entire cross section into three different regions, indicated as *DCM* sub-sections: orographic left side, central region, and orographic right side. All the comparative analyses were carried out with two different discharges.

6.2. Materials and methods

6.2.1. Estimated Manning's n hydraulic roughness coefficients: $n_{,est}$

The comparison between estimated and measured Manning's *n* was conducted for validating the proposed model, in order to extend the simulation to other riparian vegetation management scenarios and providing to water bodies managers useful predictive indications on the effect of riparian vegetation management on both aquatic water quality and hydraulic conveyance inside the 70 m long experimental vegetated reclamation channel. The water surface level at the downstream cross section was imposed as boundary condition since the water flow in the reclamation channel was in sub-critical condition. Three experiments were analyzed in the hydraulic simulation: UV_1, CC_1 and CC_2, corresponding to the two management scenarios characterized by the presence of riparian vegetation along the reclamation channel stretch. The Manning's *n* hydraulic roughness coefficients were estimated by calibrating the 1D hydraulic simulation to fit the measured surface water level profile. After the first run corresponding to UV_1, it was possible to estimate a Manning's *n* of 0.65 $s \cdot m^{-1/3}$. Then, for CC_1 and CC_2, miming vegetation removal for a 2.70 m wide central region of the reclamation channel, and leaving two buffers of undisturbed vegetation at sides, the value of $n = 0.65\ s \cdot m^{-1/3}$ was imposed for the side buffers, while *n* value for the central region clean from vegetation was calibrated, till the predicted water levels at the four monitored cross sections converged to those observed during the field experiments (*Errico et al., 2019b)*.

6.2.2. Estimated vegetative Chézy's C_r water flow resistance coefficients: $C_{r,est}$

6.2.2.1. *Bp* and *S&S* resistance models

Following the review proposed by Vargas-Luna et al. (2015), the two resistance models examined in this study (*Bp* and *S&S*) were applied for real emergent riparian vegetation, i.e., when the water level (*h*) is smaller than the height of the stems measured from the

bottom of the vegetated reclamation channel (h_v). Both resistance models were applied for a condition of partial riparian vegetation cover.

6.2.2.2. DCM and composite cross section methods

Four composite cross section methods were employed for characterizing the effect of the non-uniform vegetation distribution along the wetted perimeter on the global water flow resistance: Colebatch (1941), Horton (1933), Pavlovskii (1931) and Yen (2002). The outcomes of these methods are hereinafter defined as $C_{r,est}$. These methods consider different weights for parametrizing the contribution of the three *DCM* sub-sections to C_r, according to the following expressions:

Colebatch composite cross section method:

$$C_{r,est} = \frac{1}{\left[\frac{\sum_{i=1}^{N}(\sigma_i \cdot {n_i}^{1.5})}{\sigma}\right]^{\frac{2}{3}}} \cdot R^{\frac{1}{6}} \tag{6.1}$$

Horton composite cross section method:

$$C_{r,est} = \frac{1}{\left[\frac{\sum_{i=1}^{N}(\chi_i \cdot {n_i}^{1.5})}{\chi}\right]^{\frac{2}{3}}} \cdot R^{\frac{1}{6}} \tag{6.2}$$

Pavlovskii composite cross section method:

$$C_{r,est} = \frac{1}{\left[\frac{\sum_{i=1}^{N}(\chi_i \cdot {n_i}^{2})}{\chi}\right]^{\frac{1}{2}}} \cdot R^{\frac{1}{6}} \tag{6.3}$$

Yen composite cross section method:

$$C_{r,est} = \frac{\frac{\chi}{R^{\frac{1}{6}}}}{\sum_{i=1}^{N}\left(\frac{\chi_i \cdot n_i}{R_i^{\frac{1}{6}}}\right)} \cdot R^{\frac{1}{6}} \tag{6.4}$$

where N is the number of the *DCM* sub-sections, while σ_i, χ_i, R_i, and n_i respectively are the water flow cross sectional area, the wetted perimeter, the hydraulic radius, and the Manning's coefficients calculated employing both *Bp* and *S&S* resistance models at each of the three *DCM* sub-sections (excluded *DCM* sub-section 2 in which the riparian vegetation was absent), while σ, χ, and R are referred to the entire *ADV* cross section.

6.2.2.3. Comparative analysis between $C_{r,est}$ and $C_{r,meas}$

The estimated vegetative Chézy's water flow resistance coefficients, indicated as $C_{r,est}$, were compared with the measured ones, indicated as $C_{r,meas}$, in order to evaluate their capability in predicting the global water flow resistance for a condition of partial reed cover at field scale. We first compared $C_{r,meas}$ with the outcomes of *Bp* and *S&S* resistance models, estimated without considering the actual cross sectional water flow velocity distributions, and then, we carried out a second analysis comparing $C_{r,meas}$ with those obtained by combining *Bp* and *S&S* resistance models with the four cross section methods. In both cases, the predictive efficiencies of the two examined resistance models were assessed by computing the relative prediction error (ε_r, in %), according to the following equation:

$$\varepsilon_r(\%) = \frac{C_{r,est} - C_{r,meas}}{C_{r,meas}}. \quad (6.5)$$

6.3. Results and discussion

6.3.1. Estimated and measured Manning's n hydraulic roughness coefficients: n,est

In the following Figures 29a-e the outcomes of the HEC-RAS 1D hydraulic simulation are shown in terms of water surface profile for the simulated vegetated reclamation channel (Fig. 29a) and at the four measuring cross sections (I - IV in Fig. 29b-e), referred to UV_1.

Estimated and measured water flow average velocities U ($m \cdot s^{-1}$) and Manning's n roughness coefficient exhibited a good correlation (Fig. 30a), with values of *RMSE* respectively equal to 0.02 $m \cdot s^{-1}$ and 0.10 $s \cdot m^{-1/3}$, comparable with those obtained by Galema (2009), who exploited a dataset retrieved by Stone & Shen (2002), which referred to emergent rigid plants. Similar results were also retrieved by Vinatier et al. (2017), who simulated the cross sectional plants' distribution employing 3D voxels (i.e., volumetric picture elements). The Authors achieved predictive performances (Fig. 30b) comparable to those obtained in our study, by comparing measured and estimated Manning's n for different plant species (*Asparagus acutifolius*, *Elytrigia repens*, *Lythrum salicaria* and *Scirpoides holoschoenus*).

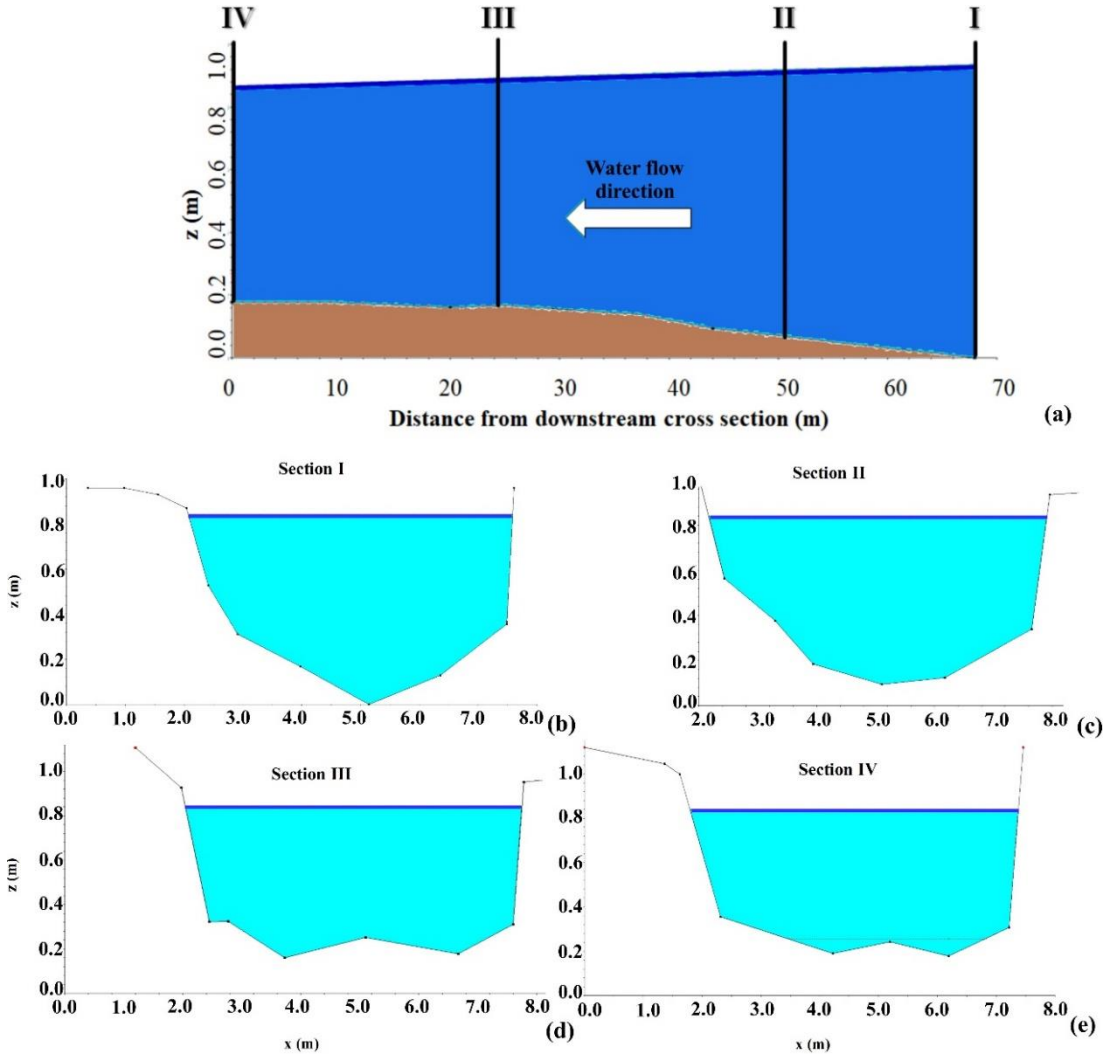

Fig. 29. (a) Simulated water surface profile for the vegetated reclamation channel and (b-e) at the four measuring cross sections (I - IV), referred to UV_1. The vertical black continuous lines in Figure 30a represent the four cross sections exploited for the measurement of the water levels, while the dark blue continuous lines in Figure 29b-e represent the water surface levels.

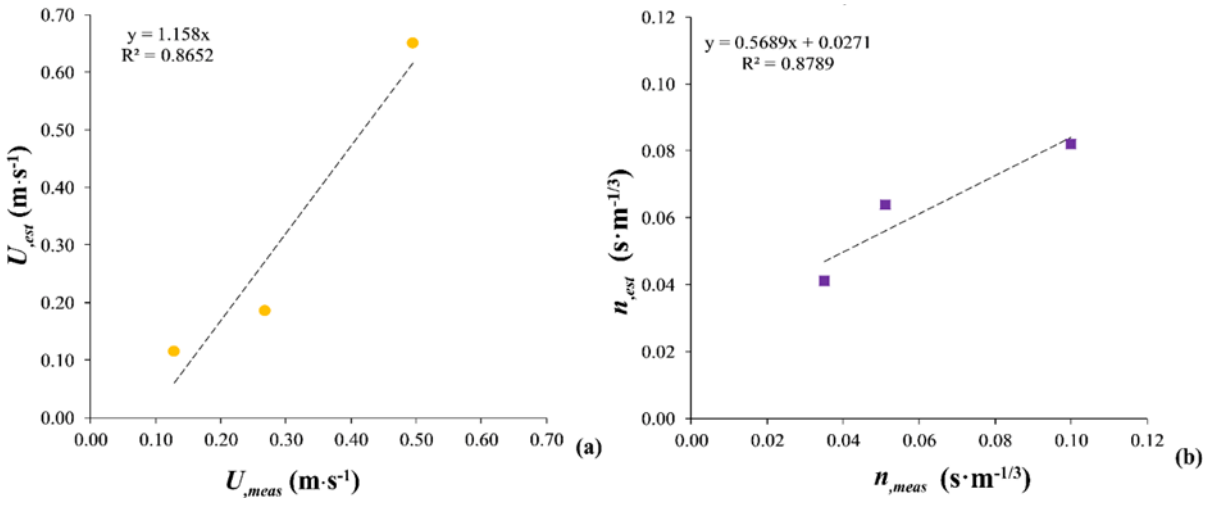

Fig. 30. Comparisons between measured and estimated (a) water flow average velocities

(yellow circles) and (b) Manning's *n* hydraulic roughness coefficients (purple squares).

6.3.2. Estimated vegetative Chézy's C_r water flow resistance coefficients: $C_{r,est}$

6.3.2.1. *Bp* and *S&S* models combined with composite cross section methods

The experimental isotachs, corresponding to the two analyzed experimental discharge regimes CC_1 (= 0.16 $m^3 \cdot s^{-1}$) and CC_2 (= 0.33 $m^3 \cdot s^{-1}$), are respectively shown in Figure 31a and Figure 31b. Three distinct *DCM* sub-sections were then defined by applying the *DCM*, after a detailed analysis of the experimental isotachs.

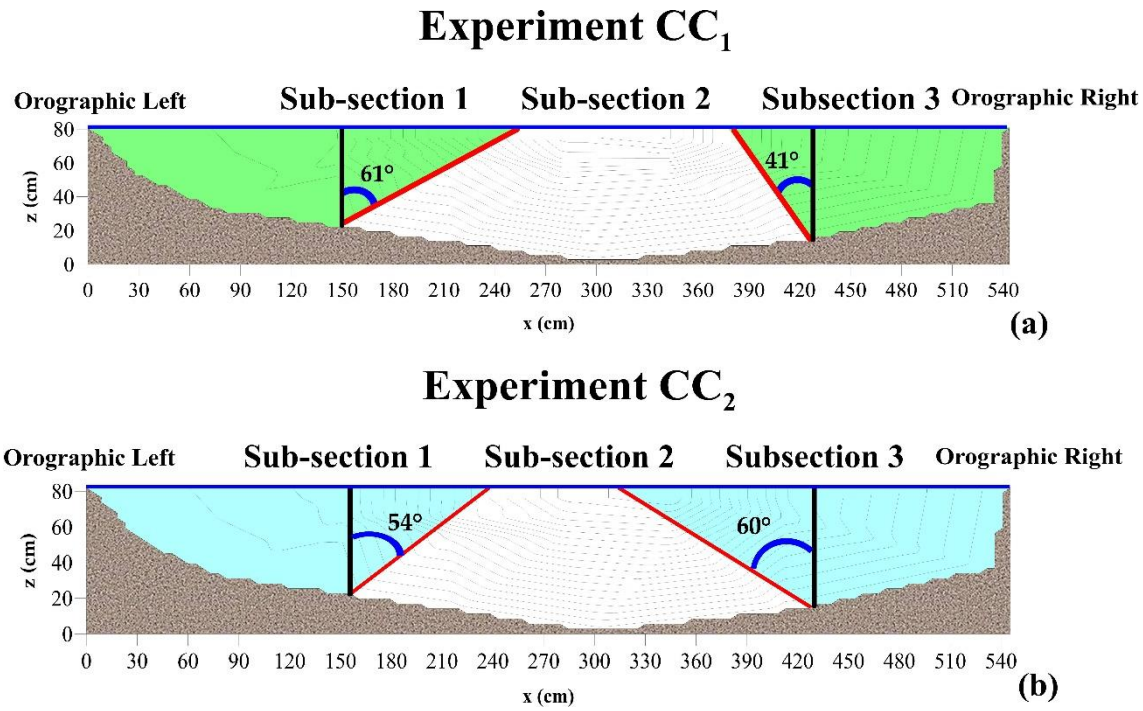

Fig. 31. *DCM* sub-sections. The continuous dark blue line indicates the water level at bankfull. The continuous vertical black lines indicate the boundary of the side buffers of undisturbed riparian vegetation, while the red lines represent the borders of the *DCM* sub-sections, which slopes were equal to 61° and 41° for CC_1 and to 54° and 60° for CC_2, respectively referred to *DCM* sub-section 1 and *DCM* sub-section 3. The experimental isotachs were derived from the same measuring grid adopted in Chapter 5 for the *ADV* measurements.

As shown in the figures, the boundaries of the three *DCM* sub-sections were delineated by drawing lines orthogonal to the isotachs starting from the channel bottom. Then, the slopes of these lines were easily determined using simple geometrical computations. These lines correspond to the physical interface between water flow and riparian vegetation. The momentum exchange is null through these lines.

The side buffers of undisturbed riparian vegetation notably influenced the cross sectional water flow velocity distribution for both CC_1 and CC_2 discharge regimes, concentrating the water flow in the central region, cleared from vegetation. This phenomenon generates strong water flow velocity gradients at the physical interface between the riparian

vegetation buffers and the water flow (continuous vertical black lines in Fig. 32a and Fig. 32b) and affects significantly the slope of the boundary lines of the three *DCM* sub-sections: *DCM* sub-section 1, *DCM* sub-section 2 and *DCM* sub-section 3 (continuous slanting red lines in Fig. 32a and Fig. 32b).

The two examined discharge regimes were characterized by a turbulent water flow regime since the Reynolds numbers *Re* (= $U \cdot h / \nu$, where U ($m \cdot s^{-1}$) is the average water flow velocity, h (m) is the water level and ν ($m^2 \cdot s^{-1}$) is the kinematic viscosity of water, equal to approximately 10^{-6} $m^2 \cdot s^{-1}$) referred to these discharge regimes were respectively equal to 4.1 x 10^4 and 8.3 x 10^4. These values refer to the original values of hydraulic radius *R*, but they can be considered acceptable also for the condition of partial riparian vegetation cover, since the new values of *R*, referred to *DCM* sub-section 2 in which the water flow motion was essentially concentrated, are similar to the original ones. The input parameters of the formulas of the four composite cross section methods tested in the present study, for each of the three *DCM* sub-sections individuated in the previous Section, are summarized in the following Table 5 and Table 6, respectively referred to the two examined .discharges. Their values were computed by considering separately the three *DCM* sub-sections.

Table 5. Hydraulic and vegetative parameters for CC_1: χ_i (m), σ_i (m^{-2}), h_i (m) and m_i (m^{-2}) are respectively the wetted perimeter, the water flow cross sectional area, the water level and the riparian vegetation density of each *DCM* sub-section.

***DCM* sub-section**	**χ_i (m)**	**σ_i (m^{-2})**	**h_i (m)**	**m_i (m^{-2})**
1	1.71	0.97	0.68	49
2	2.77	1.46	0.71	-
3	1.52	0.80	0.65	78

Table 6. Hydraulic and vegetative parameters for CC_2: χ_i (m), σ_i (m^{-2}), h_i (m) and m_i (m^{-2}) are respectively the wetted perimeter, the water flow cross sectional area, the water level and the riparian vegetation density of each *DCM* sub-section.

***DCM* sub-section**	**χ_i (m)**	**σ_i (m^{-2})**	**h_i (m)**	**m_i (m^{-2})**
1	1.88	1.04	0.72	49
2	2.82	1.21	0.77	-
3	1.82	0.96	0.68	78

The riparian vegetation density m_i at *DCM* sub-section 2, corresponding to the central region of the examined drainage channel, is null because the Common reed plants were completely removed from there.

6.3.2.2. Comparative analysis between $C_{r,est}$ and $C_{r,meas}$

A comparative analysis between $C_{r,est}$ and $C_{r,meas}$ was carried out, to evaluate the predictive efficiency of the *Bp* and the *S&S* global water flow resistance models in the condition of partial vegetation cover of a reclamation channel. As shown in the following Figure 32, a first comparison was carried out between $C_{r,est}$ and $C_{r,meas}$, the latter calculated without applying the composite section methods (indicated by filled orange and black squares). Then, by applying the methodology proposed in the present study to parametrize the effect of riparian vegetation on the actual cross sectional water flow velocity distribution, a comparative analysis was performed by combining *DCM* with the four composite cross section methods analized in the present study: Colebatch (1941), Horton (1933), Pavlovskii (1931) and Yen (2002).

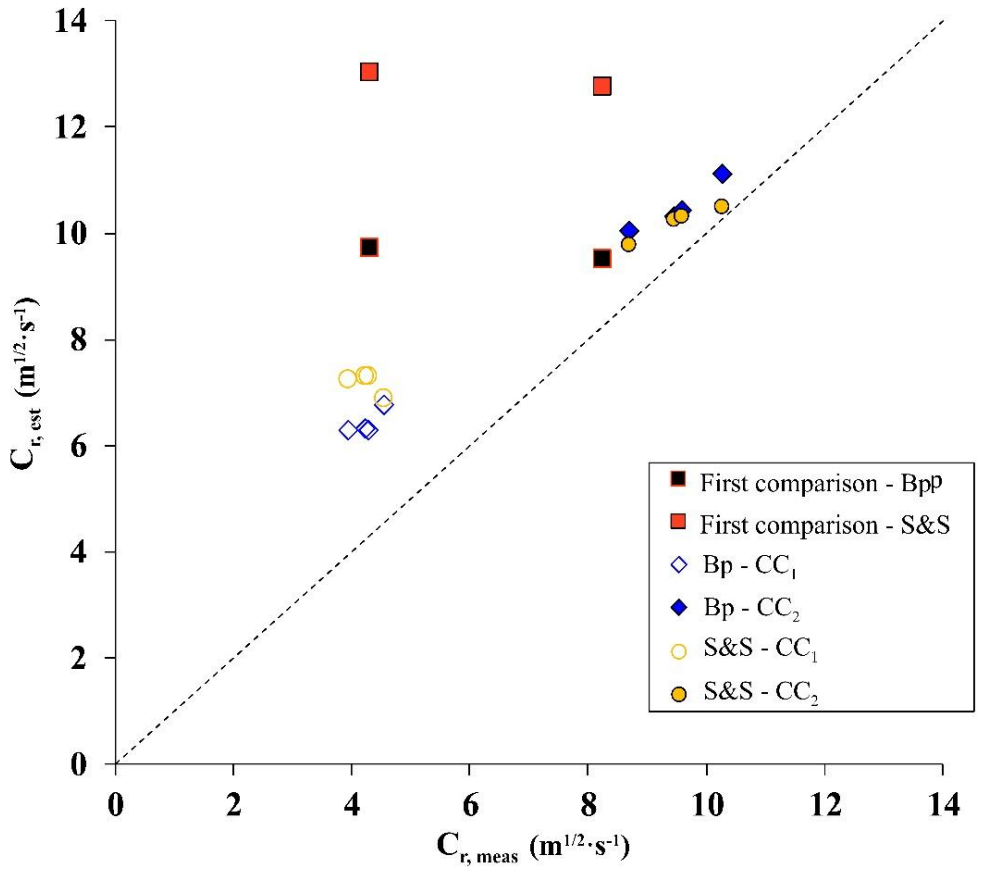

Fig. 32. Measured and estimated C_r ($m^{1/2}\cdot s^{-1}$) for the *Bp* and *S&S* resistance models, by not applying (black and orange filled squares) and applying the four composite cross section methods: the blue diamonds and the yellow circles correspond respectively to *Bp* and *S&S* resistance models, for CC_1 = 0.16 $m^3\cdot s^{-1}$ (unfilled symbols) and CC_2 = 0.33 $m^3\cdot s^{-1}$ (filled symbols). The dashed black line represents the perfect agreement between estimated and measured C_r.

Both *Bp* and *S&S* resistance models overestimated the measured C_r. The only remarkable difference between the two selected resistance models is represented by the changing trend of the estimated C_r, depending on the two different investigated discharges, as it can be noticed in Figure 32. In fact, for the CC_1 discharge, *Bp* resistance model returned higher values than *S&S*, while this behavior was inverted when considering CC_2.

The relative prediction error ε_r (%) between $C_{r,\,mod}$ and $C_{r,meas}$ for the two examined resistance models, with two discharges are shown in Figure 33.

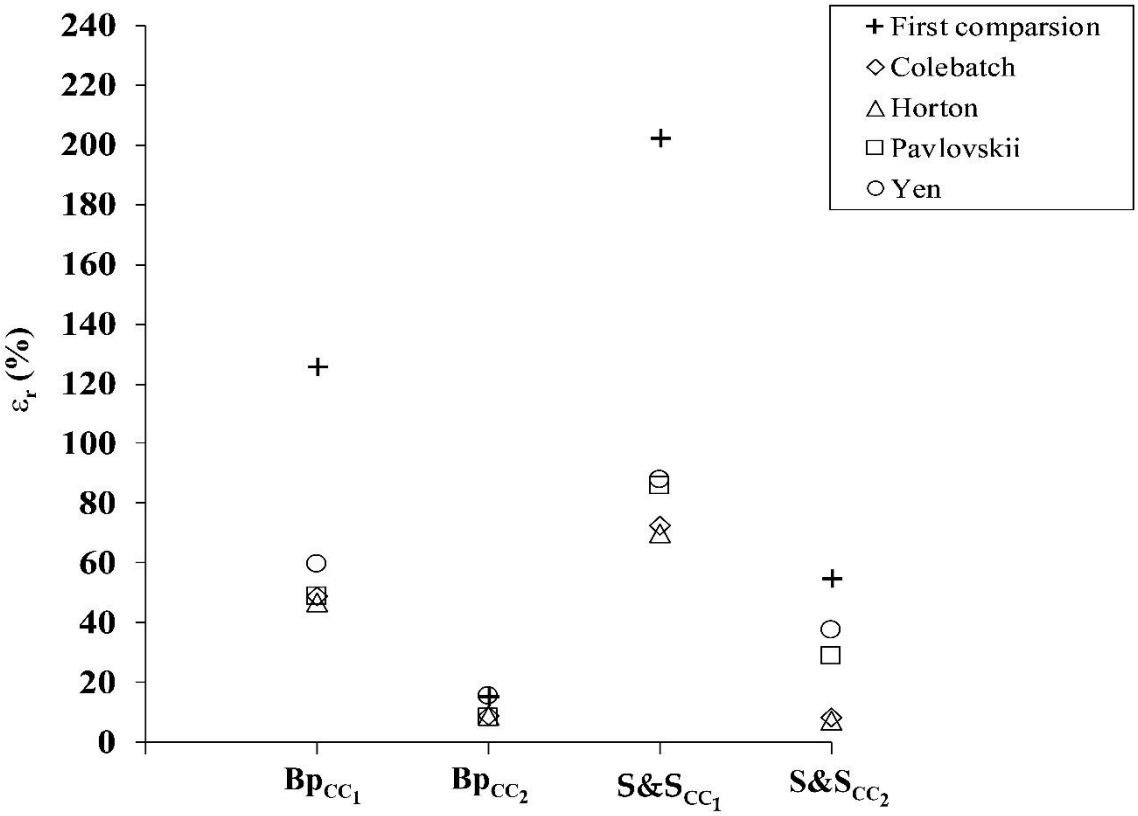

Figure 33. Relative prediction errors ε_r (%) of *Bp* and *S&S* resistance models, computed under the two discharge regimes respectively pair to CC_1 = 0.16 $m^3 \cdot s^{-1}$ and CC_2 = 0.33 $m^3 \cdot s^{-1}$, corresponding to the condition of partial riparian vegetation cover of the reclamation channel, without employing the proposed methodology (black crosses), and by applying the four examined composite cross section methods: Colebatch (diamonds), Horton (triangles), Pavlovskii (squares) and Yen (circles).

As it appears from Figure 33, the combination of the two resistance models examined in the present study with the four composite cross section methods for CC_1 and CC_2 discharges are respectively labeled as Bp_{CC_1}, Bp_{CC_2}, $S\&S_{CC_1}$ and $S\&S_{CC_2}$. It can be easily observed that the Yen composite cross section method systematically returned the highest ε_r value, for both *Bp* and *S&S* resistance models under both CC_1 and CC_2 discharges. On the other hand, we can observe that in three cases Horton method always returned the lower ε_r values, except for the case of *S&S* resistance model in combination with Pavlovskii method under the CC_2 discharge. In just one single case, corresponding to *Bp* resistance model under the CC_2 discharge regime, Yen composite cross section method returned ε_r = 16%, close to that obtained by applying *Bp* and *S&S* resistance models without combining them with the four composite cross section methods, equal to 15%. For the CC_1 discharge, ε_r reduced from 126% to 47% by combining *Bp* model with Horton composite cross section method, and from 202% to 70% for *S&S* resistance model combined with the same method, while, for the CC_2 discharge, ε_r decreased from 15% to 8% for *Bp* model combined with Pavlovskii composite cross section method, and from

55% to 7% for *S&S* model in combination with Horton method. Moreover, as it can be easily noticed, the highest reduction of ε_r with respect to the first comparison was obtained by combining *Bp* resistance model with Horton composite cross section method, for CC_1. Our result agrees with that obtained by Yang et al. (2019), in which the Authors achieved the minimum predictive error (indicated in their work as relative accuracy) of 9.14%, computed between measured global water flow resistance and those retrieved by employing a model based on Unmanned Aerial Vehicles (*UAV*) techniques for a river partially covered by emergent riparian vegetation. This is a promising finding since it demonstrates the application of a simple method, like *DCM* with one of the four examined composite cross section methods, which can lead to results comparable with those obtained by using more complex models. The satisfactory levels of accuracy reached by the methodology proposed in the present study, testified by small ε_r values, have been achieved thanks to the detailed analysis of the experimental *ADV* cross sectional water flow velocity fields (or distributions) that significantly and inevitably affect the contributions of the different parts of the reclamation channel cross section to the global water flow resistance for a partial vegetation cover. Moreover, the range of variabilities exerted by the ε_r values is very similar to those obtained by Errico (2017), which compared estimated and measured roughness coefficients by applying different predictive models (*Nepf & Vivoni, 2000*; *James et al., 2004*; *Yang & Choi, 2010*) in combination with the same composite cross section methods tested in the present study, for a different condition of partial vegetation cover of a reclamation channel colonized by green and flexible Common reed plants. The main difference with respect to our outcomes is represented by the choice of the borders of the *DCM* sub-sections. In fact, in the study by Errico (2017), the Author considered just the vertical physical interfaces between riparian vegetation and water flow, instead of those derived from the analysis of the experimental isotachs.

6.5. Conclusions

A 1D Hydraulic simulation was carried out for reproducing the outcomes of field tests conducted in a reclamation channel covered by mature Common reed in order to evaluate the effects of different riparian vegetation management scenarios on average water flow velocity and vegetative Manning's *n* roughness coefficient. Two vegetation scenarios were simulated: natural cover and side vegetation cover - according to two configurations: CC_1 and CC_2. For the three flow rates examined within the present study, it was observed that the measured and the estimated water flow average velocities and vegetative Manning's *n* roughness coefficient exhibited a high correlation, testified by values of *RMSE* respectively equal to 0.02 $m \cdot s^{-1}$ and 0.10 $s \cdot m^{-1/3}$. The achieved predictive performances are comparable with those obtained by previous studies (*Galema, 2009*; *Vinatier et al., 2017*) for similar experimental conditions.

A direct comparative analysis between modeled and measured vegetative Chézy's coefficients C_r was carried out, for assessing the predictive efficiencies of the *Bp* and the *S&S* resistance models for an experimental reclamation channel partly vegetated by rigid and emergent riparian Common reed plants, under two different flow rates. The accuracy

of both resistance models has been sensibly improved with respect to those obtained without applying the composite cross section methods. These results were achieved by applying a more rigorous methodology, that considers the actual influence of the cross sectional riparian vegetation distribution on the water flow velocity fields in conditions of partial reed cover. The proposed methodology, preliminarily introduced by Lama et al. (2019), is founded on the analysis of the experimental isotachs retrieved from local *ADV* measurements at the upstream channel cross section. We combined the *Bp* and *S&S* resistance models with *DCM* and with four composite cross section methods: Colebatch, Horton, Pavlovskii and Yen. From the outcomes of the direct comparison between modeled and measured vegetative Chézy's coefficients, it was observed that the combination of the *S&S* resistance model and the Horton composite cross section method returned the lowest value of relative prediction error ε_r, equal to 7%. The results of this study are limited to channels having a width of an order of magnitude larger than the water levels.

From a Computational Fluid Dynamics (*CFD*) perspective, the *DCM* constitutes a very simple model, based on basic theoretical assumptions. At the same time, it represents a quick method for describing the contribution of the distinct portions of the entire cross section characterized by the condition of partial riparian vegetation cover. A significant improvement to the accuracy of the outcomes of the present study can be obtained implementing 2D and 3D numerical simulations, aiming at reproducing the actual impacts of the full and partial riparian vegetation cover on the water flow velocity and turbulence fields by modeling the Common reed stems as rigid cylindrical elements (i.e.,, *Ozan & Yilmazer, 2019*). Another improvement to this methodology can be achieved by analyzing the water flow velocity vertical profile in detail, especially in correspondence of the interface between riparian vegetation buffers and water flow. In these cases, we can consider also other methods (i.e., *Kouwen et al., 1969*) aiming at defining the influence of vegetation patches on global water flow resistance. Further applications of the proposed methodology will be carried out on datasets obtained by remote sensing techniques from *UAV*, already largely employed for the measurement and monitoring of morphometrical and bio-mechanical properties of vegetation in many agricultural, forestry, as well as in Ecohydraulic studies referred to different vegetation species and phenological stages (*Sarghini & De Vivo, 2017*; *Giannetti et al., 2018*; *Yang et al., 2019*). It is possible to conclude that the outcomes of this study can provide to administrators of reclamation areas a simple and accurate methodology for modeling the effects of the cross sectional streamwise distributions on the global water flow resistance of real natural and manmade partly vegetated water bodies.

References

Baptist, M.J. Modelling floodplain biogeomorphology. 2005. PhD Thesis, Delft University of Technology, Delft, The Netherlands.

Baptist, M.J., Babovic, V., Rodríguez, J., Keijzer, M., Uittenbogaard, R., Mynett, A., Verwey, A. 2007. On inducing equations for vegetation resistance. J. Hydraul. Res., 45(4), pp. 435-450. https://doi.org/10.1080/00221686.2007.9521778.

Colebatch, G.T. 1941. Model tests on the Lawrence Canal roughness coefficients. Journal Inst. Civil Eng. (Australia), 13(2), pp. 27-32.

Errico, A. 2017. The effect of flexible vegetation on flow in drainage channels. Field surveys and modelling for roughness coefficients estimation. PhD Thesis, University of Florence, Florence, Italy.

Errico, A., Pasquino, V., Maxwald, M., Chirico, G.B., Solari L., Preti, F. 2018. The effect of flexible vegetation on flow in reclamation channels. Estimation of roughness coefficients at real scale. Ecol. Eng. 2018, 120, pp. 411-421. https://doi.org/10.1016/j.ecoleng.2018.06.018.

Errico, A., Lama, G.F.C., Francalanci, S., Chirico, G.B., Solari L., Preti F. 2019. Flow dynamics and turbulence patterns in a reclamation channel colonized by *Phragmites australis* (common reed) under different scenarios of vegetation management. Ecol. Eng. 2019, 133, pp. 39-52. https://doi:10.1016/j.ecoleng.2019.04.016.

Errico, A., Lama, G.F.C., Francalanci, S., Chirico, G.B., Solari, L., Preti, F. 2019. Validation of global flow resistance models in two experimental drainage channels covered by *Phragmites australis* (common reed), in Proceedings of the 38th IAHR World Congress, Panama, pp. 1313 - 1321. https://doi:10.3850/38WC092019-1215.

Galema, A. 2009. Vegetation resistance; evaluation of vegetation resistance models for flood management. Master Thesis, University of Twente, Enschede, The Netherlands.

Giannetti, F., Chirici, G., Gobakken, T., Næsset, E., Travaglini, D., Puliti, S. 2018. A new approach with DTM-independent metrics for forest growing stock prediction using UAV photogrammetric data. Remote Sens. Environ., 213, pp. 195-205. https://doi.org/10.1016/j.rse.2018.05.016.

Horton, R.E. 1933. Separate roughness coefficients for channel bottoms and sides. Eng. News-Rec., 111(22), pp. 652-653.

James, C.S., Birkhead, A.L., Jordanova, A.A., O'Sullivan, J.J. 2004. Flow resistance of emergent vegetation. J. Hydraul. Res., 42(4), pp. 390-398. https://doi.org/10.1080/00221686.2004.9728404.

Lama, G.F.C., Errico, A., Francalanci, S., Solari, L., Preti, F., Chirico, G.B. 2019. Hydraulic modeling of field experiments in a reclamation channel under different riparian vegetation scenarios. Book of Abstract of AIIA International Mid-Term Conference, Matera 12-13 September, Italy, p. 54.

Lama, G.F.C., Errico, A., Francalanci, S., Chirico, G.B., Solari L., Preti F. 2019. Comparative analysis of modeled and measured vegetative Chézy's flow resistance coefficients in a reclamation channel vegetated by dormant riparian reed. Proceedings of the International IEEE Workshop on Metrology for Agriculture and Forestry, Portici, Italy, pp. 180-184. ISBN: 978-1-7281-3611-0.

Nepf, H.M., Vivoni, E.R. 2000. Flow structure in depth-limited, vegetated flow. J. Geophys. Res., 105(C12), pp. 28457-28557. https://doi.org/10.1029/2000JC900145.

Ozan, A.Y., Yilmazer, D. 2019. Near-Wake Flow Structure of a Suspended Cylindrical Canopy Patch. Water, 12, 84. https://doi.org/10.3390/w12010084.

Pasquino, V., Saulino, L., Pelosi, A., Allevato, E., Rita, A., Todaro, L., Saracino, A., Chirico, G.B. 2018. Hydrodynamic behaviour of European black poplar (Populus nigra L.) under coppice management along Mediterranean river ecosystem. River Res. Appl., 34(6), pp. 1-9. https://doi.org/10.1002/rra.3276.

Pavlovskii, N.N. 1931. On a design formula for uniform flow in channels with nonhomogeneous walls. Trans. All-Union Sci. Res. Inst. Hydraulic Eng., 157-164.

Rowinski, P.M., Västilä, K., Aberle, J., Järvelä J., Kalinovska, M.B. 2018. How vegetation can aid in coping with river management challenges: A brief review. Ecohydrol. Hydrobiol., 8, pp. 345-354. https://doi.org/10.1016/j.ecohyd.2018.07.003.

Sarghini, F., De Vivo, A. 2017. Analysis of Preliminary Design Requirements of a Heavy Lift Multirotor Drone for Agricultural Use. Chem. Eng. Trans., 58, pp. 625-630. https://doi.org/10.3303/CET1758105.

Stone, B.M., Shen, H.T. 2002. Hydraulic resistance of flow in channels with cylindrical roughness. J. Hydraulic Eng., 128(5), pp. 500-506. https://doi.org/10.1061/(ASCE)0733-9429(2002)128:5(500).

Vargas-Luna, A., Crosato A., Uijttewaal, W.S.J. 2015. Effects of vegetation on flow and sediment transport: comparative analyses and validation of predicting model. Earth Surf. Proc. Land., 40(2), pp. 157-176. https://doi.org/10.1002/esp.3633.

Västilä, K., Järvelä, J. 2014. Modeling the flow resistance of woody vegetation using physically based properties of the foliage and stem. Water Resour. Res., 50, pp. 229-245. https://doi.org/10.1002/2013WR013819.

van Velzen, E., Jesse, P., Cornelissen, P., Coops, H. 2003. Stroming-sweerstand vegetatie in uiterwaarden; Handboek. Part 1 and 2. Technical Report, RIZA Reports, Arnhem, The Netherland.

Vinatier, F., Bailly, J.S., Belaud, G. 2017. From 3D grassy vegetation point cloud to hydraulic resistance: Application to close-range estimation of Manning coefficients for intermittent open channels. Ecohydrology, 10(8), e1885. https://doi.org/10.1002/eco.1885.

Yang, S., Wang, P., Lou, H., Wang, J., Zhao, C., Gong, T. 2019. Estimating River Discharges in Ungauged Catchments Using the Slope-Area Method and Unmanned Aerial Vehicle. Water 2019, 11 (11), 2361. https://doi.org/10.3390/w11112361.

Yang, W., Choi, S.-U. 2010. A two-layer approach for depth-limited open-channel flows with submerged vegetation. J. Hydraulic Res., 48(4), pp. 466-475. https://doi.org/10.1080/00221686.2010.491649.

Yen, B.C. 2002. Open channel flow resistance. J. Hydraul. Eng., 128(1), pp. 20-39. https://doi.org/10.1061/(ASCE)0733-9429(2002)128:1(20).

7. Sensitivity of flow resistance modeling to the uncertainty of non-submerged Phragmites australis Leaf Area Index derived by Digital Hemispherical Photography

The present Chapter is based on the following article:

- **Lama**, **G**.**F**.**C**. et al. 2020. Sensitivity of Ecohydraulic modeling to the uncertainty of Common reed Leaf Area Index derived by Digital Hemispherical Photography. *In preparation.*

7.1. Introduction

This Chapter aims at analyzing the sensitivity of Västilä & Järvelä model for the prediction of the flow resistance of vegetated streams (*Järvelä, 2004*; *Aberle & Järvelä, 2013*; *Västilä & Järvelä, 2014*) to *DHP* processing uncertainty in determining *LAI* of 2 m high Common reed plants' stands. A field campaign was carried out inside a study area 20 m x 20 m located in a vegetated riverine floodplain, covered for almost its entire extension by 2 m high rigid Common reed plants. The field campaign aimed at evaluating the accuracy of *DHP* processing in predicting *LAI* comparing them with the direct and the *LI-COR*-derived *LAI* (hereinafter referred to as *L*) by considering 187 *DHPs*. The Västilä & Järvelä model was calibrated based on the results of field hydraulic experiments performed inside a vegetated reclamation channel colonized by mature emergent Common reed plants (*Errico et al., 2019*). The sensitivity of water flow average velocity U ($m \cdot s^{-1}$) to the uncertainty of the *DHP*-derived *LAI* was evaluated according to a functional perspective.

7.2. Materials and methods

7.2.1. Västilä & Järvelä model for emergent mature Common reed stands

According to most experimental studies (*Fathi-Moghadam & Kouwen, 1997*; *Järvelä 2002*; *Järvelä, 2004*; *Aberle & Järvelä, 2013*), it has been observed a linear relationship between *LAI* and vegetative Darcy-Weisbach friction factor $f'' = 4 \cdot \overline{C_D} \cdot A_{p_0}/A_B$, where $\overline{C_D}$ is the bulk drag coefficient and A_{p_0} (m^2) and A_B (m^2) are respectively the frontal projected area in still air (*Armanini et al., 2005*) and the channel's bottom surface area. For non-submerged mature Common reed stands, it is possible to consider $\frac{A_{p_0}}{A_B} \equiv LAI$, thus $f'' = 4 \cdot \overline{C_D} \cdot LAI$. The Manning's n hydraulic roughness coefficient of vegetated open channels can be expressed as a function of the vegetative friction factor f'', as follows:

$$n = R^{\frac{1}{6}} \cdot \sqrt{\frac{f''}{8 \cdot g}}, \tag{7.1}$$

where g (m·s^{-2}) is the gravity acceleration and R (m) is the hydraulic radius, given by the ratio between the water flow cross sectional area σ (m^2) and the wetted perimeter χ (m). Under these assumptions, U (m·s^{-1}) can be expressed as follows:

$$U = \frac{1}{n} \cdot R^{\frac{2}{3}} \cdot \sqrt{J}, \tag{7.2}$$

Then, combining Eq. (7.1) and Eq. (7.2), the new expression of U becomes the following:

$$U = \sqrt{\frac{2 \cdot g}{C_D \cdot LAI}} \cdot R \cdot J. \tag{7.3}$$

7.2.2. Field LAI determinations

A field campaign was conducted inside a study area 20 m x 20 m for retrieving direct and indirect *LAI* (Fig. 34a), located on the orographic left bank of a 700 m long vegetated reclamation channel situated in a riverine floodplain, aiming at estimating the accuracy of *DHP* processing in predicting the *LAI* of low riparian plants' stands. The entire study area was almost completely covered by 2 m high *Phragmites australis (Cav.)* Trin. ex Steud. (Common reed) plants. Only a small percentage of its surface (11%) was covered by *Alnus glutinosa A (L.)* Geartn. trees, also known as black alder (Fig. 34b-c). The field campaign took place in the period June - August (2018) since in other seasons the study area is generally flooded and thus inaccessible.

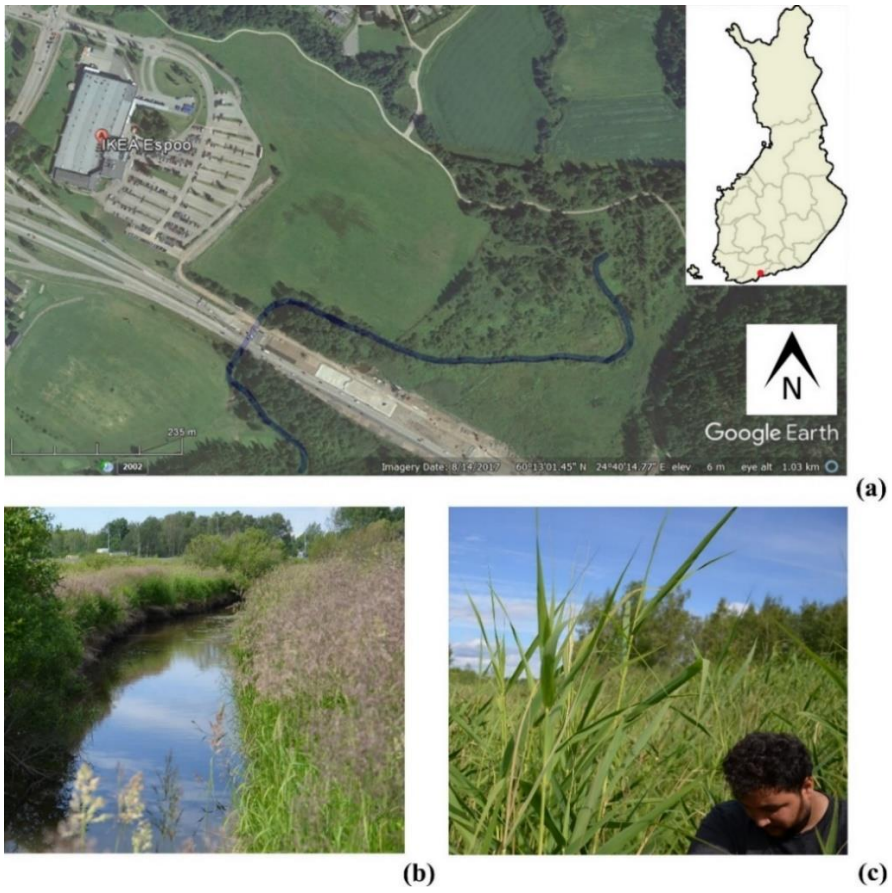

Fig. 34. (a) Aerial view of the entire riverine floodplain. (b) Vegetated drainage channel and (c) Investigated Common reed plants' stand.

In order to compare the examined direct and indirect methods employed for assessing *LAI* of the Common reed plants, ten measuring points were uniformly selected across the whole study area 20 m x 20 m, aiming at extending the analysis to the entire area. First, *LAI* was retrieved by means of *LI-COR* device (*L*) and *DHP* processing methodologies, and then the riparian vegetation samples were uniformly harvested from the study area for obtaining direct *LAI* measurements at laboratory (hereinafter referred to as *D*).

(a)

(b)

Fig. 35. (a) Aerial view of the study area 20 m x 20 m (red square). (b) Picture of Common reed stands covering the study area.

The 10 riparian vegetation samples can be considered representative of the whole Common reed plants' stand since the riparian vegetation distribution at field can be assumed as uniform, including the 0.30 - 0.40 m high *Phalaris aquatica* (bulbous canary-grass), an invasive herbaceous species highly diffuse in riparian habitats. The assumption of the statistical significance of the ten *LAI* measurements with respect to the whole study area 20 m x 20 m will be demonstrated in the next paragraphs, by employing a two-sample *T-test* (p = 0.05) for the differences of the *L* mean values. Other 200 measuring points were selected in the same study area 20 m x 20 m (Fig. 35a-b), aiming at comparing *L* and *DHP*-derived *LAI*, according to a measuring grid characterized by meshes having a spacing of 1 m and 2 m in the E-W and the S-N directions, respectively. A subset of 23 measuring points was excluded from the analyses after it was verified that *L* values were affected by the black alder dominating the canopy structure of the lower Common reed

plants' stands. Then, both *L* and *DHP*-derived *LAI* were computed at just the 177 remaining measuring points.

7.2.2.1. Field indirect *LAI* determinations

Indirect LAI by DHP processing

Due to the lack of studies dealing with *DHP* processing for determining *LAI* of low riparian plants, the tuning of the most suitable *DHP* acquisition system was crucial for the main purpose of the present study. The majority of studies and reviews on *DHP* processing was essentially focused on tall trees of forestry interests (e.g. *Chianucci & Cutini, 2012*; *Glatthorn & Beckschäfer, 2014*; *Oirgo et al., 2017*), in which the distance from the sensor and the top of the canopy is two - or even three - order of magnitude higher than in the present study case, or in agricultural studies, in which the influence of distinct surrounding plants is null or, at most, neglecting (e.g. *Demarez et al., 2008*). In this study, then, we employed a SONY® NEX-7 mirrorless camera, in combination with a Lensbaby® Circular Fisheye E-mount lens, having an *AOV* of 185°. This specific lens was specifically selected because of its very low minimum focusing distance, equal to 6.35 mm, extremely appropriate for the examined 2 m high Common reed plants.

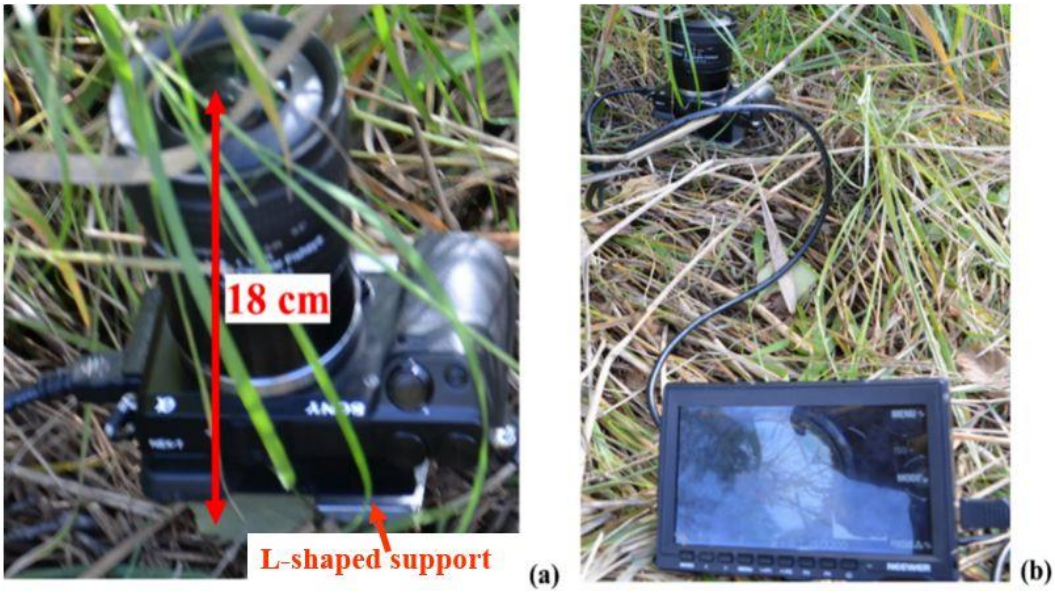

Fig. 36. (a) Camera+lens system on the L-shaped steel support. (b) External HD monitor.

The camera+lens system (Fig. 36a) was employed under an upward-facing configuration, in order to guarantee the verticality of the system itself. Moreover, it was fixed on a L-shaped steel support aiming at ensuring its stability and the perfect horizontal position of the lens. According to this set-up, the system was not able to include in its Field-Of-View (*FOV*) the portion of plants below the lens top, which was located 18 cm above the ground. A remote controller and an external HD monitor (Fig. 36b) were employed for shooting the *DHP*s at a minimum distance of 5 m from the target, aiming at excluding from the *DHPs* the external elements to the lens' view. The *DHP*s, which resolution was equal to 3008 x 2000 pixels, were acquired under uniform sky conditions in order to contain the uncertainties related to the sunlight fluctuations occurring during the day, and

they were successively processed according to two different strategies of spatial analysis: single and ensemble-based *DHP* analyses.

Single DHP analysis

All the single *DHP*s were binarized by applying two different methods: the iterative automatic IsoData algorithm and the global threshold method (*Leblanc et al., 2005*). *LAI* retrieved from IsoData algorithm is hereinafter indicated as F_A. The global threshold method attributed a black colour to *DHP* pixels with brightness in the blue wavelength region (320 - 490 nm), in which the recorded light scattering from leaves is minor (*Fournier & Hall, 2017*), below a user-defined given threshold value of the Digital Number, hereinafter referred to as *DN*. In image processing, the *DN* is a variable assigned to each image pixel, usually in the form of a binary integer included in the range of 0 - 255 (i.e., a byte). Thus, the range of the reflectance is partitioned into 256 bins. To any single pixel may be assigned several *DN* values, for different recorded bands. In the present study, the global threshold method was applied by considering three increasing *DN* values: 100, 150 and 200. A MATLAB® script (*Korhonen et al., 2011*) was employed for calculating the canopy gap fraction in the binarized *DHP*s, defined as the amount of open area within the canopy (*Weiss et al., 2004*). The *LAI* values derived from global threshold method were indicated as F_{100}, F_{150} and F_{200}, respectively.

Ensemble-based DHP analysis

As already introduced, the software allows the user to perform manual masking instead of the MATLAB® script, based on fixed threshold values of the *DN* of the whole *DHP*s. Another distinction between the two spatial analysis approaches lied in the capability of CAN_EYE of being able to consider different orientations and light exposures because it analyses more than one *DHP* a time. The 177 measuring points were re-grouped into 20 *ESU*s, defined by considering the closest measuring points falling into a cell 8 m x 2 m, representing the C_1 and C_2 maps of the study area 20 m x 20 m (Fig. 37a-b): the 15 *ESU*s named with numbers from 1 to 15 included 8 points, the 4 *ESU*s ranging from 16 to 19 included 11 points, and *ESU* number 20 included 13 points.

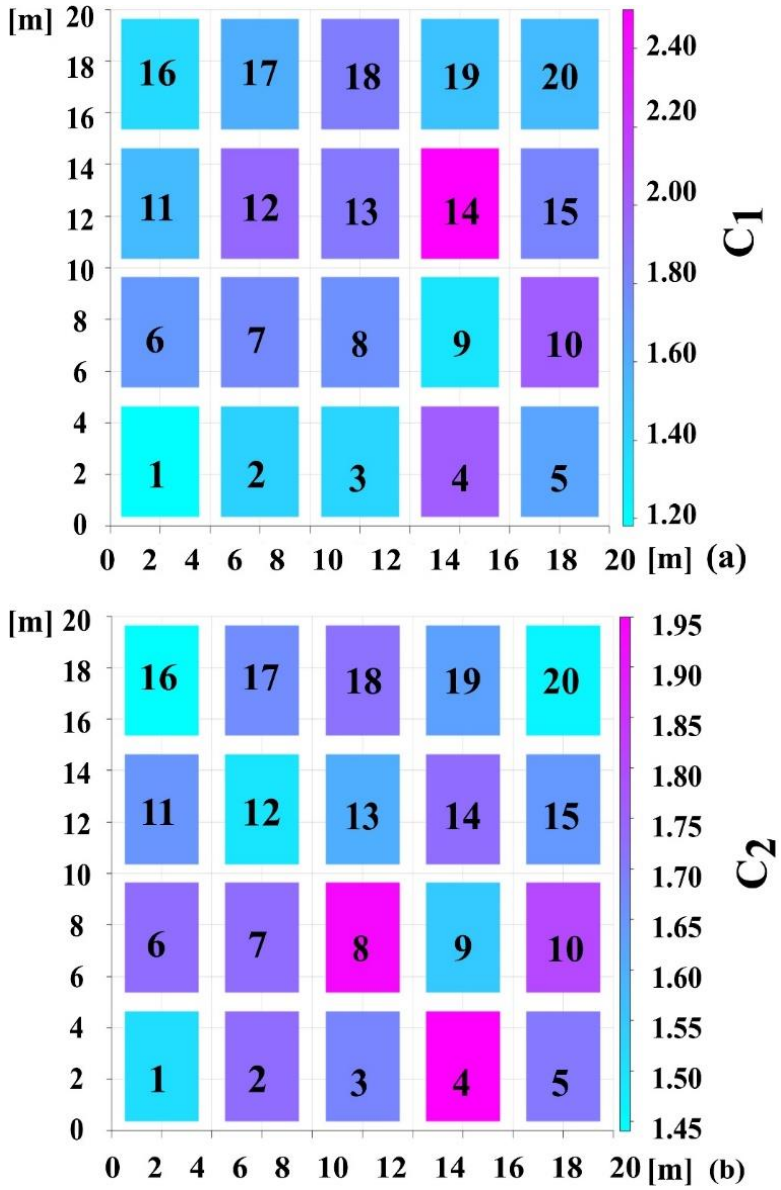

Fig. 37. (a) C_1 and (b) C_2 maps referred to the study area 20 m x 20 m.

LI-COR-derived LAI

The *LI-COR* portable device measures the attenuation of the diffusive sky radiation at five zenith angles simultaneously, considering the above- (*LI-COR*$_A$) and the below- (*LI-COR*$_B$) canopy pair readings at the same plant, for calculating the transmittance. The sensor projects the image of its nearly hemispheric view onto 5 sensors arranged in concentric rings, and 5 transmittances are then calculated by diving *LI-COR*$_A$ and *LI-COR*$_B$ corresponding pairs. In the present study, the *LI-COR* device was employed in a "one sensor mode" condition, particularly indicated for low plants. It has required the use of just one device to be employed both as trigger and receiver. A 90° black view cap was placed on the optical sensor for reducing the presence of the operator into the sensor's *FOV*. As for the *DHP*-derived *LAI*, it was possible retrieving the *L* values both at the 10 sampling points and at the original 200 measuring points of the study area 20 m x 20 m. The following Figure 38 shows a colour map representing the *L* values inside the study area 20 m x 20 m. As mentioned in the previous Section, 23 measuring points were

excluded by the analyses after it was verified that *L* values were inevitably affected by black alder trees dominating the surrounding lower Common reed plants.

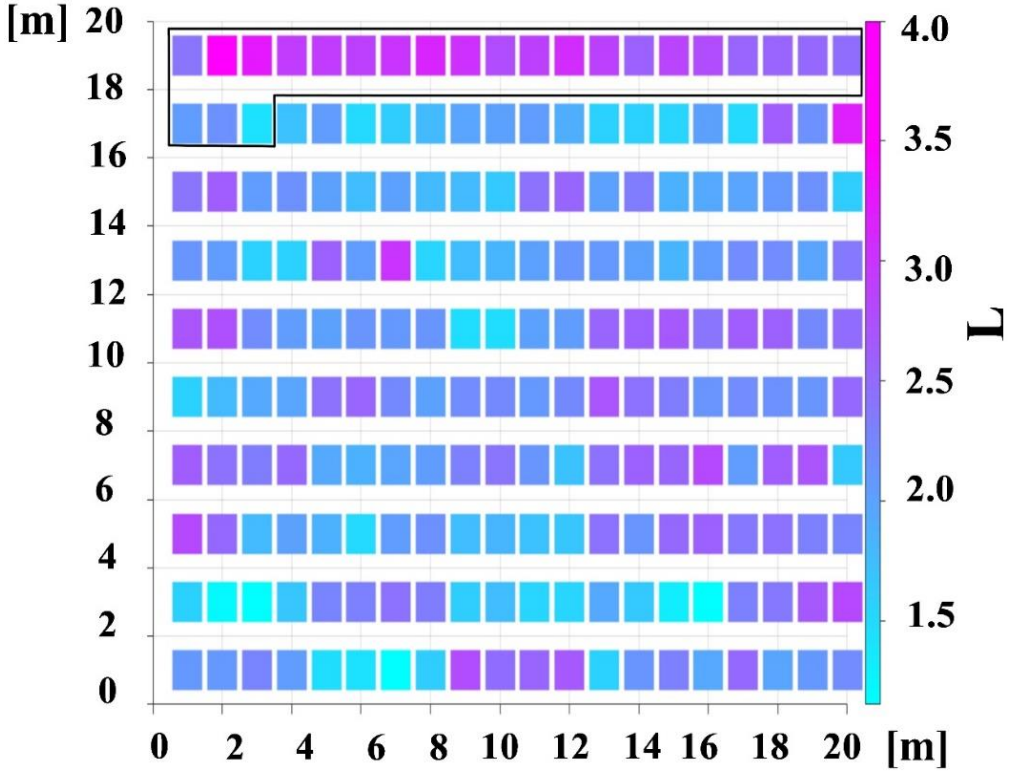

Fig. 38. *L* map of the examined study area 20 m x 20 m. The black continuous line represents the borders of the 23 excluded measuring points, representing the *L* of the black alder trees.

7.2.2.2. Direct LAI derived from harvested riparian vegetation samples

Ten Common reed samples were uniformly collected from the study area 20 m x 20 m (Fig. 39a) by placing on the ground a reference PVC circular frame with a diameter of 15 cm (Fig. 39b), having a cross sectional area A_{Ref} = 176.71 cm^2, and harvesting for all its height the whole riparian vegetation falling inside. The 10 samples were analyzed for carrying out direct *LAI* measurements (*D*).

As shown in Table 7, the wet-weights exhibited a small variability, with an average value of 29.7 g, and a standard deviation of 4.6 g. The harvested riparian vegetation samples were then laid on a horizontal whiteboard, and 10 HD pictures - each for every analyzed riparian vegetation sample - were acquired by a NIKON® D5100 camera, mounted on a tripod at a fixed height of 1.80 m above the floor. The camera sensor exposure was managed by accurately checking the single HD histograms (i.e. number of pixels of a certain value of brightness) - ranging from black (0% brightness) to white (100% brightness) - directly on an external portable HD monitor connected to the camera. The acquisition system was carefully oriented to reduce the HD distortion by choosing as fixed reference a grid composed of 54 black crosses regularly distributed on the horizontal whiteboard. Each black cross corresponded to a measured area of 0.36 cm^2.

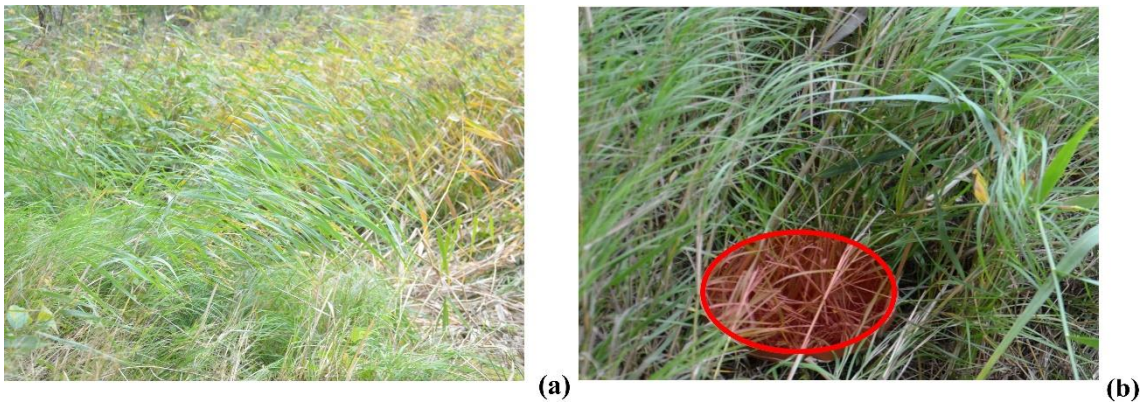

(a) (b)

Fig. 39. (a) View of the vegetation sampling area. (b) Example of harvested vegetation samples, falling inside the PVC circular frame, indicated in the figure by the red ellipse.

Each of the 10 riparian vegetation samples harvested was wrapped by a double layer of greaseproof paper for maintaining its original wetness at field, and then stored in a refrigerator at a fixed room temperature of 4°C, after being weighted utilizing a system of precision digital scales. It was observed that the riparian vegetation samples were composed for the 89% of their weight by 2 m high reed, and for the remaining 11% by 30 - 40 cm high bulbous canary-grass. The wet-weights of the harvested riparian vegetation samples are summarized in the following Table 7.

Tab. 7. Wet-weights of the 10 riparian vegetation samples harvested at field.

Sample	Wet-weight (g)
1	29.6
2	21.0
3	31.0
4	20.3
5	27.0
6	30.3
7	31.1
8	26.9
9	27.0
10	35.5

Firstly, the HD images acquired at laboratory were binarized by employing the IsoData algorithm (*Ridler, 1978*), implemented in the freeware image processing software ImageJ (available at *https://www.imagej.net/Downloads*); then, we computed the number of black pixels referred to each HD image corresponding to the riparian vegetation elements and thus, given the size of each pixel based on the HD image resolution equal to 2646 x 4216 pixels, the total black area was easily computed. It was then reduced by the area of the black crosses visible in each HD image to obtain the total black area corresponding to the

riparian vegetation elements, hereinafter referred to as A_{HD}. Thus, the *D* values, representative of all the riparian plants falling inside the PVC circular frame for each of the 10 samples, were then calculated as follows, in order to characterize the entire green volume of the riparian vegetation samples:

$$D = \frac{A_{HD}}{A_{Ref}}. \quad (7.4)$$

7.2.3. Comparative analyses of direct and indirect LAI methods

Different comparative analyses were performed for evaluating the accuracy of *DHP*-derived *LAI* of the 2 m high Common reed plants. The performances of linear regression methods were tested for obtaining simple mathematical relations between the outcomes of the examined direct and indirect methods. First, a comparison of direct (*D*) and indirect (*LI-COR* and *DHP* processing) methods for assessing *LAI* was carried out, based on the 10 riparian vegetation samples, uniformly harvested across the study area 20 m x 20 m. It has confirmed the high level of correlation existing between *D* and *LI-COR*-derived *LAI* observed in many previous works on low plants. Then, the *DHP*-derived *LAI*, based on the two different strategies of spatial analysis (single *DHP* and ensemble-based *DHP*) were compared with *LI-COR*-derived *LAI*, respectively indicated with *L* for the single *DHP* analysis, and with L_m, representing the average *L* of all the measuring points falling into each of the 20 *ESU*s individuated for the ensemble-based *DHP* analysis. The variabilities of *L* values in each of the 20 *ESU* individuated in the present study are shown in the following Figures 40a-b.

As depicted in Figure 40a, *L* exhibited different variabilities depending on the selected *ESU*; in some cases (*ESU* 5, *ESU* 10, *ESU* 11, *ESU* 14 and *ESU* 15), they seem to be far from the be normally distributed, but, in all the examined cases, the Coefficients of Variations (*CV*), calculated as the ratio between the standard deviation and the average *L* value in each *ESU*, are very low - at most equal to 0.35 for *ESU* 5 - as indicated in Figure 40b. Hence, in the present study, it was considered acceptable employing the average *L*, hereinafter indicated as L_m, for characterizing the *LI-COR*-derived *LAI* of each *ESU*.

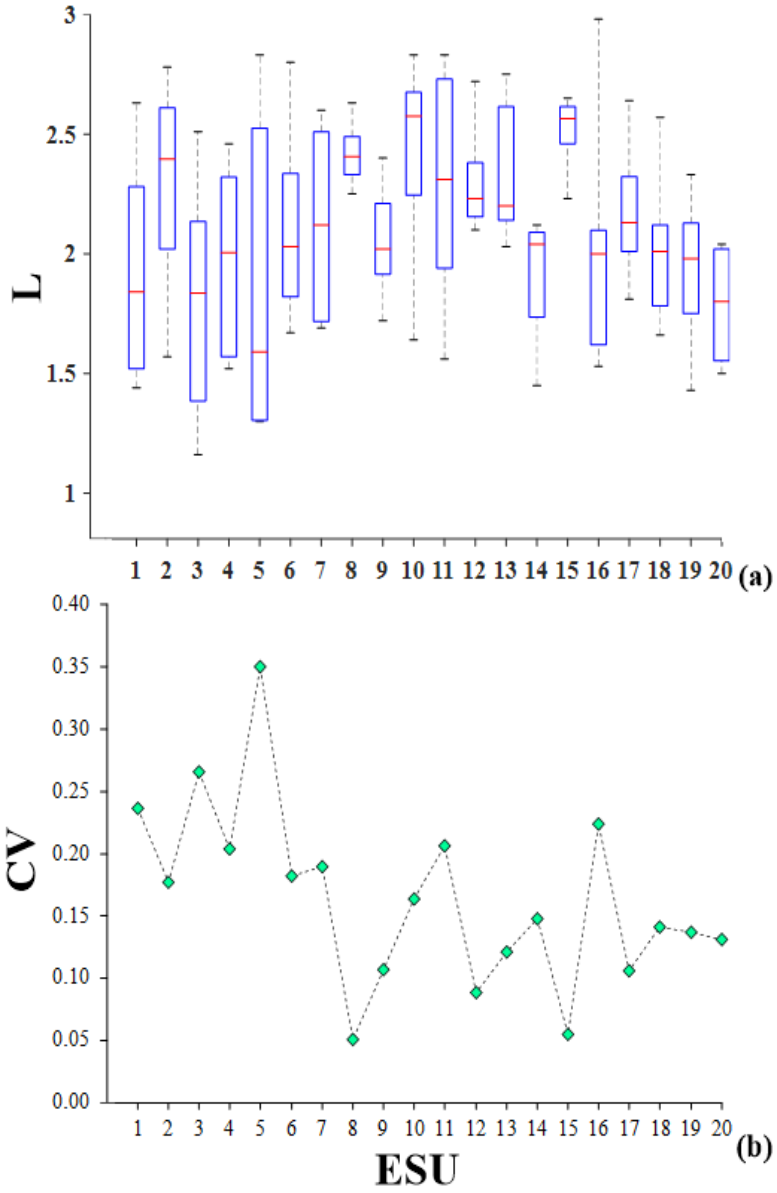

Fig. 40. (a) *L* and (b) *CV* variability ranges for each *ESU*.

7.2.4. Accuracy of direct and indirect LAI methods

The *BIAS* and the *RMSE* of each method were computed to quantitatively compare the accuracy of the direct and indirect *LAI* methods, according to the following expressions:

$$BIAS = \frac{1}{N}\sum_{i=1}^{N}(y_i - x_i) \tag{7.5}$$

$$RMSE = \sqrt{\frac{1}{N}\sum_{i=1}^{N}(y_i - x_i)^2}\,, \tag{7.6}$$

where x_i and y_i indicate respectively the predictionary and response variables of each comparative analysis, represented by *D* and *L* for the comparison based on the 10 harvested riparian vegetation samples, while by *D* and F_A, F_{100}, F_{150} and F_{200} for the single

DHP analysis, and by L_m and C_1 and C_2, for the ensemble-based *DHP* analysis. In this final case, L_m was selected as predictionary variable owing to the high correlation existing between *D* and *L* in low plants (i.e., *Sonnentag et al., 2007*; *Lopez-Lozano & Casterad, 2013*), confirmed in this study.

7.2.5. Sensitivity analysis of Västilä & Järvelä model to DHP-derived LAI uncertainty

In the following analysis, the only F_{200} was considered as *DHP*-derived *LAI*, given the higher accuracy exerted by this binarization method in predicting the actual *LAI* of the examined Common reed stands. The uncertainty of the average flow velocity *U* (σ_U) predicted by Västilä & Järvelä model due to the uncertainty of F_{200} (σ_{LAI}) can be evaluated as follows:

$$\sigma_U{}^2 = \left(\frac{\partial U}{\partial LAI}\right)^2 \cdot \sigma_{LAI}{}^2, \tag{7.7}$$

where $\frac{\partial U}{\partial LAI}$ is the partial derivate of *U* with respect to *LAI*, represented by *DHP*-derived *LAI*, and σ_{LAI} obtained from the comparative analysis of F_{200} with *L*. Thus, it is possible to express Eq. (7.7) according to the following:

$$\left.\frac{\sigma_U}{U}\right|_{\sigma_{LAI}} = \frac{1}{2} \cdot \frac{\sigma_{LAI}}{LAI}. \tag{7.8}$$

7.3. Results and discussion

7.3.1. Comparison of direct and indirect LAI methods

The direct (*D*) and indirect (*L*, F_A, F_{100}, F_{150} and F_{200}) *LAI* referred to the 10 vegetation samples are summarised in Table 8:

Tab. 8. Direct and indirect *LAI*, referred to the 10 harvested Common reed samples, with relevant statistics

Sample	*D*	*L*	F_A	F_{100}	F_{150}	F_{200}
1	1.93	2.19	1.40	1.58	1.38	1.84
2	1.85	2.07	1.49	1.48	1.68	1.94
3	2.22	2.47	1.50	1.49	1.78	2.22
4	2.00	1.76	1.19	1.17	1.35	1.52
5	2.56	2.66	1.39	1.82	2.23	2.52
6	1.83	1.76	1.20	1.18	1.39	1.64
7	2.74	3.03	1.74	1.69	2.03	2.52
8	2.06	2.25	1.49	1.46	1.66	1.92
9	1.90	2.15	1.42	1.54	1.81	2.00
10	2.20	2.42	1.70	1.73	1.96	2.21
Min	1.83	1.76	1.19	1.17	1.35	1.52
Max	2.74	3.03	1.74	1.82	2.23	2.52
Mean	2.13	2.28	1.45	1.51	1.73	2.03
St. Dev.	0.31	0.38	0.18	0.21	0.30	0.33
BIAS	-	-0.03	-0.62	-0.56	-0.35	-0.04
RMSE	-	0.06	0.36	0.20	0.14	0.07

It can be noticed from Table 8 that *L* and F_{200} can better reproduce *D* compared with the other examined methods. They exhibit two low *BIAS*, respectively equal to -0.03 and -0.04. More in detail, they both tend to underestimate *D* (Fig. 41).

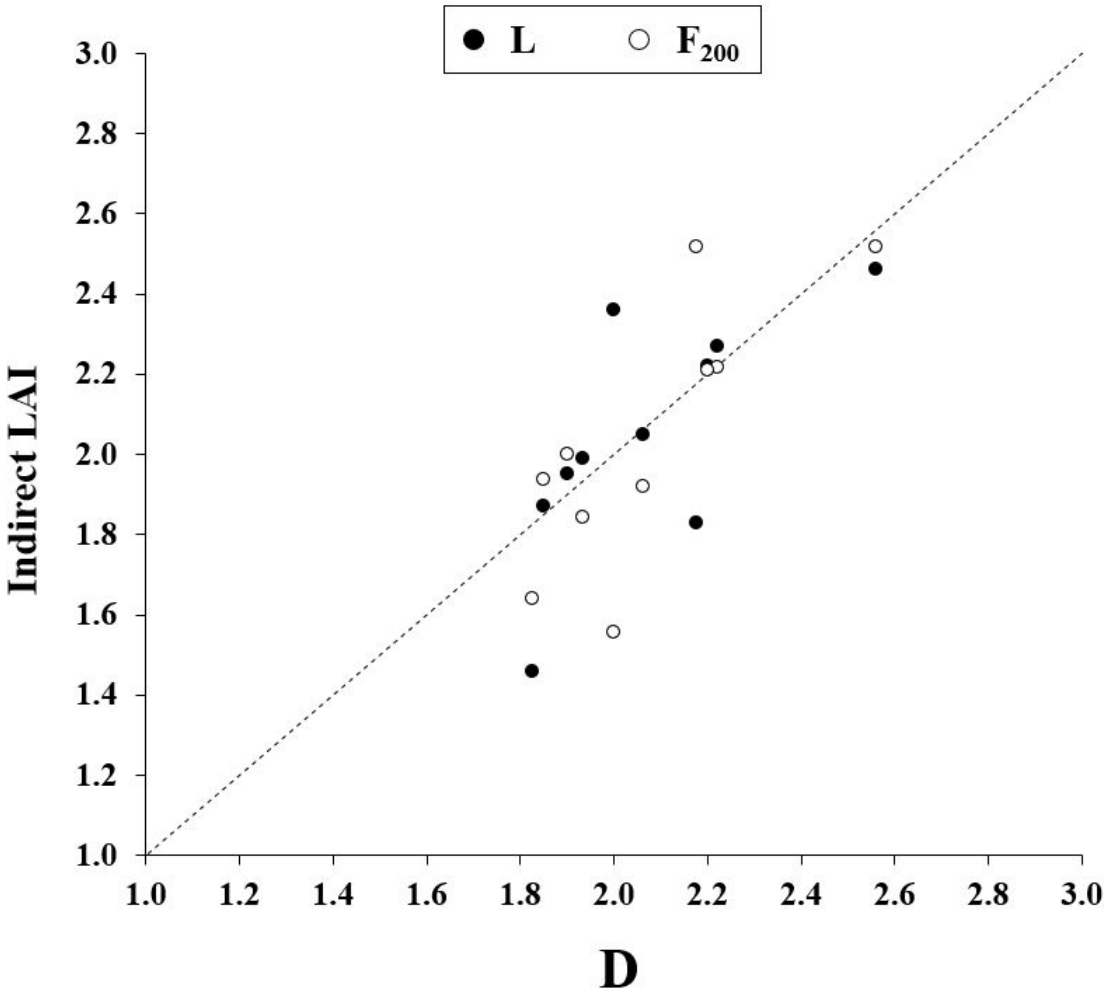

Fig. 41. Comparison of *D* with *L* and F_{200}, respectively indicated with black and white dots. The dashed line indicates the perfect agreement between response and predictionary variables.

7.3.1.1. Comparison of single DHP- and LI-COR-derived LAI

The *L* of the 177 measuring points are characterized by a mean and a standard deviation respectively pair to 2.10 and 0.40. The statistical significance of the 10 uniformly distributed *L* values with respect to the whole study area was already confirmed by the two-sample *T-test* for the differences ($p = 0.05$) of the average *L*, respectively indicating the two samples composed respectively by 10 and 177 data.

Due to the very high correlation observed between *D* and *L*, and aiming at optimizing the measuring time at filed, it was possible considering L measurements as reference to be compared to *DHP*- derived *LAI*. The dataset obtained by the sum of the 177 points of the study area 20 m x 20 m and the 10 riparian vegetation sampling points were grouped together to individuate a linear regression model by applying the Ordinary Least Square method (*OLS*) for better evaluating the accuracy of F_{200} estimations (Fig. 42):

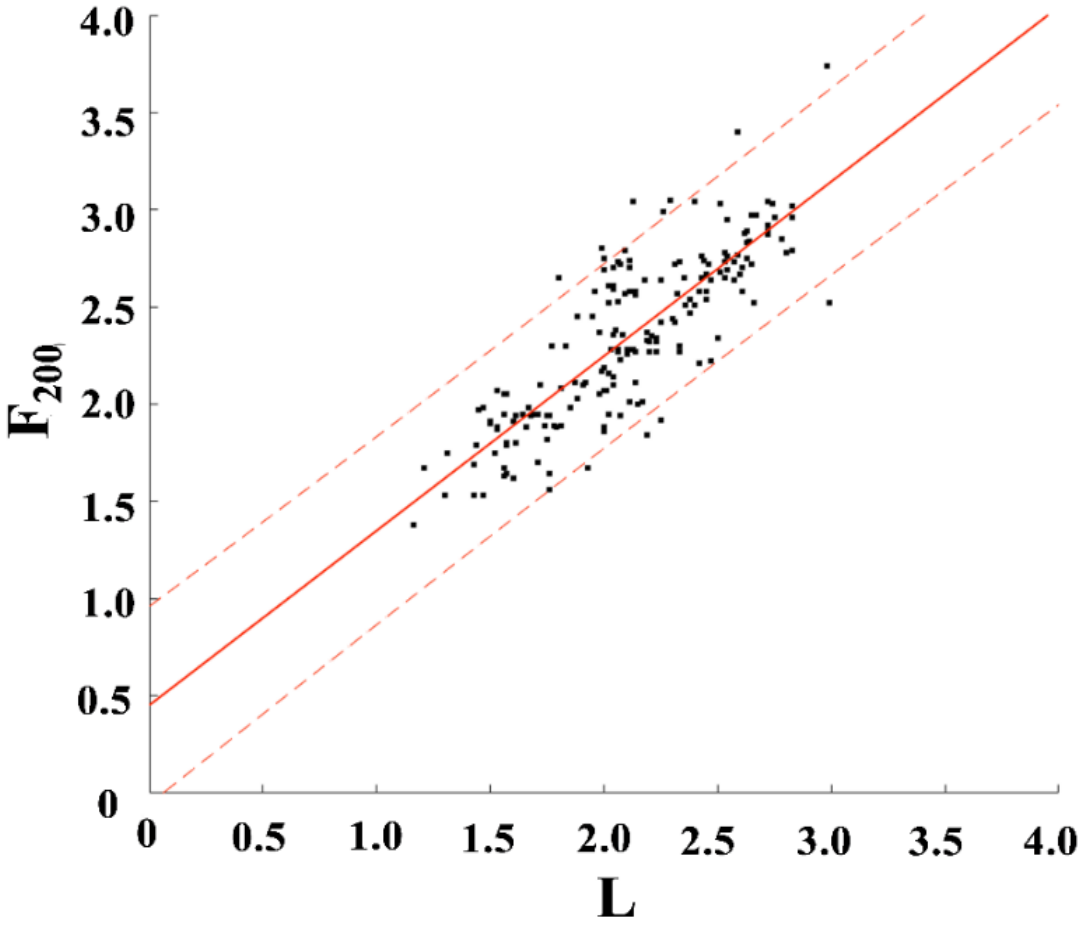

Fig. 42. Linear regression by *OLS* (continuous orange line) between L and F_{200} with prediction bounds corresponding to 95% percentile (dashed orange curves).

The linear law individuated between L and F_{200} is expressed according to the following equation:

$$F_{200} = \alpha \cdot L + \beta, \tag{7.10}$$

where α and β are the coefficients of the *OLS*. The two parameters α and β, with in brackets lower (5%) and upper (95%) percentiles of the prediction bounds, the Coefficient of Determination (R^2) and the Root Mean Square Error (*RMSE*) were summarized in the following Table 9:

Tab. 9. Parameters of the *OLS* regression between L and F_{200} referred to a dataset composed of the sum of the 177 measuring points and the 10 sampling points selected across the entire study area 20 m x 20 m.

α	β	R^2	RMSE
0.90 (0.81 - 0.98)	0.45 (0.267 - 0.66)	0.69	0.23

7.3.1.2. Comparison of ensemble-based DHP- and LI-COR-derived LAI

The following Figure 43 shows the comparison of C_1 and C_2 with L_m, referred to the 177 measuring points of the study area 20 m x 20 m:

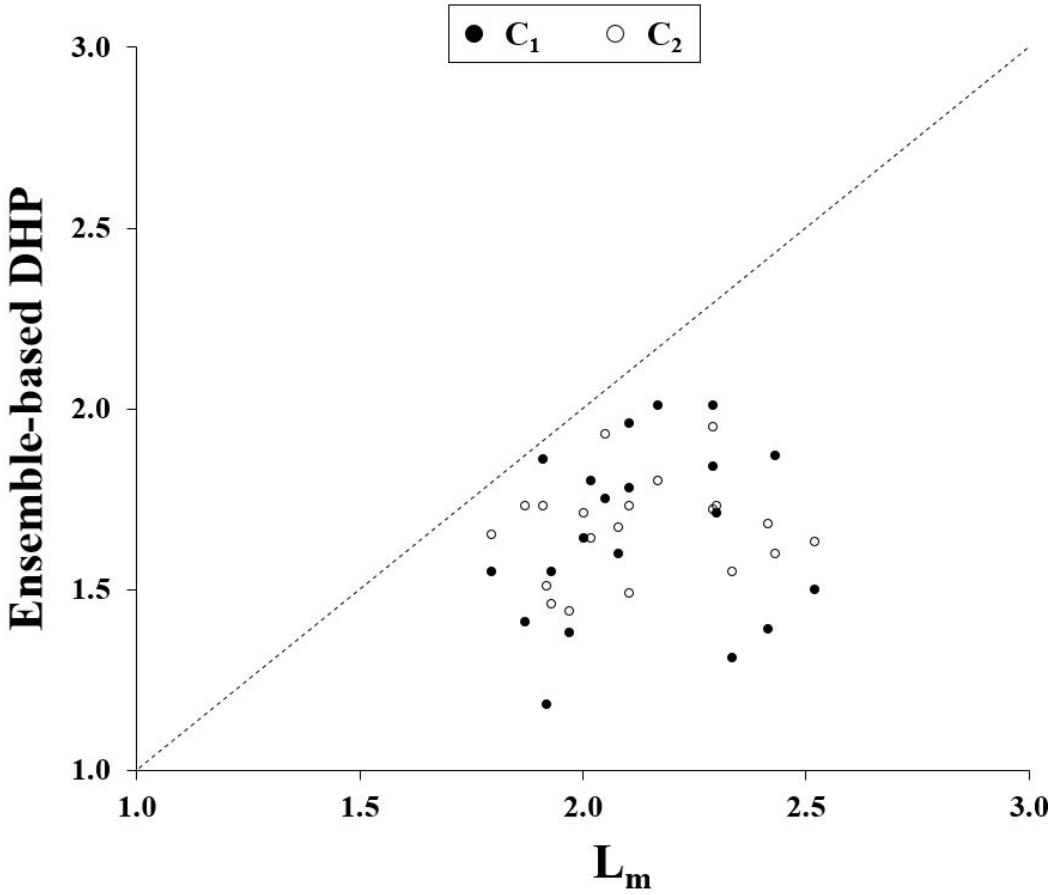

Fig. 43. Comparison of L_m with C_1 and C_2, indicated with black and white dots, respectively. The dashed line indicates the perfect agreement between response and predictionary variables.

The comparisons between C_1 and C_2 with L_m were extremely similar in terms of *BIAS* (equal to -0.46 and -0.44) and *RMSE* (equal to 0.20 and 0.17). It can be easily observed from the analysis of the *BIAS*, that both C_1 and C_2 tended to underestimate L_m. The only remarkable difference can be observed in the standard deviation (0.24 and 0.14 respectively), which highlighted a higher sensitivity of C_1 to the variability of L_m than C_2. This spread can lie into the two assumptions made by CAN_EYE; in fact, the software does not impose any constraint on the *ALA* for the computations of C_2 while the C_1 is constrained to a value of leaf angle equal to 60° ± 30°. It consequently leads to a reduction in the influence of taller vegetation covering the lower Common reed falling out of the 57° limit ring.

7.3.2. Sensitivity analysis of U to DHP-derived LAI uncertainty

The normalized sensitivity of the uniform water flow velocity *U* estimated with Västilä & Järvelä model to the uncertainty of F_{200} is illustrated in the following Figure 44:

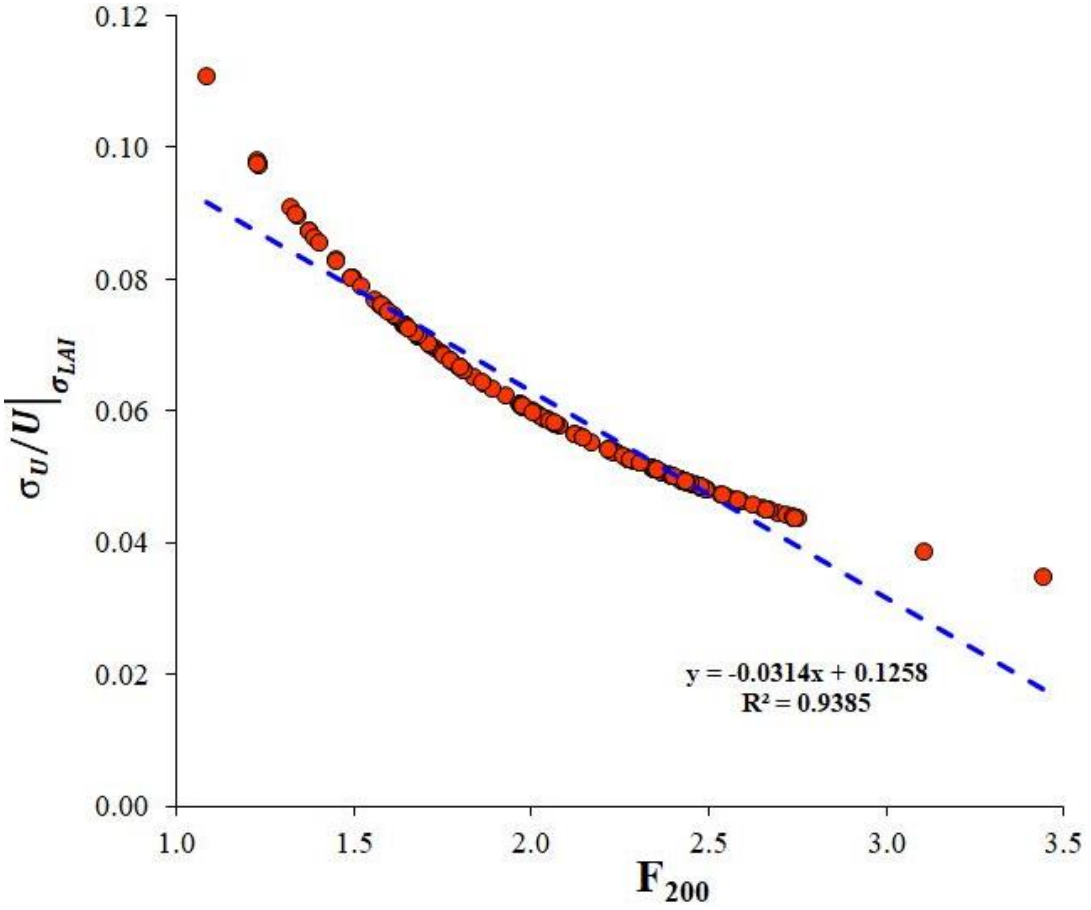

Fig. 44. Normalized sensitivity of uniform water flow velocity U $\left(\frac{\sigma_U}{U}\Big|_{\sigma_{LAI}}\right)$ estimated with Västilä and Järvelä model to the uncertainty of F_{200}.

It is easy to observe from Figure 44 that $\frac{\sigma_U}{U}\Big|_{\sigma_{LAI}}$ was equal at most to approximately 11%. This value is extremely comparable to the uncertainty affecting the measurements of water flow velocity acquired directly at field. Moreover, for low F_{200} values it reaches higher values than for high F_{200}; this is probably imputable to the fact that the model is not applicable for such low *LAI* values.

7.4. Conclusions

By comparing *L* with *D* for the 10 Common reed samples uniformly harvested across the study area 20 m x 20 m, it was possible to observe that *D* tended to be slightly underestimated by *L* (*BIAS* = -0.03). This was most probably imputable to the differences in the assessment of *LAI* between the two methods: in fact, in *D* the entire sample was considered, stem-by-stem ordinated on the white background floor, while for *L* it was considered the plant distribution directly in the field, in which two or more stems can be covered by others and the corresponding *LAI* can be influenced by this phenomenon, also known as "clumping effect". The same evidences were highlighted by Sonnetag et al. (2007). In their study, the Authors compared the so-defined "true" shrub *LAI*, computed through a destructive riparian vegetation sampling method, to *LI-COR*-derived *LAI*, examining a dataset acquired in a precipitation-fed peatland located in the near Ottawa

(Canada). In the present study, we observed a higher accuracy than the one reported in Sonnetag et al. (2007). In fact, they obtained a value of *RMSE* = 0.38, while in this study we estimated a lower value of *RMSE*, equal to 0.21. Chianucci et al. (2015) noticed a similar trend, comparing the *LI-COR*-derived *LAI* to those measured directly from leaves harvesting in three species of isolated trees (*Juglans regia*, *Liquidambar styraciflua* and *Platanus orientalis*) individuated within several Italian urban forests, for a total of 9 leaf samples. On the other hand, F_{200} was determined from a *DHP* global threshold binarization of each vegetation sample. It can lead to improperly consider as black also those pixels that do not represent the Common reed plants. *L* tends to be underestimated by F_{200}. This is most probably related to the presence of the surrounding Black alder tall trees (> 2 m). In fact, unlike the *LI-COR* device algorithm, the global threshold binarization method cannot consider the actual attenuation of the diffusive sky radiation related to the canopy structure, but it can just account for the black or white pixels from a single DHP, without discerning between the low reed and the taller vegetation.

The two *LAI* retrieved employing CAN_EYE software, respectively indicated as C_1 and C_2, exhibit practically the same accuracy, expressed in terms of *BIAS* (-0.46 and -0.44) and both underestimated L_m. This latter aspect is in accordance with the results observed by Demarez et al. (2008), in which the Authors analyzed low (≤ 1 m high) canopy wheat and maize plants, considering C_1 as best L_m , whereas they observed a *RMSE* (= 0.46), that is 2 times higher than the one observed in this study (*RMSE* = 0.24). As remarked by the Authors, the main differences between C_1 and L_m could lead to the uncertainties in gap fraction measurements, not quantified neither on their own and in the present study. The same trend was highlighted by White & Young (2007) by comparing C_1 to *LI-COR*-derived *LAI* for four different mature crop types (*Alfalfa*, *Corn*, *Sorghum* and *Soy*) examined at three different times: two at diffuse - just after sunrise and just before sunset - and one at sunny sky illumination conditions. These results well demonstrated the existence of a trend of C_1 in underestimating the *LI-COR*-derived *LAI* for low plants (≤ 2 m high), as in the case of the 2 m high reed plants analyzed in the present study. It will be interesting to study more in detail the causes of this tendency, e.g. focusing more deeply on the gap fraction measurements.

This study has proved that *DHP* processing can be a simple and effective methodology for assessing *LAI* of low (1 - 2 m high) reed plants, a widespread plant that affects the water flow features of many riverine environments of the world (*Vargas-Luna et al., 2015*; *Errico et al., 2019*; *Lama et al., 2019*). The findings of the present study were obtained through a field campaign carried out within a study area 20 m x 20 m located inside a river floodplain, in the period June - August (2018). It was possible to confirm that *LI-COR* device guarantees outcomes comparable with *LAI* obtained directly from harvested samples, in agreement with previous analyses conducted on low plants (i.e. *Sonnentag et al., 2007*; *Lopez-Lozano & Casterad, 2013*). However, *LI-COR* cost is one order larger than *DHP* techniques.

Two different spatial analytical strategies were employed for the indirect determination of *LAI* by *DHP* processing: single *DHP* and ensemble-based *DHP* analyses. With the single *DHP* analysis, a strong linear correlation was found between *DHP* and *LI-COR*-derived *LAI*, after observing that the best value of the *DN* image pixels threshold to be considered in an automatic binarization is pair to 200. Concerning ensemble-based *DHP*

analyses, C_1 and C_2 were influenced by the taller trees dominating the reed canopy, as also observed by other studies conducted on manmade monocultures (e.g., *Demarez et al., 2008*). An improvement to this aspect can be achieved by operating an accurate evaluation of the clumping effect, coupling *DHP* processing with remote sensing techniques, based on the acquisition of images characterized by high spatial resolution (i.e., *Niedzielski et al., 2016*; *Sarghini & De Vivo, 2017*; *Martone et al., 2020*).

In conclusion, it is possible to assess that *DHP* image processing methods can be effectively applied for estimating *LAI* to be employed in prediction models of the hydraulic resistance of vegetated open channels covered by rigid Common reed plants' stands (e.g., *Lama et al., 2020*). Moreover, the present study also revealed the need for realizing further field campaigns, aiming at analyzing a wider range of riparian vegetation species and a larger spectrum of hydraulic and vegetative field conditions.

References

Aberle, J., Järvelä, J. 2013. Flow resistance of emergent rigid and flexible floodplain vegetation. J. Hydraul. Res. 51(1), pp. 33-45. https://doi.org/10.1080/00221686.2012.754795.

Armanini, A., Righetti, M., Grisenti, P. 2005. Direct measurement of vegetation resistance in prototype scale. J. Hydraulic Res. 43(5), pp. 481-487.

Boothroyd, R.J., Hardy, R.J., Warburton, J., Marjoribanks, T.I. 2018. The importance of riparian plant orientation in river flow: implications for flow structures and drag. Journal of Ecohydraulics, 3:2, pp. 108-127. https://doi.org/10.1080/24705357.2019.1573648.

Caroppi, G., Västilä K., Järvelä, J., Rowinski, P.M., Giugni, M. 2019. Turbulence at water-vegetation interface in open channel flow: experiments with natural-like plants. Adv. Water Resour., 127, pp. 180-191. https://doi.org/10.1016/j.advwatres.2019.03.013.

Casas-Mulet, R., King, E., Hoogeveen, D., Duong, L., Lakhanpal, G., Baldwin, T., Stewardson, M.J., Webb, J.A. 2016. Two decades of ecohydraulics: trends of an emerging interdiscipline. Journal of Ecohydraulics, 1, pp. 1-29, http://dx.doi.org/10.1080/24705357.2016.1251296.

Chianucci, F., Cutini, A. 2012. Digital hemispherical photography for estimating forest canopy properties: current controversies and opportunities. iForest - Biogeosciences and Forestry, 5(6), pp. 290-295. https://doi.org/10.3832/ifor0775-005.

Chianucci, F., Ferrara, C., Pollastrini, M., Corona, P. 2015. Development of digital photographic approaches to assess leaf traits in broadleaf tree species. Ecological Indicators, 106, 105547. https://doi.org/10.1016/j.ecolind.2019.105547.

Demarez V., Duthoit, S., Baret, F., Weiss, M., Dedieu, G. 2008. Estimation of leaf area and clumping indexes of crops with hemispherical photographs. Agricultural and Forest Meteorology, 148, 644-655. https://doi.org/10.1016/j.agrformet.2007.11.015.

Errico, A., Lama, G.F.C., Francalanci, S., Chirico, G.B., Solari L., Preti F. 2019. Flow dynamics and turbulence patterns in a reclamation channel colonized by Phragmites australis (common reed) under different scenarios of vegetation management. Ecol. Eng. 2019, 133, pp. 39-52. https://doi:10.1016/j.ecoleng.2019.04.016.

Fathi Moghadam, M., Kouwen, N. 1997. Nonrigid, non-submerged vegetative roughness on floodplains. J. Hydraul. Eng., 123(1), pp. 51-57.

Fournier, R.A., Hall, R.J. 2017. Hemispherical Photography in Forest Science: Conclusions, Applications, Limitations, and Implementation Perspectives. In: Hemispherical Photography in Forest Science: Theory, Methods, Applications, pp. 287-302. Springer, Netherlands.

Glatthorn, J., Beckschäfer, P. 2014. Standardizing the Protocol for Hemispherical Photographs: Accuracy Assessment of Binarization Algorithms. PLoS ONE 9(11): e111924. https://doi.org/10.1371/journal.pone.0111924.

Järvelä, J. 2002. Flow resistance of flexible and stiff vegetation: A flume study with natural plants. J. Hydrology 269, pp. 44-54. https://doi.org/10.1016/S0022-1694(02)00193-2.

Järvelä, J. 2004. Determination of flow resistance caused by non-submerged woody vegetation. International Journal of River Basin Management, 2:1, pp. 61-70. https://doi.org/10.1080/15715124.2004.9635222.

Korhonen, L., Korpela, I., Heiskanen, J., Maltamo, M. 2011. Airborne discrete-return LIDAR data in the estimation of vertical canopy cover, angular canopy closure and leaf area index. Remote Sensing of Environment,115(4), pp. 1065-1080. https://doi.org/10.1016/j.rse.2010.12.011.

Lama, G.F.C., Errico, A., Francalanci, S., Chirico, G.B., Solari L., Preti F. 2019. Comparative analysis of modeled and measured vegetative Chézy's flow resistance coefficients in a reclamation channel vegetated by dormant riparian reed. Proceedings of the International IEEE Workshop on Metrology for Agriculture and Forestry, Portici, Italy, pp. 180-184. ISBN: 978-1-7281-3611-0.

Lama, G.F.C., Errico, A., Francalanci, S., Solari, L., Preti, F., Chirico, G.B. 2020. Evaluation of flow resistance models based on field experiments in a partly vegetated reclamation channel. Geosciences, 10(2), 47. https://doi.org/10.3390/geosciences10020047.

Leblanc, S.G., Chen, J.M., Fernandes, R., Deering, D.W., Conley, A. 2005. Methodology comparison for canopy structure parameters extraction from digital hemispherical photography in boreal forests. Agricultuiral and Forest Meteorology, 129, pp. 187-207. https://doi.org/10.1016/j.agrformet.2004.09.006.

Lopez-Lozano, R., Casterad, M.A. 2013. Comparison of different protocols for indirect measurement of leaf area index with ceptometers in vertically trained vineyards. Australian Journal of Grape and Wine Research, 19, pp. 116-122. https://doi.org/10.1111/ajgw.12005.

Martone, I., Gualtieri, C., Endreny, T. 2020. Characterization of Hyporheic Exchange Drivers and Patterns within a Low-Gradient, First-Order, River Confluence during Low and High Flow. Water, 12(3), 649. https://doi.org/10.3390/w12030649.

Niedzielski, T., Wytek, M., Spallek, W. 2016. Observing river stages using unmanned aerial vehicles. Hydrol. Earth Syst. Sci., 20, pp. 3193-3205. www.hydrol-earth-syst-sci.net/20/3193/2016/doi:10.5194/hess-20-3193-2016.

Origo, N., Calders, K., Nightingale, J., Disney, M. 2017. Influence of levelling technique on the retrieval of canopy structural parameters from digital hemispherical photography. Agricultural and Forest Meteorology, 237-238, pp. 143-149. http://dx.doi.org/10.1016/j.agrformet.2017.02.004.

Ridler, T.W. 1978. Picture thresholding using an iterative selection method. IEEE Transactions on Systems, Man, and Cybernetics, 8(8), pp. 630-632. https://doi.org/10.1109/TSMC.1978.4310039.

Sarghini, F., De Vivo, A. 2017. Analysis of Preliminary Design Requirements of a Heavy Lift Multirotor Drone for Agricultural Use. Chem. Eng. Trans., 58, pp. 625-630. https://doi.org/10.3303/CET1758105.

Sonnentag, O., Talbot, J., Chen, J.M., Roulet, N.T. 2007. Using direct and indirect measurements of leaf area index to characterize the shrub canopy in an ombrotrophic peatland. Agricultural and Forest Meteorology, 144, pp. 200-212. https://doi.org/10.1016/j.agrformet.2007.03.001.

Vargas-Luna, A., Crosato, A., Uijttewaal, W.S.J. 2015. Effects of vegetation on flow and sediment transport: Comparative analyses and validation of predicting models. Earth Surf. Proc. Land. 40 (2), pp. 157-176. https://doi.org/10.1002/esp.3633.

Västilä, K., Järvelä, J. 2014. Modeling the flow resistance of woody vegetation using physically based properties of the foliage and stem. Water Resour. Res. 4, 50, pp. 229-245. https://doi.org/10.1002/2013WR13819.

Weiss, M., Baret, F., Smith, G.J., Jonckheere, I., Coppin, P. 2004. Review of methods for in situ leaf area index determination Part II: Estimation of LAI, errors and sampling. Agricultural and Forest Meteorology, 121, pp. 37-53. https://doi:10.1016/j.agrformet.2003.08.001.

White, H.P., Young, E.R. 2007. Comparison of in situ LAI retrieval of two instruments for mature agricultural crops, Geomatics Canada, Technical Note 1. https://doi.org/10.4095/224133.

8. Summary and conclusion

The field experiments performed inside a reclamation channel colonized by mature and emergent Common reed stands, demonstrated the importance of analyzing the mean hydrodynamic and turbulent features directly at field scale, in order to develop more realistic theories and models of water flow resistance in real vegetated water bodies. The effects of different riparian vegetation management scenarios have been experimentally investigated to provide a contribution to understanding the impact of the riparian vegetation - water flow interactions on the hydrodynamics of vegetated open channels. The field experiments described in Chapter 5 focused on the analysis of the cross sectional distribution of water flow velocity and main turbulence features under three riparian vegetation management scenarios: abandoned riparian vegetation in undisturbed conditions; central cut of riparian vegetation as an example of gentle management practice, aiming at balancing the hydraulic efficiency and the water quality; and the total riparian vegetation removal. The analysis of these three scenarios showed that the hydraulic conveyance in the central cut scenario was comparable to that obtained in the total riparian vegetation removal scenario and that the side buffers of undisturbed riparian vegetation assured an adequate level of auto-purification to the entire vegetated reclamation channel. In Chapter 6, the vegetative hydraulic resistance coefficients for partial riparian vegetation cover, related to the central cutting scenario, were compared with those estimated by applying two predictive models proposed and validated for real riparian vegetation: Stone & Shen (2002) and Baptist et al. (2007). The accuracy of these two models was improved by considering the contribution of the different regions of the entire cross section to the global water flow resistance. To this aim, a methodology based on the analysis of the experimental isotachs and on the combination of the two predictive models with four composite cross section methods was proposed. The Horton method in combination with the Stone & Shen (2002) model leads to the highest accuracy. It also emerges that further improvements could be achieved by implementing two- or three-dimensional simulations, with Common reed stems represented by rigid cylinders. Further applications of this methodology could be carried out on datasets obtained by remote sensing techniques from *UAV*, to be employed for monitoring different riparian vegetation species at different phenological stages. In Chapter 7, the sensitivity of the estimated water flow velocity to the uncertainty of *LAI* measurements retrieved with the *DHP* technology was assessed for the case of mature and rigid Common reed plants. A cheap and fast technology as *DHP* can be effectively implemented for assessing *LAI* of mature and emergent Common reed plants' stands, to be employed in prediction models of the hydraulic resistance of vegetated water bodies. In fact, the uncertainty of uniform water flow velocity due to *DHP*-derived *LAI* uncertainty is acceptable (equal at most to 11%). This value is comparable to the uncertainties affecting the measurements of water flow velocity acquired during field experiments. It has been highlighted the need for evaluating the sensitivity of predictive ecohydraulic models to the *DHP*-derived *LAI* by investigating a wider range of riparian vegetation species and a larger spectrum of hydraulic and vegetative conditions, aiming at determining the models' limitation.

Notation

A_B	unit ground area.
A_C	reference area
ADV	acoustic Doppler velocimeter.
A_{HD}	total HD black area.
A_L	one-sided leaf area.
ALA	average leaf inclination angle.
AOV	angle-of-view.
Ap_0	projected area in still air.
A_{Ref}	PVC reference circular frame area.
a_x	longitudinal cylinders' spacing.
B	width of the channel's cross section.
Bp	Baptist et al. (2007) resistance model.
Bp_{CC_1}	Baptist et al. (2007) resistance model results for CC_1.
Bp_{CC_2}	Baptist et al. (2007) resistance model results for CC_2.
C_1	CAN_EYE *LAI* for *ALA* = 60° ± 30.
C_2	CAN_EYE *LAI* for a view angle of 57°.
CC_1, CC_2	discharge regimes corresponding to the second riparian vegetation management scenario.
C_b	Chézy's coefficient flow resistance due to the bed roughness.
C_D	stem's drag coefficient.
$\overline{C_D}$	bulk drag coefficient.
CFD	Computational Fluid Dynamics.
COI	circle of interest.
$CORR$	signal averaged Correlation.
C_r	vegetative Chézy's water flow resistance coefficient.
$C_{r,\,est}$	estimated vegetative Chézy's water flow resistance coefficient.
$C_{r,\,meas}$	measured vegetative Chézy's water flow resistance coefficient.
CV	coefficient of variation.
D	direct *LAI* measurements.
d	stems' average diameter.
DCM	divided channel method.
DHP	digital hemispherical photography.
DN	digital number.
E	elastic modulus of the material.
EC_1, EC_2, EC_3	discharge regimes corresponding to the third riparian vegetation management scenario.
ESU	elementary sampling unit.
F_{100}	*DHP*-derived *LAI* from binarized *DHP*s with *DN* = 100 as threshold.
F_{150}	

F_{200}	*DHP*-derived *LAI* from binarized *DHP*s with *DN* = 150 as threshold.
F_A	*DHP*-derived *LAI* from binarized *DHPs* with *DN* = 200 as threshold.
f	*DHP*-derived *LAI* from binarized *DHP*s with automatic *DN* threshold.
f'	total Darcy-Weisbach's friction factor.
f''	bed Darcy-Weisbach's friction factor.
F_D	vegetative Darcy-Weisbach's friction factor.
F_L	drag force.
FOV	lift force.
F_R	field-of-view.
$G(\theta_i, \varphi_i)$	resultant force.
g	mean projection of the leaf area per unit surface.
h	gravitational acceleration.
h_i	water level.
h_v	water level of each *DCM* sub-section.
i	riparian vegetation height from the channel's bottom.
I	bed longitudinal slope.
J	second moment of area.
K_i	energy line slope.
k_s	leaves contact frequencies.
L	characteristic bed roughness coefficient, equal to 50 $m^{1/2} \cdot s^{-1}$ for sand.
LAI	*LI-COR*-derived *LAI*.
l_c	leaf area index.
$LI\text{-}COR$	characteristic length.
$LI\text{-}COR_A$	LI-COR® LAI-2000 Plant Canopy Analyser.
$LI\text{-}COR_B$	above-canopy *LI-COR* reading.
L_m	below-canopy *LI-COR* reading.
m	average *L* values of the measuring points of the 20 *ESU*s.
m_i	riparian vegetation density.
N	riparian vegetation density for each *DCM* cross section.
n	number of the *DCM* sub-sections
$n_{,est}$	Manning's hydraulic roughness coefficient.
$n_{,meas}$	estimated Manning's hydraulic roughness coefficient.
n_i	measured Manning's hydraulic roughness coefficient.
$num.$	Manning's hydraulic roughness coefficient for each *DCM* cross section.
OLS	number of stems in each measuring cross section.
p	ordinary least square method.
$P_0(\theta_v, \varphi_v)$	probability value, also known as *p*-value.
Q_i	gap fraction.

R	leaves contact weights.
R^2	hydraulic radius.
Re	coefficient of determination.
Re_s	Reynolds number.
RGB	stem's Reynolds number.
R_i	red-green-blue additive colour model.
$RMSE$	hydraulic radius for each *DCM* cross section.
s	root mean square error.
$S\&S$	distance between adjacent stems.
$S\&S_{CC_1}$	Stone & Shen (2002) resistance model.
$S\&S_{CC_2}$	Stone & Shen (2002) resistance model results for CC_1.
SNR	Stone & Shen (2002) resistance model results for CC_2.
$T_j(\theta_i)$	Signal-to-Noise Ratio.
$T\text{-}test$	transmittance at arbitrary point *j*.
TKE	statistical hypothesis test based on Student's t-distribution.
U	Turbulent Kinetic Energy.
u	water flow average velocity.
$\overline{u}$	instantaneous streamwise water flow velocity.
u'	time-average streamwise water flow velocity.
UAV	turbulent streamwise water flow velocity fluctuation.
u_C	unmanned aerial vehicle.
$U_{, est}$	approach velocity.
$U_{, meas}$	estimated water flow average velocity.
U_v	measured water flow average velocity.
UV_1	water flow velocity averaged only over the riparian vegetation layer.
$u(z)$	discharge regime corresponding to the first riparian vegetation management scenario.
v	vertical profile of water flow velocity.
$\overline{v}$	spanwise instantaneous water flow velocity.
v'	time-average spanwise water flow velocity.
V_p	turbulent spanwise water flow velocity fluctuation.
W	submerged plant volume.
w	plant's weight.
$\overline{w}$	vertical instantaneous water flow velocity
w'	time-average vertical water flow velocity.
x	turbulent vertical water flow velocity fluctuation.
x_i	water flow direction.
y	predictionary variables of the comparative analyses.
y_i	transverse direction.

z	response variables of the comparative analyses.
	vertical direction.

Greek symbols

α, β	
ε_r	coefficients of the *OLS* regression method.
φ_i	relative prediction error.
λ	azimuth angle.
ν	riparian vegetation surface density.
π	kinematic viscosity of water, equal to approximately 10^{-6} $m^2 \cdot s^{-1}$.
ρ	pi, equal to approximately 3.14.
σ	water density.
σ_i	water flow cross sectional area.
σ_{LAI}	water flow cross sectional area of each *DCM* sub-section.
σ_U	uncertainty of *DHP*-derived *LAI*.
χ	uncertainty of *U* estimated with Västilä and Järvelä model.
χ_i	wetted perimeter referred to the cross section.
θ_i	wetted perimeter of each *DCM* sub-section.
τ	zenith angle.
τ_0	total shear stress.
τ'	shear stress on the substrate surface per unit ground area.
τ'_{xz}	bed shear stress.
τ''	Reynolds shear stress on the *x*-*z* plane.
	vegetative shear stress.